Increasing Coverage and Improving Efficiency for RFID Systems and Wireless Sensor Networks

by

Li Chen

Submitted in Partial Fulfillment of the Requirements for the Degree Doctor of Philosophy

Supervised by

Professor Wendi B. Heinzelman

Department of Electrical and Computer Engineering

Arts, Sciences and Engineering

Edmund A. Hajim School of Engineering and Applied Sciences

University of Rochester

Rochester, New York

2015

Biographical Sketch

The author, Li Chen, was born in Shanghai, China. He received his Bachelor of Science degree in Electrical Engineering from Tongji University, Shanghai, China, in July 2005. From 2005 to 2006, he worked in Intel Asia-Pacific Research Center as a signal integrity engineer. After that, he joined a local electrical design firm, Onsig Technology, as a hardware engineer. In August 2008, he began his master's program at the University of Rochester in the Department of Electrical and Computer Engineering and has been a member of the Wireless Communications and Networking Group at the University of Rochester since August 2008. He began doctoral studies in the Department of Electrical and Computer Engineering at the University of Rochester in 2010. He pursued his research in the field of wireless communications and networking under the direction of Prof. Wendi Heinzelman. He received his Master of Science degree in 2011. He worked as a graduate intern at the General Electric Global Research Center, Advanced Communication Systems Laboratory from May 2014 to November 2014. His current research interests lie in the areas of wireless communications and networking, RFID, sensor networks and radio wake-up systems.

The following publications were a result of work conducted during doctoral study:

Li Chen, Jeremy Warner, Wendi Heinzelman, Ilker Demirkol "MH-REACH-Mote: Supporting Multi-hop Passive Radio Wake-up for Wireless Sensor Net-

works," Proceedings of the IEEE International Conference on Communication (ICC), 2015.

Li Chen, Ilker Demirkol and Wendi Heinzelman, "Token-MAC: A Fair MAC Protocol for Passive RFID Systems," IEEE Transactions on Mobile Computing, Vol. 13, Issue 6, June 2014.

Li Chen, Stephen Cool, He Ba, Wendi Heinzelman, Ilker Demirkol, Ufuk Muncuk, Kaushik Chowdhury, and Stefano Basagni, "Range Extension of Passive Wake-up Radio Systems through Energy Harvesting," Proceedings of the IEEE International Conference on Communication (ICC) 2013, June 2013.

Li Chen, He Ba, Wendi Heinzelman and Andre Cote , "RFID Range Extension with Low-power Wireless Edge Devices," Proceedings of the IEEE International Conference on Computing, Networking and Communications (ICNC) 2013, January 2013.

He Ba, Li Chen, Wendi Heinzelman, Melissa Sturge-Apple and Zeljko Ignjatovic, "A Method For Signal Detection and Quantification of Heart Rate Data in Human Research: Insights From Engineering and Psychology," Society for Research in Child Development (SRCD) Themed Meeting, 2012.

Li Chen, Ilker Demirkol and Wendi Heinzelman, "Token-MAC: A Fair MAC Protocol for Passive RFID Systems," Proceedings of the IEEE GLOBECOM 2011, November, 2011.

Acknowledgments

I would like to express my deepest gratitude to my advisor, Wendi Heinzelman, for her excellent guidance, caring, patience, and providing me with an excellent atmosphere for doing research. During my 7 years of study at the University of Rochester, she spent endless amount of time proofreading my research papers and giving me excellent suggestions. Her professional support and advise in my research guided me through the difficulties in my research and lead to this dissertation.

I would like to thank Professors Mark Bocko and Muthu Venkitasubramaniam for acting as members of my thesis committee.

I would like to thank all my lab-mates and colleagues in the Wireless Communications and Networking Group. It is my pleasure to work with all members in the lab. I am especially thankful for the friends who worked with me on my projects, Dr. Ilker Demirkol, Dr. He Ba, Stephen Cool, Jeremy Warner, Pak Lam Yung and Dawei Zhou.

I would like to express thanks to all of my friends in Rochester. I am grateful for the invaluable friendship and support they provided; here I only name a few: Yanwei Song, Na Yang, Xuefei Zhang, Jianbo Wu, Dehua Zhou, Changxu Liu, Shuai Zhu, Yu Gu, Wei Feng, Mitchell Lin and Anna Cha.

Above all I would like to thank my parents, Long Chen and Xinglian Li, as well as my girlfriend, Weili Huang, for their endless love, support, encouragement and patience. It is to them that I dedicate this dissertation.

Abstract

Radio-frequency identification (RFID), which uses radio-frequency electromagnetic fields to transfer data between an RFID reader and RFID tags in order to identify and track objects, has been widely deployed in recent years. RFID systems have the advantages of low cost, easy deployment and high design flexibility, and hence are used for access control, commercial tracking, toll collection and asset management. Compared to other identification methods such as bar codes and QR codes, RFID tags can be accessed without a line of sight, which increases the flexibility of ID tracking.

One of the key limitations for RFID technology is coverage. An RFID system with better coverage can access more tags in a larger area with fewer RFID readers, which leads to lower cost, less access delay and higher tag access efficiency. My research begins with an investigation of the coverage problem for passive RFID tags. Due to the limitations of the transmission power, the coverage is limited. I developed and implemented a range extension approach for passive RFID tags using devices called edge devices (ZigBee-based, battery-powered, low-power readers). With the help of edge devices, the coverage of a single RFID reader can be doubled. Also, multiple edge devices can work cooperatively to further extend the coverage area.

Another challenge in RFID system design is the MAC (Media Access Control) protocol. Due to some hardware limitations, most RFID systems are designed to use a contention based MAC protocol, which leads to high collisions, low fairness

and low scalability. I proposed a token based RFID MAC protocol called Token-MAC to address these issues. Token-MAC can achieve a higher tag rate than contention based protocols. Also, Token-MAC can provide higher fairness performance, and it increases the scalability of the RFID system as well. I implemented the Token-MAC protocol in a programable RFID tag and evaluated the performance of Token-MAC. I also compared the performance of Token-MAC with a TDMA approach and the standard RFID protocol called C1G2 in experiments and through simulations.

As passive RFID tags can be powered by an electromagnetic field, it is possible to use these devices to build a wake-up radio for Wireless Sensor Networks (WSNs). Passive wake-up radios can greatly increase the operational lifetime for a wireless sensor node by eliminating idle listening, when the node is awake but not transmitting or receiving data. However, due to the limited amount of energy harvested by an RFID tag, the limited wake-up range is a problem for passive wake-up radio sensor nodes. Most passive wake-up radio receivers can only work with a wake-up distance much shorter than the communication range. In this thesis, I present a passive wake-up radio design for Wireless Sensor Networks with extended wake-up range. This wake-up radio utilizes a high efficiency power harvesting receiver, a low power wake-up trigger circuit, and a wireless sensor node to build a passive wake-up sensor node called a REACH-Mote.

Furthermore, due to the high efficiency power harvesting receiver and the compact RFID transmitter, it is possible to build a sensor node that operates using the energy obtained from the power harvester rather than from a battery and utilizes the harvested energy to transmit energy to nodes further away, waking up a second level of nodes. This potential network topology may lead to a new design in wireless sensor networks.

In summary, I have developed 1) an RFID range extension method using edge devices that improves the coverage of RFID systems; 2) Token-MAC, an RFID

MAC protocol that improves the performance of the RFID system; 3) passive wake-up radio sensor nodes called REACH-Mote and REACH^2-Mote designed for wireless sensor networks; and 4) a multi-hop passive radio wake-up sensor node. These designs improve the performance of RFID systems and wireless sensor networks, enhancing the network stability, throughput and lifetime and enabling new applications of RFID systems and wireless sensor networks.

Contributors and Funding Sources

This work was supported by a dissertation committee consisting of Professor Wendi Heinzelman and Mark F. Bocko of the Department of Electrical and Computer Engineering and Professor Muthu Venkitasubramaniam of the Department of Computer Science. The energy harvester circuit in Chapter 5 was provided by Ufuk Muncuk, Professor Kaushik Chowdhury and Professor Stefano Basagni of the Department of Electrical and Computer of Northeastern University. All other work conducted for the dissertation was completed by the student independently. The RFID Range Extension research in Chapter 3 was supported by Omni-ID. The research on wake-up radio was supported by the National Science Foundation under research grant CNS-1143662.

Table of Contents

List of Tables

List of Figures

1 Introduction

Wireless communication technology has experienced a boom in the last decade, mainly through the introduction and mass adoption of cell phones and WiFi. Additionally, other types of wireless systems, including RFID systems and wireless sensor networks, have developed substantially in recent years. The development of these systems, as well as advances in energy harvesting technologies, with a focus on eliminating the need for batteries in the devices, have given rise to a host of potential applications, such as the Internet of Things (IoT) [1], wearable devices [2] and body-area networks [3].

1.1 RFID Systems

Radio Frequency IDentification, or RFID, is a generic term for technologies that use radio waves to identify people or objects [5]. Most common is to store the identification on a microchip that is attached to an antenna (the chip and the antenna together are called an RFID tag). The antenna enables the chip to transmit the identification information to a reader. The reader receives and processes the radio waves from the RFID tag and obtains the identification information. RFID systems generally are composed of RFID readers and RFID tags, which are either active, using a battery to operate [6], or passive, using energy harvested from the

reader [7]. Using passive RFID tags has the advantage of not requiring batteries on the tag, which leads to a nearly infinite lifetime for the tags. However, the communication abilities of passive RFID tags are limited and unstable, as this depends on the energy received by the tags, which itself is determined by the distance between the tag and the RFID reader, differences in tag design, and slight differences in the manufacturing of the tags. Moreover, as some antennas of RFID readers and tags are not omnidirectional, the orientation of the tags as well as the orientation of the RFID reader antenna may impact the communication abilities. Nevertheless, passive RFID systems are widely used in inventory management, object tracking and access control.

In an RFID system composed of passive RFID tags, RFID readers emit electromagnetic energy to power the tags as well as to send commands to the tags. RFID tags, which store the identification information, are powered by the energy radiated from the RFID readers and respond to commands accordingly. In practice, passive ultrahigh frequency (UHF) RFID readers and tags are designed to communicate in the frequency band from 860 MHz to 960 MHz [8]. UHF RFID systems have a reasonable access range (on the order of 3-30 m) while at the same time supporting tags that cost less than $0.10. Thus, UHF RFID systems are currently being used in a wide range of applications [9] [10].

1.2 Challenges for RFID Systems

For different applications, the requirements for the RFID system are different. For example, in an inventory management application, the time to access all tags attached to the merchandise is very important. On the other hand, in the application of an electronic toll-collection system such as E-Zpass [11], the delay between when a new tag enters the network and the reader detects this new tag is crucial. In general, the following are the most significant metrics for evaluating

the performance of RFID systems [12]:

- The maximum range of tag access (i.e., the read range). This metric represents the coverage capability for the RFID system. A system with a long tag access range can cover more area for tag access (e.g., for inventory tracking), and thus can track more assets with fewer RFID readers and can provide more alerts in an access control system.

- Tag rate, which represents the number of tags that can be read in a unit time. This metric describes the achievable throughput of the system. A good throughput enables the RFID reader to access multiple tags within a small amount of time. This metric is important for inventory checking applications, as an RFID system with high tag rate can access more tags in the same amount of time as a system with low tag rate. Also, this metric is crucial for continuous identification applications, where the tags are continuously tracked by the RFID reader. A high tag rate can increase the resolution of the target tracking without missing any important tag reads.

- Fairness, which specifies the relative tag read rate of multiple tags. For most applications of RFID systems, it is important for tags to share channel access equally so that the RFID reader can access all of the tags within its read range. Fairness is especially important for a dense network, in which some tags are more likely to capture the channel and prevent the access to some other tags. Also, fairness is important for some applications like RFID sensing [13], where the tag send its ID as well as sensed data, such as temperature, humidity and velocity, to the RFID reader. Good fairness can assure all tags have a fair chance to send data back to the reader.

- The time delay between when a new tag enters the network and the reader detects this new tag. This metric is especially important when there are

mobile tags in the network. An RFID system that requires a long time to detect a new tag is more likely to miss detecting a tag with high velocity. A well designed MAC protocol should ensure a low delay to detect a new tag without compromising on tag rate. Furthermore, the delay should not increases significantly as the number of tags in the system increases.

It is difficult to build an RFID system with good coverage, high tag rate, good fairness and low delay between when a new tag enters the network and the reader detects this new tag, as there are some hardware/protocol limitations that need to be overcome to meet these goals.

Good coverage can be achieved by increasing the transmission power. However, the United States Federal Communications Commission (FCC) limits the maximum transmit power of an RFID reader [32]. Most RFID readers transmit at the maximum allowable power to achieve as much coverage as possible. Another solution to increase the coverage of RFID systems is applying multiple RFID readers or multiple RFID antennas. However, both of these solutions increase the cost of the system as well as increasing the complexity in system deployment.

High tag rate, good fairness and low delay in detecting a new tag can be achieved by a well designed MAC protocol. Generally, a carrier sense multiple access (CSMA) approach can achieve very high throughput and steerable low delay in detecting new devices. On the other hand, a time-division multiple access (TDMA) approach can guarantee good fairness for channel access for the devices. However, due to some hardware limitations, neither approach can be utilized directly in RFID systems. Tags cannot detect communication from other tags, due to the low antenna gain (the size of the tags is limited) and lower transmission power of the tags (the power consumption of the tag is limited by the power harvested by it), which means that carrier sensing is not possible, and hence CSMA cannot be used. Additionally, the unstable power supply of the tags causes issues with time synchronization, and hence TDMA is difficult to implement. RFID

standards such as the ISO 18000-6C, also know as Class 1 Generation 2 UHF Air Interface Protocol (C1G2 protocol) [44], define mainly contention-based MAC protocols. Since tags contend to control the channel to transmit packets back to the readers, the collisions increase with an increase in the number of tags in the network. Also, the capture effect occurs when a few tags are located closer to the reader than others, as those closer to the reader will harvest more energy and transmit with high energy. Therefore, it is another main challenge to build a MAC protocol that will provide good performance in terms of tag rate, fairness and delay.

1.3 Contributions: RFID systems

This thesis aims to extend the access range of RFID systems by developing an RFID system that consists of multiple ZigBee-based, battery-powered, low-power readers, which we call *edge* devices. These edge devices work cooperatively with the main RFID reader, which we called the *base station*, to extend the access range of the RFID system. Additionally, we propose Token-MAC, a new MAC protocol for UHF passive RFID systems that aims to ensure multiple tags are accessed by the reader efficiently to achieve high tag rate, good fairness, and low tag detection delay, even in the presence of a large number of tags. The contributions of my research in RFID systems include:

RFID Range Extension with Low-power Wireless Edge Devices

- Design of low-power wireless *edge* devices to cooperate with the *base station*. The edge devices are designed to be battery powered and communicate with the base station via Zigbee. Since no wires are needed, it is easy and fast to deploy the RFID system with range extension. Also, the cost of the edge device is lower than a typical RFID reader, so that the entire system will cost less than using multiple readers to achieve a similar coverage. Furthermore,

this approach is scalable. Multiple edge devices can work cooperatively to extend the coverage.

- Implementation of the hardware of the *edge* devices as well as the *base station*. I evaluated the performance of the system in terms of range extension through field tests. I optimized the deployment of *edge* devices to maximize the range extension.

Token-MAC Protocol

- Development of a new RFID MAC protocol, Token-MAC, to achieve high tag rate, good fairness and low detection rate by reducing the probability of collisions in a token based protocol. Token-MAC uses different kinds of tokens to control the communication between the reader and the tags, where tokens with different functions are either allocated by the reader or generated by the tags.

- Implementation of Token-MAC on 4 WISP programmable passive RFID tags. I evaluated Token-MAC by comparing the performance of Token-MAC to that of the standard C1G2 protocol as well as a TDMA approach.

- Using implementation results, derived energy harvesting and communication models for simulations.

- Exploration, through simulations, of the behavior of Token-MAC, C1G2 and a TDMA protocol for a large number of tags as the distances between the tags and the reader vary.

1.4 Wireless Sensor Networks

A wireless sensor network (WSN) consists of distributed sensor nodes that monitor physical or environmental conditions [14], such as temperature, sound, video, etc.

and pass the data they collect through the network to a data sink. A sensor node is typically composed of one or more processing units to process the data; memory to store the data before transmission; different types of sensors to sense the data; a power source such as a battery or an energy harvesting system, and a wireless communication transceiver. Nodes generally operate as an ad hoc network to transmit data back to the base station [15]. There are many areas that can benefit by using such sensor networks, such as:

- Military applications such as battlefield surveillance and enemy tracking. Elimination of the need for the hard/impossible to set up fixed infrastructure makes sensor networks a perfect solution for such applications [16] [17].
- Sensing the environment in an extreme or dangerous environment, such as an active volcano. Sensor nodes can be deployed remotely (e.g., dropped from an airplane), and they can build a self-organized network to collect seismic and infrasonic (low-frequency acoustic) signals in order to predict the potential volcano activity [18] [19].
- Healthcare monitoring using wireless sensors to build body sensor networks. The low power, flexible and compact design of sensor networks enable ease of deployment for a body sensor network [20] [21].
- Internet of Things, in which objects are uniquely identifiable by their virtual representations, will be easy to develop using wireless sensor networks, since they provide additional sensor information as well as identification and location information [22] [23].

1.5 Radio Wake-up

One of the most important challenges for WSNs is network lifetime [24]. Most WSN nodes are battery powered, which leads to limited network lifetime. Due to

the constraints of size/cost, the batteries attached to the sensor nodes can provide only limited energy. It is a challenge to either improve the efficiency of utilizing this limited energy or to increase the battery capability to provide an extended lifetime for WSNs. Duty cycling [25] [26], which puts the sensor node into the idle/sleep state when it is neither sensing the data nor transmitting the data, is widely used in WSNs to prolong the network lifetime. However, this approach requires accurate time synchronization between sensor nodes [27]. Also, duty cycling trades the performance of data delivery delay for network lifetime [28], which is not a beneficial trade-off for some delay sensitive applications.

Wake-up radio is another approach to increase network lifetime without trading the performance of delay by utilizing passive RF wake-up radio hardware [29]. However, the wake-up range of passive RF wake-up radios is much shorter than the communication range, which limits the performance of passive wake-up radios. Also, the power consumption of passive radio wake-up transmitters is high. It is a challenge to support a wake-up transmitter on a sensor node to build a multi-hop wake-up radio sensor network.

Energy harvesting is an approach that increases the battery capability in order to prolong the network lifetime, through re-charging the battery/capacitor by capturing energy from the environment [30] [31]. Theoretically, energy harvesting systems can increase the network lifetime to infinity. However, the non-stable amount of energy harvested and the high cost for the additional hardware increase the total cost of network deployment.

1.6 Contributions: Radio Wake-up and Energy Harvesting

This thesis aims to design a novel long range radio wake-up system with RFID technology to achieve a low latency, long network lifetime wireless sensor network. Moreover, an energy harvesting system may also be applied to the sensor node to utilize the energy of the wake-up radio to re-charge the sensor node. The contributions of my research in radio wake-up and energy harvesting include:

Wake-up Radio

- Design and implementation of a long range wake-up radio based on RFID technology, called REACH-Mote, to increase network lifetime, increase network stability, and decrease transmission latency of the sensor network. The wake-up radio circuit is designed to consume low energy while it is inactive and can be controlled by the sensor node.

- Building a range improved REACH-Mote called REACH^2-Mote, to increase the wake-up range by lowering the wake-up requirement of the sensor mote.

- Design of a multi-hop radio wake-up system utilizing RFID technology and the REACH-Mote. I have developed a multi-hop wake-up radio sensor node, called MH-REACH-Mote to achieve even lower latency in a multi-hop network scenario.

- Creation of a simulation model for the REACH-Mote and REACH^2-Mote wake-up radio sensor nodes. I utilize this model to run simulations to determine the performance of these two approaches.

- Implementation and evaluation of the performance of both single-hop long range radio wake-up sensor nodes (REACH-Mote and REACH2-Mote) and

multi-hop radio wake-up sensor networks (MH-REACH-Mote) through field tests.

1.7 Thesis Organization

This thesis is organized as follows. The thesis begins in Chapter 2 by exploring the related research and products available for RFID range extension, RFID MAC protocols, radio wake-up and energy harvesting. Chapter 3 describes the detailed design of RFID range extension using EDGE devices, providing a description of the basic concept, hardware implementation and performance evaluation. In Chapter 4, Token-MAC, an RFID MAC protocol, is introduced, along with hardware experimental results, simulation results and analysis. This thesis explores long range radio wake-up, the REACH-Mote, REACH^2-Mote as well as energy harvesting design in Chapter 5. The design and evaluation of the multi-hop wake-up mote, MH-REACH-Mote, is provided in Chapter 6. Finally, Chapter 7 concludes the thesis.

2 Related Work

2.1 RFID Range Extension

Several methods have been developed to achieve range extension beyond what is possible with a single RFID reader. These methods can be broadly divided into two categories: 1) increasing the number of antennas, and 2) increasing the number of readers. These two approaches can both achieve access range increases with some cost.

2.1.1 Range Extension Based on Multiple Antenna

The CS468 16-Port RFID Reader [37] is one example of a reader that achieves range extension using multiple antennas. This RFID reader can support up to 16 antennas. Each antenna can cover the same area within its access range. Thus, this system can achieve high overall area coverage. One problem for this system is the difficulty in deployment. Deploying 16 antennas with coaxial cables is not easy in an inventory management scenario. Furthermore, although the attenuation of the coaxial cable is low, the signal and power lost through long distance power transmit in the coaxial cable is not negligible. Scalability is another problem, as the antenna port designed on an RFID reader limits the maximum area the

system can cover. Other range extension solutions through increasing the number of antennas [38] [39] [41] also have similar limitations in terms of latency, difficulty in deployment and poor scalability.

2.1.2 Range Extension Based on Multiple Readers

Another solution for range extension is deploying multiple readers in the reading area. A multiple reader solution can provide more flexibility in deploying devices, as it is not constrained by the attenuation of the coaxial cable. However, one big issue in the multiple reader scenario is the interference between readers. Zhou et al. [40] proposed a slotted scheduled tag access method in a multiple reader scenario to reduce the possibility of reader interference at the expense of added complexity. Also, an additional reader increases the cost of the entire system in order to cover the area. Finally, there is some work that focuses on the collisions when multiple readers work cooperatively [43], but this work simply identifies the appropriate distance to place different readers from each other.

2.1.3 Range Extension Based on Zigbee Module

Bellantoni proposed a ZigBee-Enabled RFID Reader Network [42]. The idea of this work is to attach a ZigBee module to a standard RFID reader so that it can communicate with a control computer directly. The design can build a self-sufficient, battery powered Distributed Autonomous Reader Network (DARN) that can achieve flexiblility in the deployment of the RFID reader. However, this work mainly focuses on building a ZigBee based network rather than increasing the RFID access range. Furthermore, this work does not provide any evaluation of the system, so we cannot determine the performance of their proposed system. Neither RFID range nor system lifetime are analyzed, and use of multiple readers will increase the system cost dramatically.

2.2 RFID MAC Protocols

Several studies propose MAC protocols for RFID systems. These approaches can be broadly divided into two categories: contention-based approaches such as ALOHA, slotted ALOHA and carrier-sense multiple access (CSMA), and time division multiple access (TDMA)-based approaches.

2.2.1 Listen Before Talk Protocol on RFID Systems

Listen-Before-Talk (LBT) [54] [55] is a multiple access scheme that is based on CSMA, requiring all readers and tags to "listen" to the channel before transmitting data. If the channel is sensed idle, the reader begins reading tags, otherwise, it waits for a certain amount of time. However, carrier sensing does not solve the tag collision problem. In most cases, a passive RFID tag cannot receive packets from other tags due to the limitations of the antenna gain and the power of the tags' transmitted signals. That is the reason why LBT, which is the MAC protocol in the ETSI RFID standard EN 302 208 [56], is only used at the reader to detect unoccupied sub-bands prior to transmitting.

2.2.2 TDMA-based Approach

Simplot-ryl et al. propose a hybrid protocol to solve the collision problem [57]. The protocol is a TDMA-based algorithm and assumes that the number of tags is known in advance, since the algorithm allocates a slot for each tag based on the number of tags. This protocol can lead to good performance in a static RFID system. However, information about the number of tags is generally not known a-priori, and the TDMA approach requires strict synchronization for each tag. If a tag fails to receive the synchronization signal due to low energy or the movement of the tag, the TDMA approach will fail. In this thesis, we implement and present

performance results for a dynamic TDMA protocol that can support a varied and unknown number of tags as a comparison to our RFID MAC protocol, Token-MAC.

2.2.3 Standard C1G2 Protocol

The contention-based MAC protocol of C1G2 is based on Framed Slotted ALOHA [52]. Each frame has a number of slots, and each tag replies to a reader "Query" message in a randomly selected slot. The number of slots in a frame is determined by the reader and can be varied on a per frame basis by announcing the number of slots in the Query message. When this protocol is used in a dense network, the collision probability is extremely high and the throughput is low. Also, C1G2 suffers from the capture effect, where one or more powerful tags (due to their distances to the reader or manufacturing differences) may capture the channel and prevent the weaker tags from replying. We also implement C1G2 and compare its performance to Token-MAC in this thesis.

2.2.4 Round Based Protocol

Kalinowski et al. provide a simulation-based evaluation of round-based tag access algorithms such as polling or TDMA, and ALOHA-based algorithms [58]. Their work shows that ALOHA does not work well in dense networks, and the round-based methods perform better. However, their evaluation assumes that the energy of the tags is sufficient for continuous operation. In reality, we will show in our experiments that the energy supply is not stable, and a passive RFID tag may only be able to reply once it accumulates enough energy. This would result in the passive RFID tag possibly not being active in the frame during its assigned slot time for round-based methods, as we will demonstrate.

2.3 Radio Wakeup and Energy Harvesting

Reducing the energy dissipation of the sensor nodes is an important goal in the design of wireless sensor networks (WSNs). Duty cycling is one approach to reducing energy dissipation, where the radio is periodically turned off to save energy that would be wasted on idle listening. However, as communication can only occur when the transmitter and receiver nodes are both awake, the duty cycles must either be synchronized or the nodes waste energy in idle listening waiting until both nodes are awake.

2.3.1 MAC for Sensor Network

Both synchronized protocols and asynchronous protocols have been developed for conventional wireless sensor networks to support duty cycling. Synchronized protocols such as S-MAC [73] and T-MAC [74], negotiate a schedule between sensor nodes so that the nodes can wake up at the same time to communicate. Asynchronous protocols such as B-MAC [75], WiseMAC [76] and X-MAC [77], also known as low power listening protocols, apply preamble sampling to establish communication between the sender and the receiver. Both synchronized protocols and asynchronous protocols need to wait until both nodes are awake before communication can begin, which wastes energy from the battery and increases the transmission delay. Increasing the wake-up/sleep ratio can improve the latency performance at the expense of wasting more energy due to unnecessary wake-ups. Thus, it is difficult for duty cycling protocols to achieve both energy efficiency and low latency.

2.3.2 Active Wakeup and Semi-passive Wake-up Radios

Active wake-up radios utilize low power wake-up circuits for the wake-up receivers (WuRxs), which are powered by the batteries of sensor nodes. Thus, the energy consumption of these wake-up circuits are critical for determining the energy performance of the active wake-up sensor network. Doorn et al. [79] proposed a $96\mu W$ wake-up circuit and Le-Huy developed a WuRx circuit that consumes $17.8\mu W$ [80] to achieve a low power wake-up. The energy costs of active wake-up radio receivers are decreasing continuously. The wake-up circuits proposed in [81] and [82] only consume $2.4\mu W$ and $0.27\mu W$ by using integrated circuits, respectively. However, as all these active wake-up receivers only achieve a wake-up sensitivity of $-50dBm$ to $-60dBm$, compared to a $-95dBm$ sensitivity for conventional sensor nodes, the wake-up range of these active wake-up circuits is much shorter than the communication range of sensor nodes. Pletcher et al. [71] proposed an active wake-up receiver that achieves a $-72dBm$ sensitivity with an energy cost of $52\mu W$, and Petrioli et al. [78] proposed a discrete components wake-up receiver with $-85dBm$ sensitivity with $1.2mW$ energy consumption. These two approaches provide a decent wake-up range for sensor network applications. In this work, we will compare our passive wake-up approach with Pletcher's work through simulations, as it offers a good range as well as low energy consumption.

2.3.3 WISP-Mote

Wireless Identification and Sensing Platform (WISP) is a research project of Intel Research Seattle assisted by the University of Washington [85]. WISP is a batteryless device that harvests power from a standard off-the-shelf RFID reader and uses this to respond to the reader. The harvested energy operates a 16-bit ultra-low power MSP430 microcontroller that can perform a variety of computing tasks, such as sampling sensors and reporting this data back to the RFID reader [86].

WISP is an open source, open architecture EPC Class 1 Generation 2 RFID tag that includes a light sensor, a temperature sensor, a strain gauge and an accelerometer [87]. Also, WISPs can write to flash and perform cryptographic computations.

2.3.4 Passive Wake-up Radio Design

Passive wake-up radios, which are the focus of my research, do not rely on the nodes' battery power supplies while awaiting a wake-up signal from the wake-up transmiter. Sensor nodes that employ passive wake-up receivers tend to have longer lifetimes but shorter communication range compared with sensor nodes that employ active wake-up receivers. There are a few existing approaches in the literature for passive wake-up radios. In our previous work [67] [70], we proposed two single-hop passive wake-up motes: WISP-Mote and EH-WISP-Mote. WISP-Mote is a combination of a an Intel WISP [85] and a Tmote Sky sensor node [70]. Whenever the WISP harvests enough energy from the transmitter radio, it sends a pulse to wake up the Tmote Sky from the sleep state. The WISP-Mote can be awakened by an Impinj RFID reader [88] at a maximum distance of approximately $4m$. Moreover, simulations show the potential advantages of the WISP-Mote over duty cycling in terms of delay, collision, overhead, energy efficiency and protocol complexity [89]. Based on the design of the WISP-Mote, we developed the EH-WISP-Mote, which uses a parallel harvesting circuit, in order to extend the wake-up range. Implementation results show that the EH-WISP-Mote can reach $5.1m$ for the wake-up range at a height of $30cm$ above the ground, $1.3m$ further than the WISP-Mote's maximum wake-up range, representing a 20% improvement in the maximum wake-up range performance [67]. All of these represent a promising approach for passive wake-up of the sensor nodes.

2.3.5 Multi-hop Wake-up Radio Receiver

Some recent research has focused on WuRx usage in multi-hop WSNs. However, only a few active WuRx studies present results drawn from WuRx hardware implementations. The research involving passive WuRx usage in multi-hop WSNs is based on theory and simulations. For example, Zhang et al. [107] focus on active wake-up, and build a multi-hop wake-up WSN equipped with a $123\mu W$ WuRx. The use of a WuRx over a duty-cycling system improves the latency and lifetime of a multi-hop enabled WSN [107]. Ruzzelli et al. [108] propose a multi-hop WSN capable of using RFID readers and tags to achieve radio wake-up. However, the evaluation concentrates primarily on simulation results, and does not include any results from hardware implementations. To the best of our knowledge, the MH-REACH-Mote is the first reported complete implementation of a multi-hop passive radio wake-up device equipped with both a WuTx and a passive WuRx.

2.3.6 Energy Harvesting

Energy harvesting can be used to extend a wireless sensor node's lifetime without increasing the device's battery capacity. Energy harvesters capture energy from ambient vibration, wind, heat, light or electromagnetic radiation, and convert this into electrical energy. This energy can either be used to power an ultra-low power MCU, or it can be stored in a supercapacitor or battery. Supercapacitors are used when the application needs to provide large energy spikes. Batteries leak less energy and are therefore used when the device needs to provide a steady flow of energy [83]. The generated energy is usually very small and highly dependent upon the size and efficiency of the generator, thus a good energy harvester system must have very low internal loss of energy and good storage. For example, AmbiMax is an energy harvesting circuit and a supercapacitor based energy storage system for wireless sensor nodes [84]. Moreover, AmbiMax is modular and enables

composition of multiple energy harvesting sources including solar, wind, thermal and vibration.

3 RFID Range Extension Using EDGE Devices

3.1 Introduction

Radio-frequency identification (RFID) systems use RF electromagnetic fields to communicate with tags for the purpose of identification. RFID systems are widely used for managing assets and people, as well as for tracking inventory by attaching tags to merchandise. RFID systems are generally composed of RFID tags, which store the ID information, and an RFID reader, which transmits the electromagnetic energy to power the tags as well as to access or modify the tag ID information. There are three types of RFID tags: passive tags, active tags and battery-assisted passive tags. Among these three types of RFID tags, passive RFID tags have the advantages of small size and low cost, and they have close to zero maintenance. Because of these advantages, passive RFID systems have been rapidly developed in recent years. In particular, passive ultra-high frequency (UHF) RFID readers and tags communicate in the frequency band from 860 MHz to 960 MHz, where the tags communicate by backscattering the radio waves they receive from RFID readers. UHF RFID systems have a reasonable access range while at the same time supporting tags that cost less than $0.10. Thus, UHF RFID systems are currently being used in a wide range of applications.

The maximum range of tag access (i.e., the read range) is a very important metric for RFID systems, representing the coverage capability for the RFID system [4]. A system with a long tag access range can cover more area for tag reads (e.g., for inventory tracking), and thus can track more assets with fewer RFID readers and can provide more alerts in an access control system.

There are several different features of an RFID system that affect the maximum access range. First, the transmit power of the RFID reader determines the amount of energy that can be harvested by the tag. However, The Federal Communications Commission (FCC), in part 15 of its regulations, limits the transmit power in the UHF frequency band to 1 W. A typical UHF RFID reader is likely to transmit power up to the legal limit. Second, the gain of the antenna also affects the maximum access range. Different antenna can be used in different applications, leading to various access ranges. Finally, different types of tags attached to different objects will lead to different maximum access ranges. For example, an NXP HANA RFID tag [33] being accessed by an Impinj Speedway UHF RFID reader [34] can achieve a 3 m access range, while an Omni-ID Ultra tag [35] with the same reader can achieve close to a 30 m access range (based on our experiments).

Thus, with the reader using the full 1 W transmit power, a specific RFID antenna, and a specific tag attached to an object, the access range of each system can be determined. However, the area covered by this access range may not be sufficient for the application. In order to fulfill the requirements of the application, one solution is to increase the number of antennas of each reader. However, as the multiple antennas are all wired to the reader, this makes deployment difficult and messy, with wires needing to be strung in the area of deployment. Another solution is to utilize multiple readers working cooperatively for covering the area that is required for the application. However, this will dramatically increase the cost of the system (as readers can range from $500 to $1500). Moreover, since

most RFID readers are wall powered, this also makes deployment difficult, as the readers must be placed near existing outlets or extension cords must be provided.

Given these current limitations for RFID access range, in this thesis we propose a system that consists of multiple ZigBee-based, battery-powered, low-power readers, which we call *edge devices*, that cooperate with the main reader which we call *base station* to achieve range extension. Since the edge devices are battery powered and communicate with the base station using ZigBee [36], no wires are needed, which enables an easy and fast deployment of this RFID system with range extension. This system is scalable, and given that the cost of this edge device is lower than a typical RFID reader[1], this approach will cost less than using multiple readers.

The rest of this chapter is organized as follows. The description of our proposed RFID system with range extension is provided in Section 3.2. Section 3.3 describes the hardware design of the edge devices. Section 3.4 presents results from physical experiments using our system, and conclusions are drawn in Section 3.5.

3.2 The Design of RFID Range Extension: EDGE Device

The edge device we designed is composed of a ZigBee module to send the tag information back to the base station, a microcontroller (MCU) that controls the RFID C1G2 protocol and coordinates with the ZigBee module, an RFID reader chip that modulates the command and demodulates the received signal replies from the tag, and a battery pack. At the base station side, a ZigBee module is connected to the base station to collect the data received by each edge device.

[1]Edge devices are targeted at a price of $100 to $250, as they do not require the entire set of reader functions.

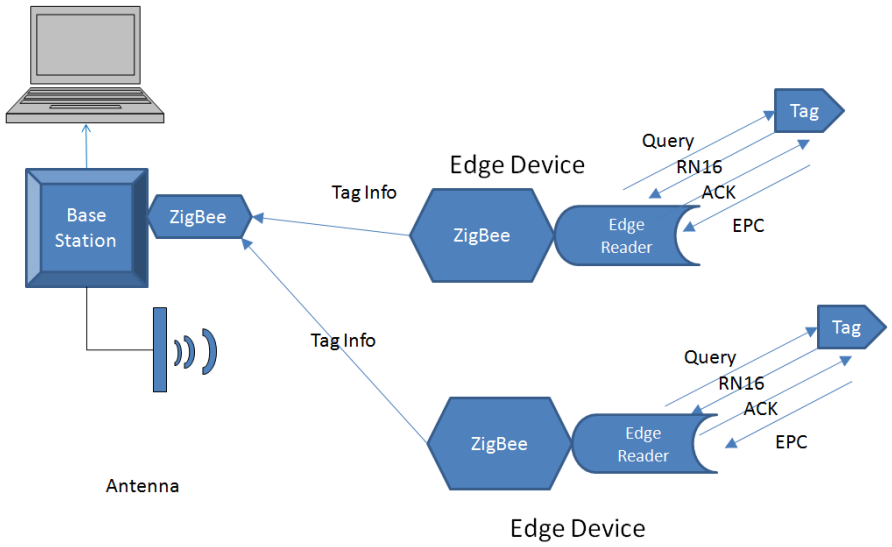

Figure 3.1: RFID system with range extension using two edge devices.

Fig. 3.1 shows the design of our RFID system with range extension using two edge devices.

When an edge device cooperates with the base station, the edge device is deployed at the edge of the access range of the base station in order to obtain the maximum range extension. For tags that are located in the access area of the base station, the tag will be accessed directly by the base station, while for those tags that are located out of the access area of base station, these tags are accessed by the edge device. When the tag information is collected by the edge device, it is sent to the base station via the ZigBee channel. Fig. 3.2 shows the resulting access area when an edge device cooperates with the main RFID reader.

In order to provide additional coverage area, multiple edge devices can be deployed. Fig. 3.3 illustrates the coverage area for an RFID reader cooperating with two edge devices to increase coverage. Additionally, edge devices can also be used with any of the existing range extension methods to obtain a hybrid system and achieve increased coverage.

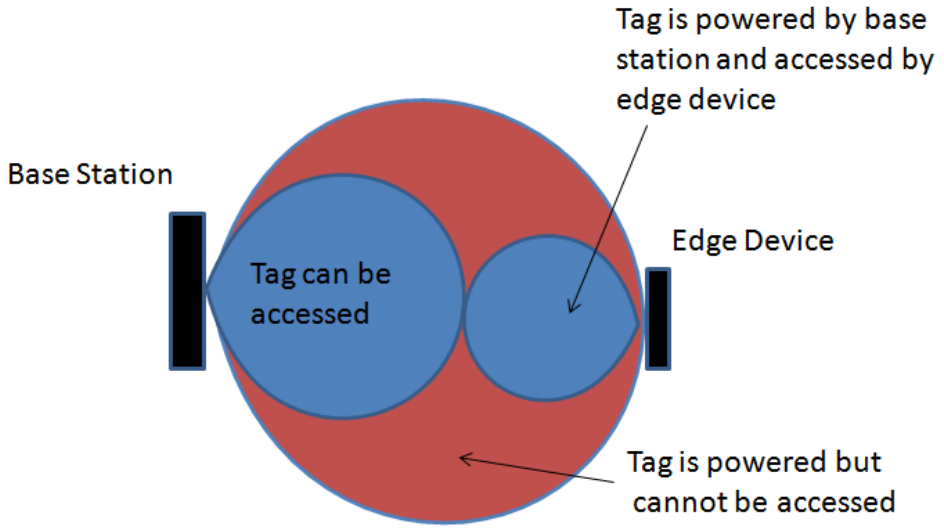

Figure 3.2: Access area and power area for a standard RFID reader cooperating with one edge device.

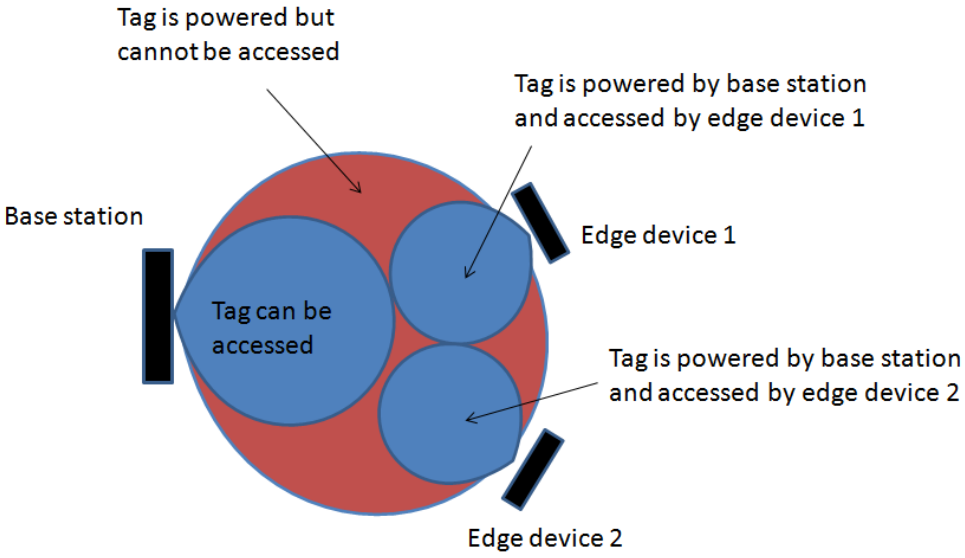

Figure 3.3: Access area and power area for a standard RFID reader cooperating with multiple edge devices.

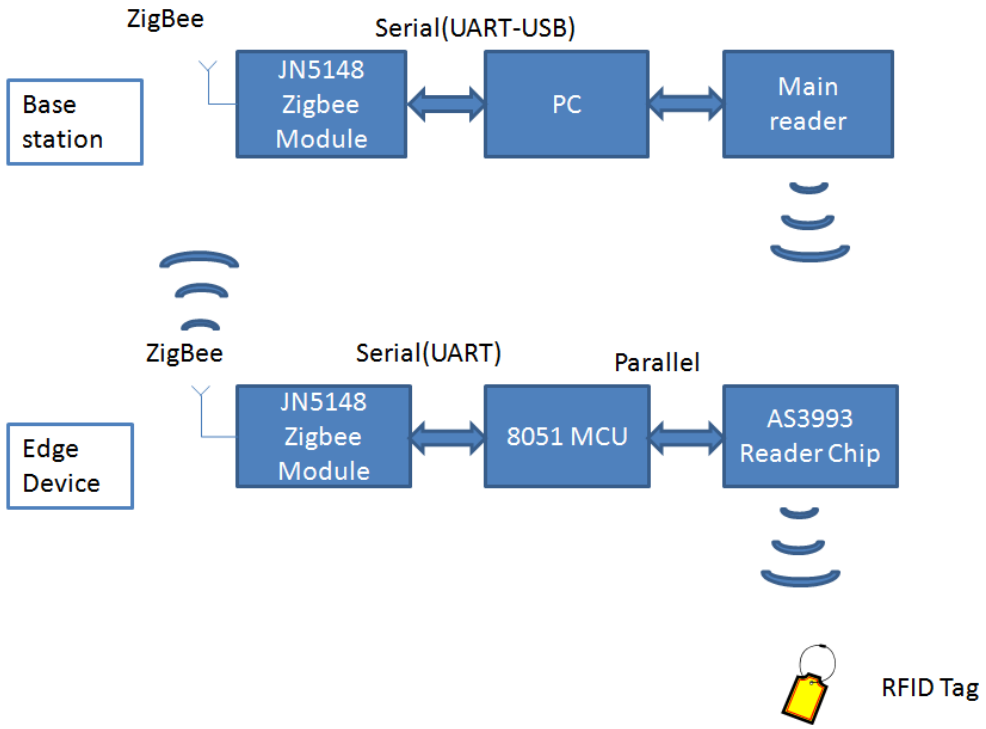

Figure 3.4: Architecture of our edge device implementation.

Table 3.1: Power Consumption (mW)

	Sleep	RFID Active	ZigBee Active	RFID Active with ZigBee
Power	0.015	636	142	778

3.3 Hardware Implementation of Edge Device

The edge device we implemented is composed of a Silicon Laboratories C8051 [45] as a control MCU to coordinate all ZigBee and RFID communication; a reader chip, Austria Microsystems AS3992 [109] RFID reader, to control the physical RFID reads; and a Jennic JN5148 [47] ZigBee communication module. Also, we connect a JN5148 to the base station in order to receive the tag information sent

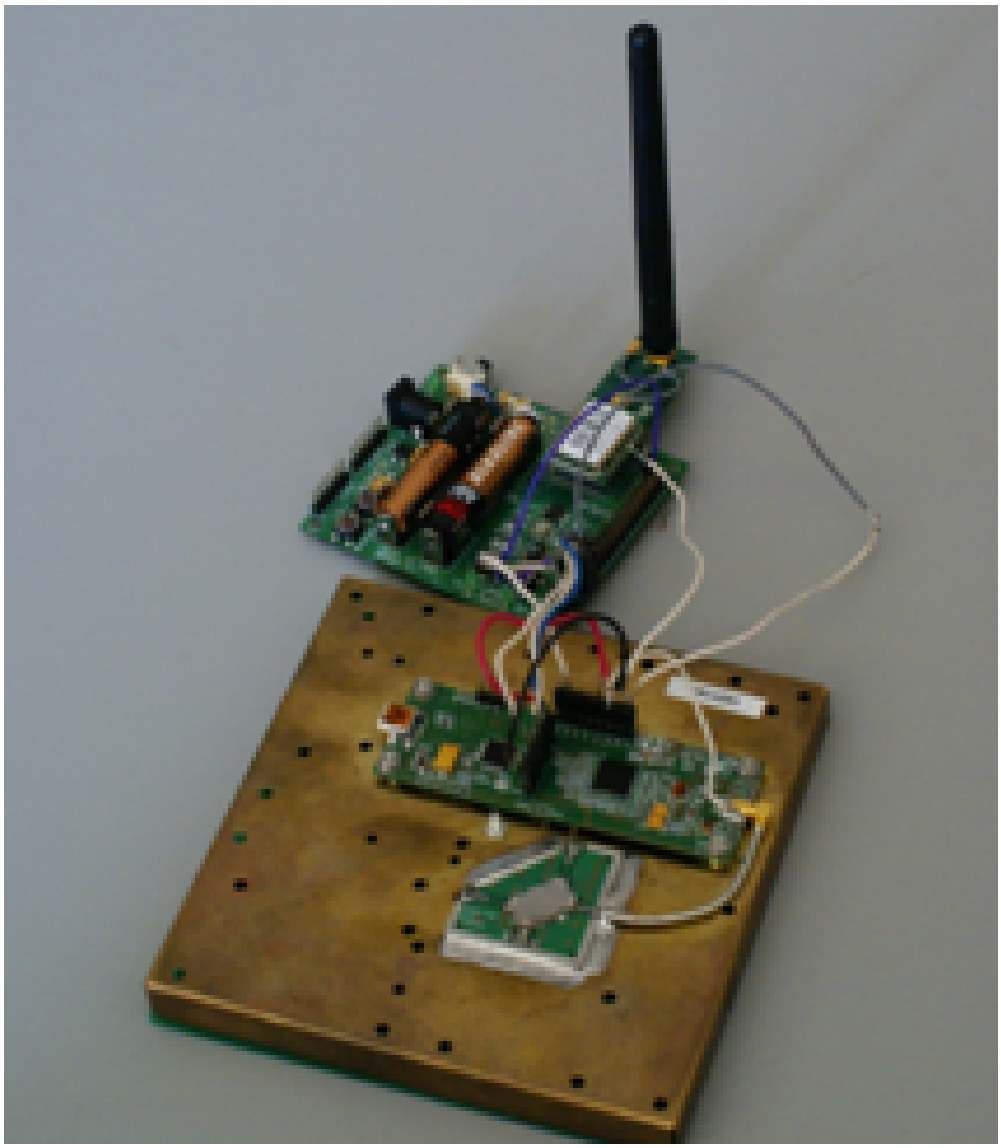

Figure 3.5: Edge device implementation.

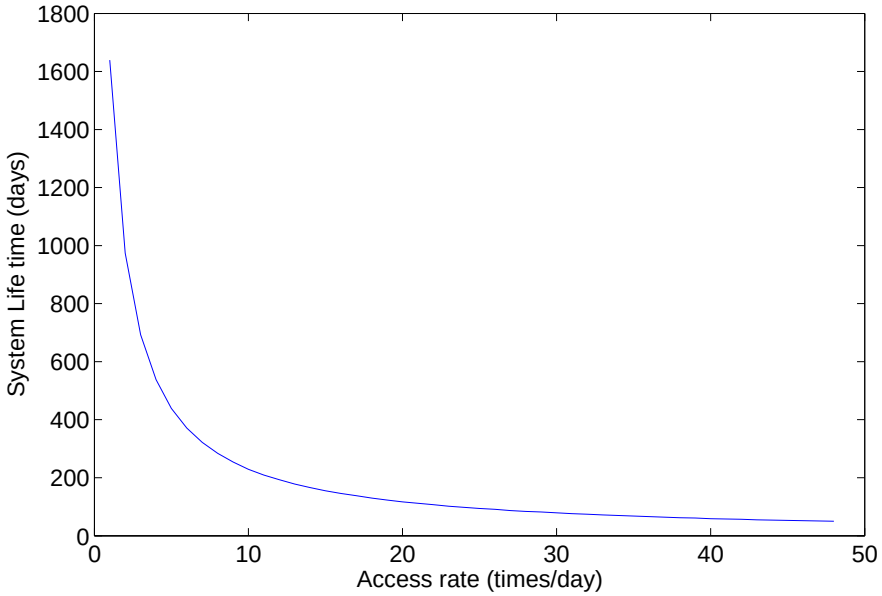

Figure 3.6: Lifetime of the edge device as the number of accesses per day increases.

by the edge device via the ZigBee channel. Fig. 3.4 shows the system architecture, and Fig. 3.5 is a picture of the actual hardware we implemented.

In order to determine expected lifetime of the system, we calculate the power consumption of different states of the edge device, as shown in Table 3.1. State "RFID Active" is the state when the edge device is sending or receiving an RFID signal; state "ZigBee Active" is the state when the Jennic JN5148 is active but the reader chip is sleeping; state "RFID Active with ZigBee" is the state when the edge device is communicating through both the RFID channel and the ZigBee channel; and state "Sleep" is the state when all of the components of the edge device are in their sleep modes.

Using these power values, and assuming that the edge device is powered by 4 AA batteries, each of which can provide 2200 mAh, we can determine the expected lifetime for our system. In particular, here we look at an inventory tracking scenario that requires the inventory to be accessed a small number of times every day. We assume that during each access, the edge device queries the

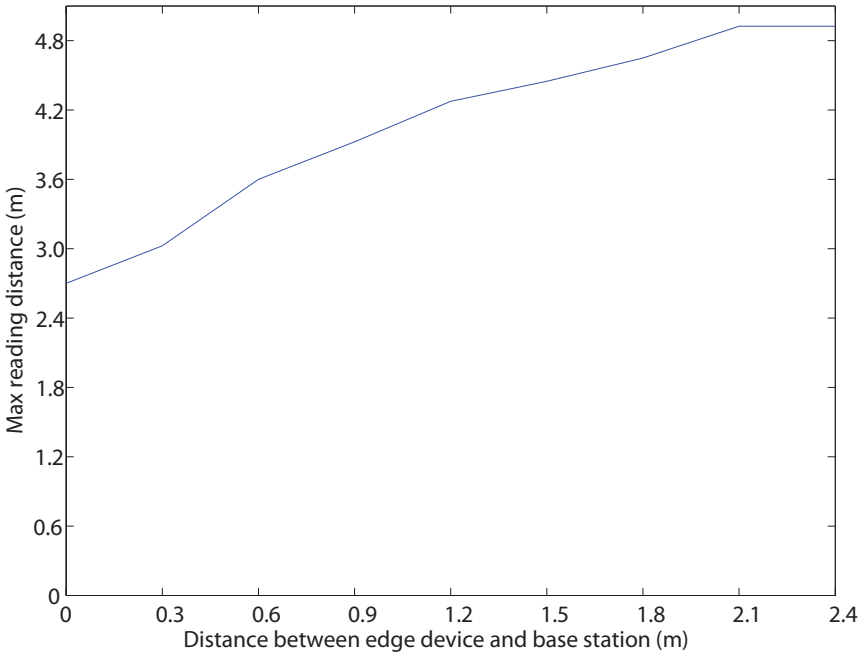

Figure 3.7: Maximum access distance as the distance between the base station and the edge device increases.

tags in its area for 30 s in order to ensure that all tags are accessed. Also, the ZigBee module needs to wake up for 10 s once every hour to handshake with the base station, keeping the ZigBee connection alive. Using these values, Fig. 3.6 shows the simulation results for the system lifetime of the edge device as we vary the number of accesses per day. From these results, we can see that if the system accesses tags once every day, the edge device can work for as long as 4 years. If the reader accesses tags every half hour, the edge device is still able to work for 1.5 months.

3.4 Experimental Results

We performed several experiments to evaluate the performance of our RFID system with range extension using edge devices. In the first experiment, the antenna of the base station is fixed, and we place the edge device very close to the base station with the edge device antenna pointed in the same direction as the base station antenna. We place tags at different distances from the base station to evaluate the maximum distance for tag access. Both the edge device and the base station as well as the tag are placed 25 cm from the ground. We repeat this experiment as we move the edge device away from the base station.

Fig. 3.7 shows the experimental results for the maximum distance the tag can be placed from the base station and still be accessed by the system. Without using our system, a single RFID reader can achieve only an 2.5 meter access range, while our experimental results in Fig. 3.7 show that using the edge device, the maximum access range is increased to 5 meter, when the edge device is $2.5m$ from the base station. If we place the edge device at a distance of more than $2.5m$ from the base station, there is an area that neither the base station nor the edge device can access. Furthermore, the maximum access distance we can achieve is 5 meter no matter where the edge device is placed. The reason for this limitation is the power harvested from the base station can only support those tags that are located within $5m$ of the base station.

In the second set of experiments, we fix both the base station and the edge device and evaluate the coverage area. We use tag rate as the performance metric, where tag rate is defined as the average number of tags that the reader as well as the edge device can access in 1 minute. The coverage result is shown in a 2-dimensional and both edge device and base station as well as the tag are placed 25 cm from the ground.

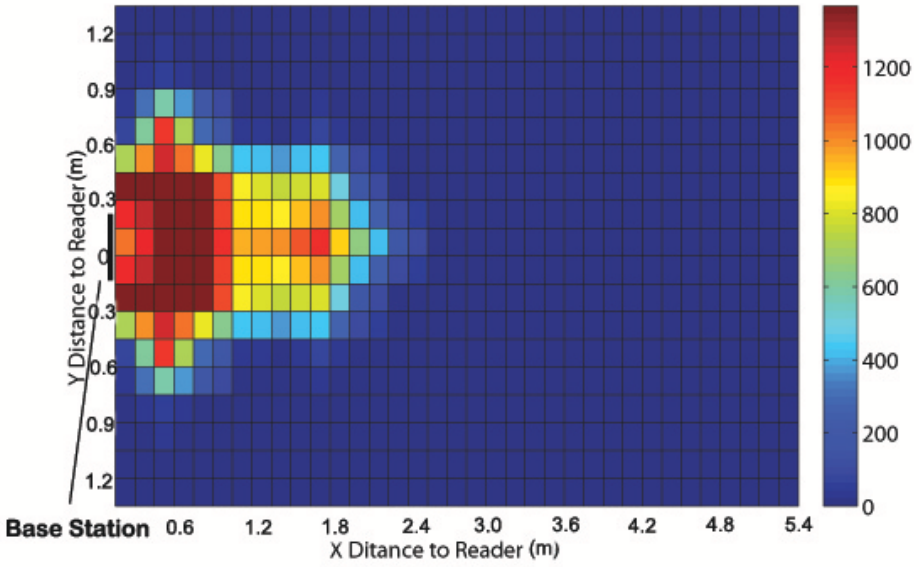

Figure 3.8: Base station coverage. Results show tag access rate in tags/min.

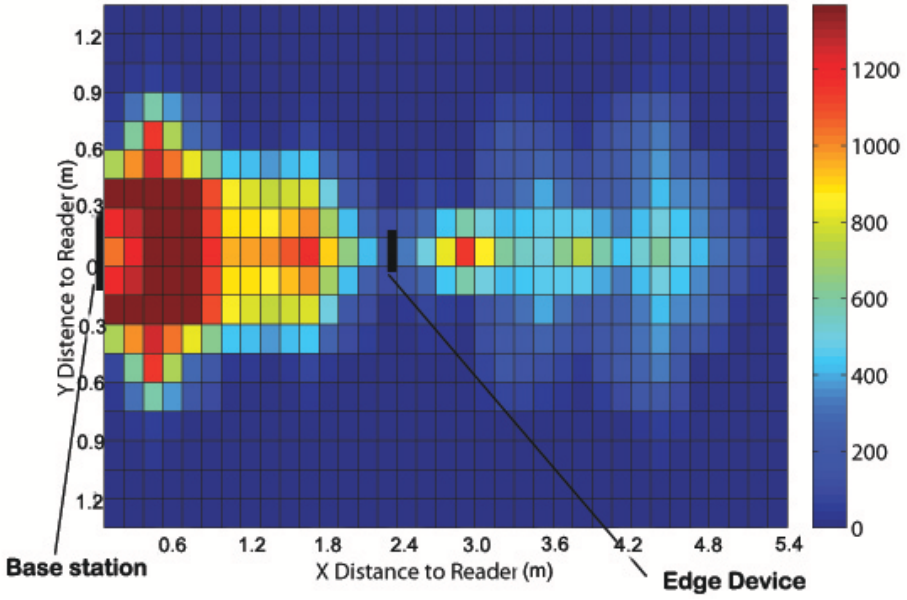

Figure 3.9: Coverage when there is one edge device with antenna pointed in the same direction as the base station antenna. Results show tag access rate in tags/min.

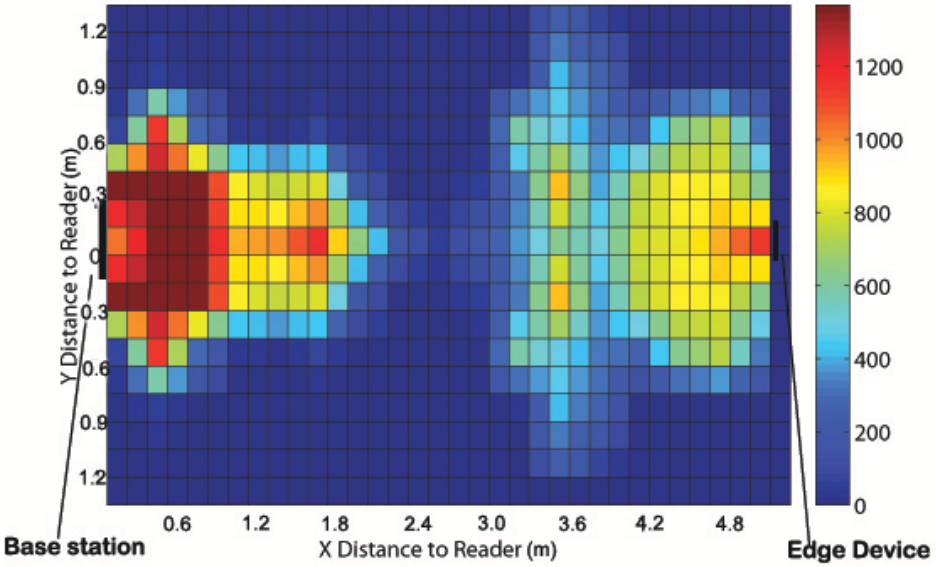

Figure 3.10: Coverage when there is one edge device with antenna pointed in the opposite direction as the base station antenna. Results show tag access rate in tags/min.

First, we evaluate the coverage of the base station without any edge devices as a baseline for coverage, as shown in Fig. 3.8. Next, we place the edge device $2.5m$ away from the base station. Both the base station and the edge device aim their antennas in the same direction. Fig. 3.9 shows the tag access rate for this scenario. Comparing Fig. 3.8 and Fig. 3.9, the additional area of coverage is the result of adding the edge device. The tags located far away from the base station have less harvested power. This is the reason the tag rate in the area that is covered by the edge device is lower than that in the area covered by the base station. With such a low power wireless edge device, we obtain a 70% increase in coverage area compared with just using the base station reader.

Fig. 3.10 shows the coverage results in tag rate when the base station and the edge device have their antennas pointed in opposite directions. The distance be-

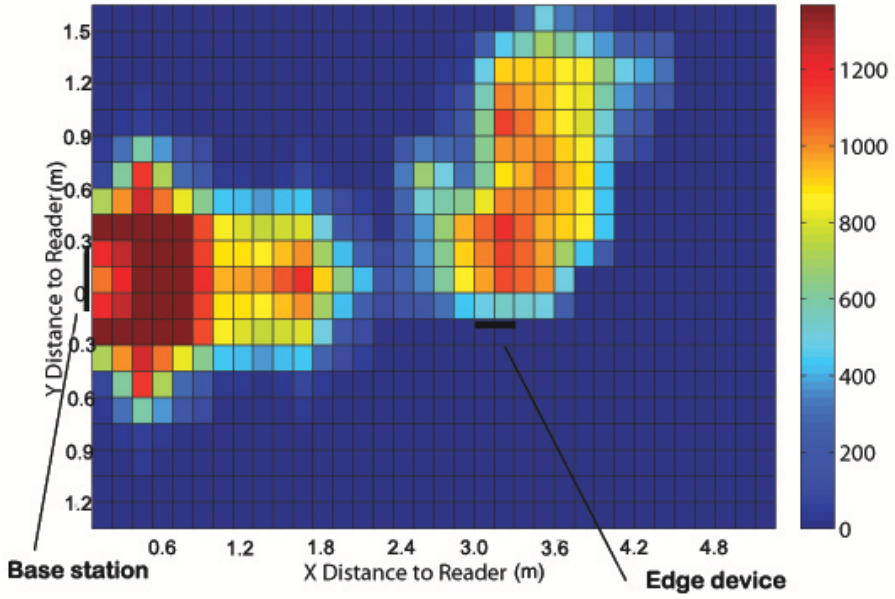

Figure 3.11: Coverage when there is one edge device with antenna pointed in the vertical direction. Results show tag access rate in tags/min.

tween the two antennas is $5m$ in order to achieve maximum access distance. Unlike the last experiment, this placement of the edge device will not block any electromagnetic waves sent by the base station. The results show that the coverage area is even better than the previous experiment's results, providing approximately 90% increase in coverage area compared with just using the base station reader. However, this deployment of the edge device leads to relatively low tag rate when the tag is located $2.5 - 3m$ from the base station, which may be an issue in real inventory management scenarios.

Fig. 3.11 shows the coverage results when the edge device is $3m$ from the base station and pointed in the vertical direction. It is easy to see that we get better coverage in the vertical direction due to the direction of the edge device, with the coverage area increasing by approximately 70% compared with just using the base station reader.

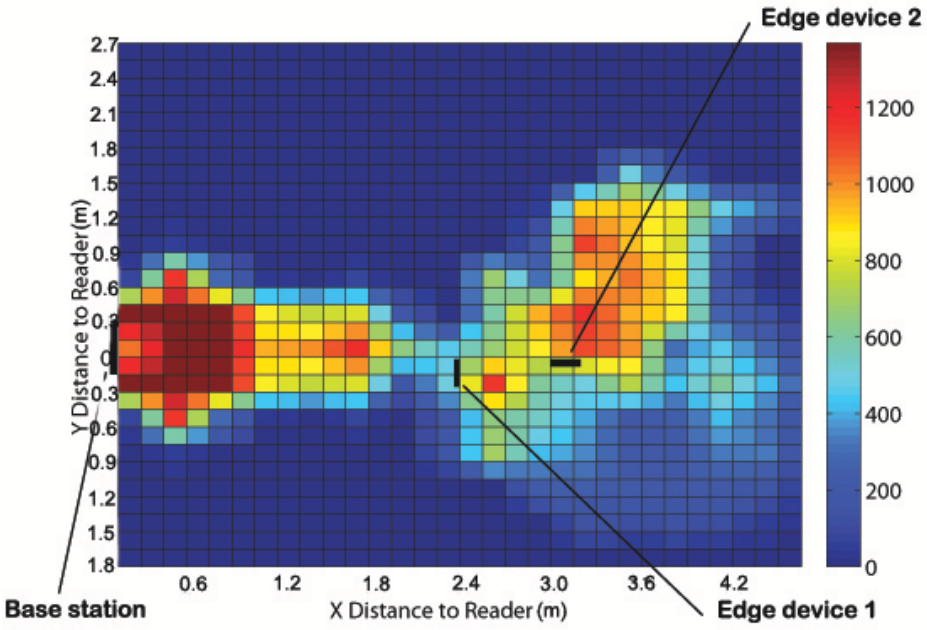

Figure 3.12: Coverage when there are two edge devices with antenna pointed in the same direction as the base station antenna and in the vertical direction. Results show tag access rate in tags/min.

Finally, we tested the scenario when the base station cooperates with two edge devices in order to further increase coverage. Fig. 3.12 shows the results from this experiment, with one edge device placed $3m$ from the base station and pointing in the vertical direction and a second edge device located $2.5m$ from the base station and pointing in the same direction as the base station. These two edge devices work together to obtain coverage extension. The results show that the coverage increases dramatically with multiple edge devices, increasing coverage by approximately 160% compared with just using the base station reader, showing that if we place more edge devices into the system, it is possible to obtain even better coverage.

3.5 Conclusions

In this chapter, we proposed an edge device that can cooperate with an RFID reader to extend the access range for RFID tags, hence increasing system coverage. This edge device has the advantage of low power operation, being easy to deploy and enabling a highly scalable system. We implemented the edge device and evaluated the performance of the system with an existing RFID reader and RFID tags. The results show that the edge device can improve the coverage and access range performance of existing RFID systems. When an RFID reader cooperates with two edge devices, the system is able to cover approximately twice the area compared to the coverage area when a single edge device is used. Also, the edge devices can work with existing range extension methods such as a multiple antenna system to create a hybrid system and obtain even more coverage.

4 The Token MAC Protocol

4.1 Introduction

Radio-frequency identification (RFID) systems are widely used for managing people and assets. Typically, RFID systems consist of RFID tags attached to objects and RFID readers that are used to interrogate (read) the RFID tags to identify the associated object. The RFID tags may be either active, using a battery to operate, or passive, using energy harvested from the reader to operate. Using passive tags has the advantage of not requiring batteries, providing a near-infinite lifetime for the tags [48]. However, the communication ability of passive tags is not stable, as it depends on the amount of energy that can be harvested, which itself depends on the distance of the tag from the reader, the environment, and slight differences in tag manufacturing, as well as on the other tags in the system. Nevertheless, passive RFID systems are deployed for a wide range of applications, such as inventory management, access control and object tracking [49].

Tag rate, which represents the number of tags that can be read in a unit time, is an important metric in passive RFID systems [50], as it represents the achievable throughput of the system. High throughput ensures the fast access of a large number of tags in a short time, which can be crucial for applications

such as inventory tracking. Fairness, which specifies the relative tag read rate of multiple tags, is another important metric in passive RFID systems. For most applications of RFID systems, it is important that each tag share channel access equally such that the reader is able to collect information on all objects within its read range. These two metrics, tag rate and fairness, are even more important in continuous identification applications, where the tags are continuously monitored by the reader to track the location of each tag. A high tag rate and good fairness can enable the continuous access of the tags without missing any important tag reads.

Another important metric for passive RFID systems is the time delay between when a new tag enters the the read range of an RFID reader and the reader detects this new tag. This metric is especially crucial when there are mobile tags in the network or when the reader is mobile. If the reader requires a long time to detect a new tag, it is possible that those tags with high velocity will be missed entirely by the reader. Not only will a good protocol ensure a low delay on accessing a new tag, but this delay should not increase significantly as the number of tags in the system increases.

RFID standards define mainly contention-based MAC protocols, where all tags contend with each other for the chance to communicate with the reader. For instance, the most widely used RFID protocol, ISO 18000-6C, also known as the Class 1 Generation 2 UHF Air Interface Protocol (C1G2 protocol) defines that tags contend to reply to the reader after they receive a Query command sent from the reader [52]. As multiple tags will receive the same Query command, there will be collisions from multiple tags accessing the channel at the same time. Thus, contention-based protocols have the issue that the throughput (tag rate) will drop sharply as the number of tags in the system increases. One other problem in contention-based protocols such as C1G2 is that a few tags that are located close to the reader may capture the channel, by responding with high power and

drowning out the other tags that are trying to communicate with the reader. This capture effect results in unfairness and impacts the reliability of the system in reading all tags.

It is not easy to achieve high throughput and low collision probability in passive RFID systems due to certain hardware limitations of the passive RFID tags [51]. One of the key issues is that a tag cannot receive or detect communication from any other tag due to the low transmit power of the tags and the low tag antenna gain, which makes channel listening employed in carrier sense multiple access, CSMA, MAC protocols infeasible for passive RFID systems. Moreover, due to the uncertainty of the tags' energy harvesting, time division multiple access (TDMA) based approaches are not reliable for passive RFID tags, as the tags may run out of energy during their allocated time slot. Also, fairness is difficult to achieve in passive RFID systems, as TDMA and CSMA approaches, which provide good fairness in conventional wireless networks, are not feasible for RFID systems. It is a challenge to design a protocol to achieve good fairness without channel listening (required for CSMA) and time synchronization (required for TDMA).

Thus, in this chapter, we present Token-MAC, a new MAC protocol for UHF passive RFID systems whose aim is to ensure that multiple tags can be accessed by the reader efficiently to achieve high tag rate, good fairness, and low tag detection delay, even in the presence of a large number of tags. Token-MAC uses tokens to control the communication between the reader and the tags, where tokens are allocated by the reader or self-generated by the tags. We choose this approach to remove the need for synchronization or channel listening and to shift the responsibility of channel management to the reader side, while providing a way to prevent the potential starvation problem of the new tags through the self-generated tokens. We present the Token-MAC protocol and implement this protocol on four WISP [85] passive RFID tags. We compare the performance of Token-MAC to that of the standard C1G2 protocol as well as a TDMA protocol. Additionally, we

derive energy harvesting and communication models based on our implementation results, which are then used to perform extensive simulations. We first show that the simulation results match the implementation results for a small number of tags, and then use the simulations to explore the behavior of Token-MAC, C1G2 and a TDMA protocol for a large number of tags as the distances between the tags and the reader vary.

The rest of this chapter is organized as follows. The description of Token-MAC is provided in Section 4.2. Section 4.3 presents the physical experiment results using Token-MAC, C1G2 and TDMA. Section 4.4 describes how we used the experimental results to devise energy harvesting and tag communication models for the simulations, and Section 4.5 provides a comparative analysis of the performance results for all the protocols through simulations. Section 4.6 presents a discussion about the results, and conclusions are drawn in Section 5.6.

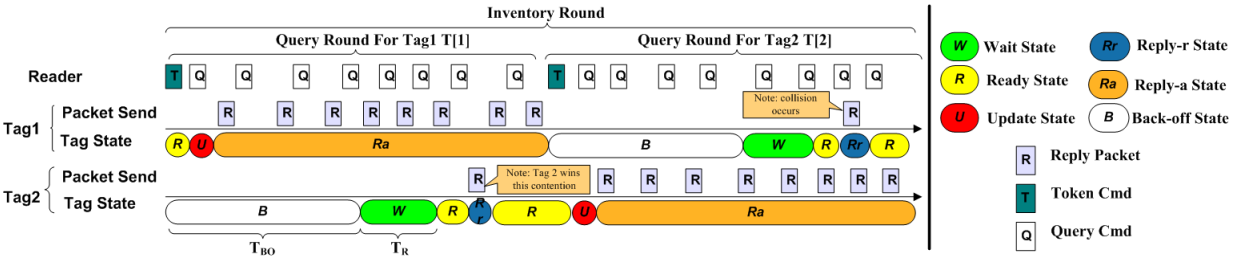

Figure 4.1: Illustration of the operation of the Token-MAC protocol.

4.2 The Token-MAC Protocol Details

To achieve low collision probability, high throughput, and good fairness, as well as a low tag detection delay, without requiring synchronization of the tags or a-priori knowledge of the tag population, Token-MAC utilizes the concept of tokens for permitting tags to access the channel. Tokens represent permission for a tag to

send data to the reader. Also, the number of tokens a tag holds represents the number of packets that the tag is allowed to send to the reader. The protocol ensures that the reader appropriately allocates tokens to different tags according to the changes in the system (e.g., the addition of new tags, the departure of tags, or the restart of tags due to power issues).

As in the C1G2 protocol, Token-MAC divides time into "Query" rounds, as illustrated in Fig. 4.1. In each Query round, the reader accesses one particular tag through a set of Query-Response exchanges. Query rounds are grouped into "Inventory" rounds, during which the reader accesses every tag that is known to the reader. We describe the Token-MAC protocol in the following sections, first discussing the use of tokens, then introducing the protocol operation at the tag and at the reader. After that, we explain the communication procedure between the reader and the tags.

4.2.1 Tokens

There are two types of tokens in Token-MAC: allocated tokens and random tokens. Allocated tokens are distributed by the reader via "Token" commands. The reader allocates tokens to tags such that tags with lower historical success rates are assigned more tokens so that they have more chances to access the channel in the next round. Hence, the fairness of the medium access is improved.

Random tokens are produced by tags themselves. The purpose of the random tokens is to give the tags permission to respond to the reader when the reader sends "Query" commands to other tags. This strategy may result in collisions. However, when the energy of the tags is uncertain, which is common for passive RFID tags, the tags may run out of energy during the wait time before they are allowed to transmit. Experimental results show that the risk of collision is worth taking, as the tags have a higher probability of successfully sending a packet to

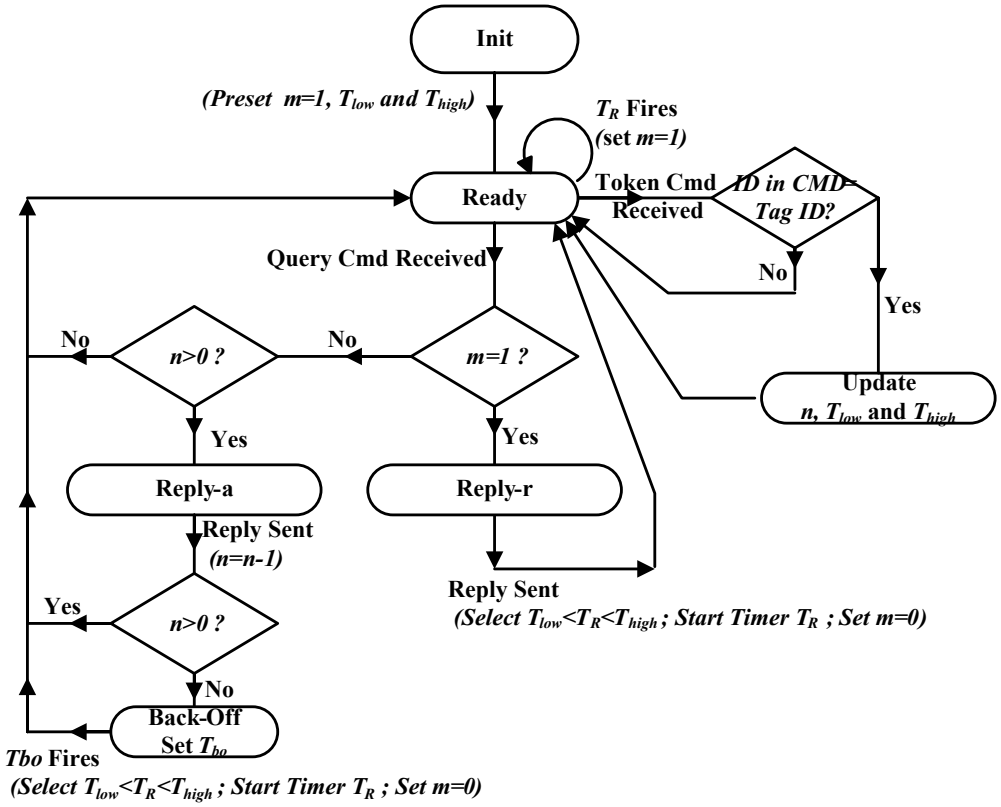

Figure 4.2: Tag operation flowchart.

the reader with this approach compared to using a separate reserved time at the end of the Inventory round for new tags.

4.2.2 Tag Operation

Tags running Token-MAC follow the flowchart shown in Fig. 4.2. Each tag has two sets of tokens: m represents the number of *random tokens* and n represents the number of *allocated tokens*. A tag begins its operation (when entering the range of an RFID reader or powering up after losing power) in the *init* state. In this state, the tag sets its internal parameters T_{low} and T_{high} to default values, and sets $m = 1$ so the tag has a random token. The tag then enters the *ready* state, where it waits to receive packets from the reader.

There are two types of packets that can be received by a tag in the *ready* state: "Token" packets and "Query" packets. When a tag receives a Token packet, it first determines whether or not it is the intended destination of the Token packet. If not, the tag goes back to the *ready* state. If the tag is the intended destination of the Token packet, the tag transitions to the *update* state, where it updates its allocated tokens, n, as well as the other parameters T_{low}, T_{high}, and T_{BO}, as specified in the Token packet. These parameters are set by the reader based on the tag density. After updating its own internal parameters accordingly, the tag goes back to the *ready* state.

When a tag receives a Query packet, its response depends on the number of allocated and random tokens it currently has. If the tag has a random token ($m = 1$), then it goes to the *reply-r* state and sends a Reply packet back to the reader. The tag then sets $m = 0$, selects a value for T_R, $T_{low} < T_R < T_{high}$, and starts a timer to fire after T_R time. The tag then goes back to the *ready* state. If the tag does not have any random tokens ($m = 0$), then the tag checks to see if it has allocated tokens ($n > 0$). If not, the tag does not have permission to respond to the Query and hence simply transitions back to the *ready* state. Note that, in this case, the timer T_R has already been set and may fire later to generate a random token. If the tag does have allocated tokens, the tag transitions to the *reply-a* state and sends a Reply packet back to the reader. After sending the reply, the tag reduces its allocated tokens by one (i.e., $n \leftarrow n - 1$). Then the tag checks to see if it still has allocated tokens remaining ($n > 0$). If so, the tag goes back to the *ready* state. If not, the tag has used up all of its allocated tokens, then the tag sets a back-off timer T_{BO} and goes to the *back-off* state, where the tag waits for the back-off timer T_{BO} to fire. Once the back-off timer fires, the tag sets $m = 0$, selects a random time T_R between T_{low} and T_{high} and starts a timer to fire then transitions into the *ready* state. After T_R time, the random token timer T_R fires and the tag sets $m = 1$, and thus the tag can reply to the next Query command

using the random token.

4.2.3 Reader Operation

In Token-MAC, the RFID reader has the following responsibilities: tag list maintenance, token allocation, tag parameter settings, and reader parameter settings. The reader maintains a tag list that specifies all known tags currently in the range of the reader. New tags are added to the list when the reader receives a Reply packet that contains a tag ID that does not exist in the current tag list. Tags that are no longer available, determined through lack of response from the tag for a timeout period, are removed from the list. The amount of time to wait before removing a tag from the tag list represents a trade-off between waiting for a tag that is low in energy and should still be accessed and continuously trying to read a tag that has left the network. In our experiments and simulations, we remove a tag from the tag list if the reader has not received a response in two Inventory rounds. This ensures that the tag has four chances to send a packet to the reader, including two Query rounds where the tag can send a reply using assigned tokens and two random tokens.

A Token packet is the first packet sent to a tag in a Query round, as shown in Fig. 4.1, and it contains parameter updates including the tag's allocated tokens. The number of tokens allocated to tag i during Inventory round j, $n[i, j]$, is based on the tag's historical response rate. Specifically, if $R[i, j-1]$ is the number of tag responses received from tag i during the last Inventory round $j-1$, then the weighted historical average of the tag rate for tag i during round j is

$$W[i, j] = R[i, j-1]\alpha + W[i, j-1](1-\alpha), \tag{4.1}$$

where α is the weight parameter. The reader calculates the number of tokens to allocate to tag i for Inventory round j based on the tag access duration (Query round duration) for tag i in round j, $T[i, j]$, and the weighted historical tag rate,

$W[i,j]$. $T[i,j]$ is set to the initial value T_{preset} when the reader is powered up, and updated at the beginning of each Inventory round as

$$T[i,j] = T_{preset} \frac{\frac{1}{p-1} \sum_{\substack{k=1 \\ k \neq i}}^{p} W[k,j]}{\frac{1}{p} \sum_{k=1}^{p} W[k,j]}, \tag{4.2}$$

where p is the number of known tags. According to (4.2), the tag duration is determined by the weighted historical tag rate of the tag and the average weighted historical tag rate of the other tags. Tags with high weighted historical tag rate are assigned low Query round duration, $T[i,j]$. The reader determines the number of tokens for node i during round j, $n[i,j]$, as

$$n[i,j] = T[i,j] \left(\frac{1}{W[i,j]} \right) \beta, \tag{4.3}$$

where β is a weight parameter. By properly setting the duration of the Query rounds for all tags, the reader can access all tags in its tag list within an Inventory round.

In addition to determining the number of allocated tokens, the reader adjusts the parameters T_{BO}, T_{low} and T_{high} of each tag according to the Query round duration $T[i,j]$, the tag density, and the application requirements. The settings used in our experiments are

$$T_{BO}[i,j] = \sum_{k=1}^{p} T[k,j] - T[i,j] - \frac{1}{2} T[v,j], \tag{4.4}$$

$$T_{low}[i] = \frac{1}{8} T[v], \quad T_{high}[i] = \frac{1}{2} T[v], \tag{4.5}$$

where v represents the tag number whose query round is before that of tag i. With these settings, a tag will wake up a half query round before its own query round, receive a random token, and after waiting a random time in the remaining

half of a query round, respond to a Query using the random token. The time of reply is bounded by the lower limit of

$$\sum_{k=1}^{p} T[k,j] - T[i,j] - \frac{1}{2}T[v,j] + \frac{1}{8}T[v],$$

and the upper limit of

$$\sum_{k=1}^{p} T[k,j] - T[i,j],$$

Note that $\sum_{k=1}^{p} T[k,j] - T[i,j] - \frac{1}{2}T[v,j]$ is the middle point of the query round. $\frac{1}{8}T[v]$ is a small offset used to ensure the tag does not respond to a Query using a random token in the first half of another node's Query round, given the clock drifts that may occur in the tags. The upper bound, $\sum_{k=1}^{p} T[k,j] - T[i,j]$, is the end of the Query round. Thus there will be no collisions in the first half of the query round from this random token. The values 1/8 and 1/2 are used because it is easy for the microcontroller unit on the tags to calculate the division by using shift operations on the unsigned integer variables.

According to the example shown in Fig. 4.1, when the reader wants to access *tag1*, it sends a Token packet and then a Query packet to *tag1*. When *tag1* receives the Query packet, since it has a token, it can respond to the Query with a Reply packet. Meanwhile, *tag2* assigns itself a random token after its T_R timer fires and sends a Reply packet. Within the Query round of *tag1*, the data rate for *tag1* is much higher than *tag2*, since *tag2* only sends one Reply packet in this duration. This is the desired behavior, since in that way, contentions decrease and hence the successful delivery probabilities of the tags increase.

Token-MAC does not eliminate collisions, since tags can send Reply packets in other tags' allocated Query rounds. However, this method enables the introduction of new tags to the reader without a separate period for new tag detections, nor synchronization. Although there is a probability that multiple Reply packets collide, this probability is low due to the small Reply packet durations. Also,

the parameters T_{low} and T_{high} set the lower and upper bounds of the interval between two random tokens. A short interval increases the probability of collision, since more random tokens will be allocated to the node, but it also improves the performance of detecting new tags as the new tag will more quickly send another response packet using a new random token if any previous response packets collided with response packets sent by other tags.

4.2.4 Communication Between the Reader and the Tags

As shown in Fig. 4.1, an RFID reader running the Token-MAC protocol accesses each known tag in one Inventory round. The Token-MAC protocol operates as follows:

- While there are no tags recorded in the tag list, the reader continuously sends the Query command until the first tag replies with its ID. When the reader receives the reply, it adds the tag ID into the tag list and starts the Inventory rounds.

- The Inventory rounds are composed of Query rounds, where the reader accesses each tag from its tag list in separate Query rounds. The reader sends the Token command to a particular tag at the beginning of the Query round. For example, in Fig. 1, the reader accesses $tag1$ by sending the Token command with $tag1$'s ID.

- When the tag receives a Token command, it goes into the *update* state and updates its parameters including n, T_{BO}, T_{low} and T_{high}. As there is a token assigned through the Token command, the tag goes into the *reply-a* state after receiving the next Query command.

- The tag continuously replies to the reader during its Query round until the number of allocated tokens goes to 0, i.e., $n = 0$. After that, the tag goes

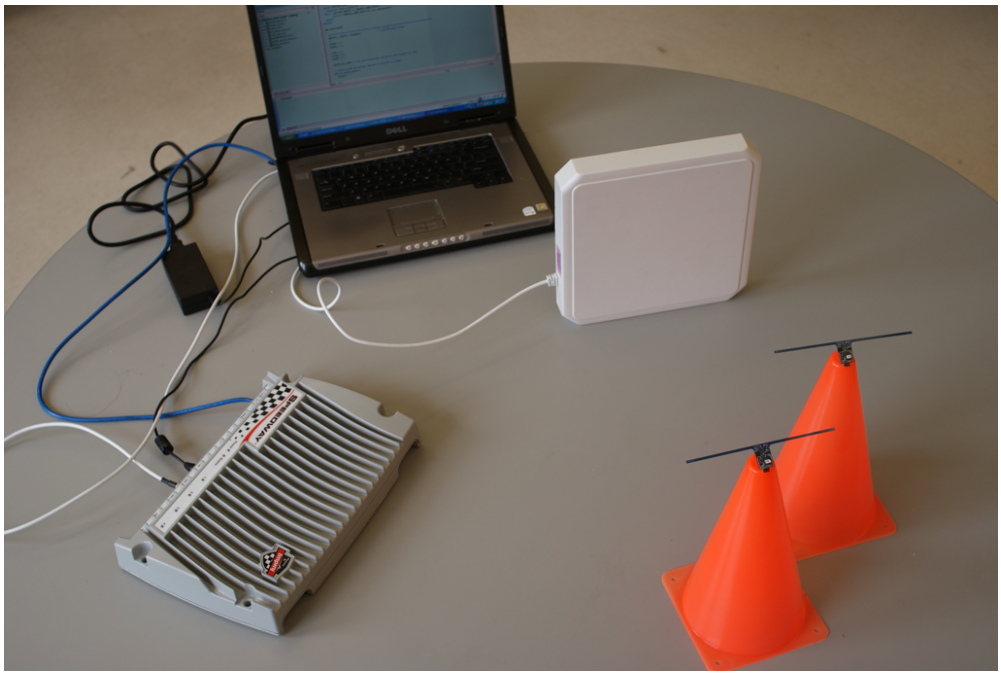

Figure 4.3: Test-bed set-up.

into the *back-off* state.

- After finishing the Query round, the reader starts the next Query round, where it accesses the next tag on the tag list.

- Any tag may go into the *reply-r* state during the Query round of the another tag by using its random token and sending a reply to the reader. The time at which a random token is generated is determined by the parameters T_{BO}, T_{low} and T_{high}.

4.3 Experimental Results

In order to evaluate the performance of the Token-MAC protocol, we built an RFID test-bed system consisting of four programmable WISP tags [85] and an

Table 4.1: Code Size and Memory Requirement

	C1G2	TDMA	Token-MAC
Code Size (bytes)	32,852	34,346	33,479
Memory Requirement (byte)	114	119	121

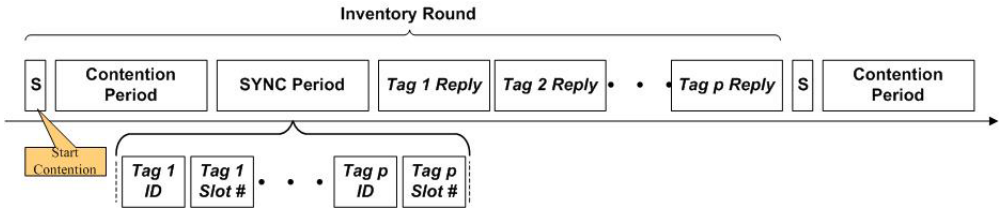

Figure 4.4: TDMA schedule.

Impinj Speedway RFID reader [66], with a computer monitoring the data collected by the RFID reader. Fig. 4.3 shows the experimental equipment. We also implemented both the C1G2 MAC protocol and a basic TDMA approach whose design details are shown in Fig. 4.4. In the TDMA approach, every Inventory round consists of a contention period in which new tags contend and announce their IDs, a synchronization period in which the reader sends a SYNC packet and allocates slots to every known tag, and a reply period in which all tags reply to the reader according to their allocated slot numbers. Through these implementations, we found that Token-MAC requires less than 2% increase in code size compared with C1G2. Also, Token-MAC requires only 7 additional bytes in memory to store the parameters for the assigned and random tokens. Thus, Token-MAC has low additional storage requirements. Table 1 shows the code size and memory requirement for all three protocols implemented.

We performed two sets of experiments. In the first set, all four tags are placed the same distance from the reader, and we vary this distance to see the performance of the three protocols. Then, to test the capture effect, in the second set of experiments, three tags are placed close to the reader while the location of the

fourth tag is varied. In both cases, the tags and RFID reader antenna are located 25 cm above the floor and moved along this plane parallel to the floor. Each experiment is repeated 4 times, and each data point is an average result for a 5 minute experiment.

We investigate two performance metrics: the tag rate achieved (or throughput), and the fairness among the tags. We used Jain's fairness index as the fairness metric, which is calculated as

$$fairness = \frac{\left(\sum_{k=1}^{p} x_i\right)^2}{p \sum_{k=1}^{p} x_i^2}, \tag{4.6}$$

where x_i represents the tag rate for tag i, and p is the number of tags. According to this definition, the fairness is a value between $\frac{1}{p}$ and 1, where the larger the index, the fairer the system is. If all of the tag rates are 0, the Jain's fairness index calculation gives an undefined value. Hence, such experiments' fairness results are not shown in the figures.

4.3.1 Tags at the Same Distance to the Reader

The aim of this set of experiments is to evaluate the performance of the protocols in an inventory management application. If we access tags attached to goods on a shelf, the distances between the reader and the tags are approximately the same.

Fig. 4.5 shows the total tag rate results when all four tags are located at the same distance to the reader. As seen in the figure, TDMA achieves better total tag rate results than C1G2 and Token-MAC for close distances (0 m – 1 m) in this scenario. However, after this range the tag rate of TDMA drops to 0. The main reason for this is that waiting for their allocated slot time consumes more energy than the tags have harvested. On the other hand, Token-MAC achieves much

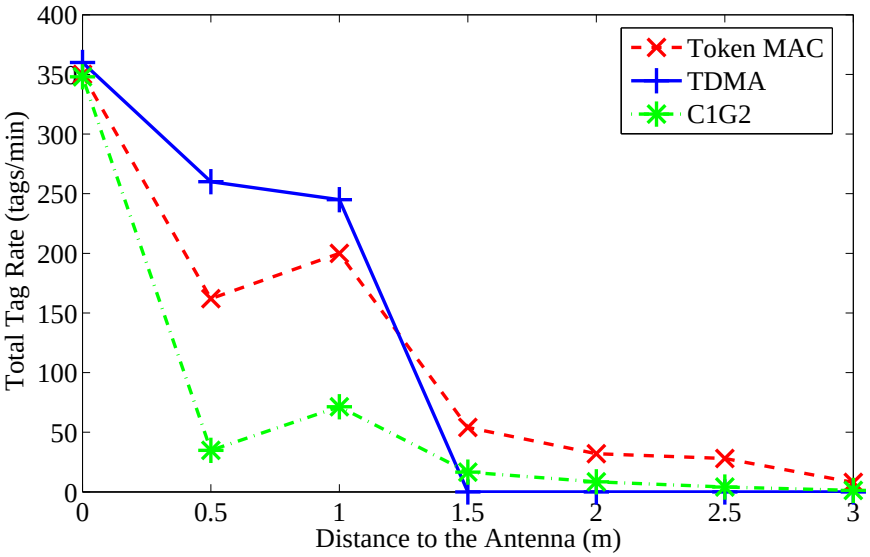

Figure 4.5: Total tag rate for tags at the same distance (4 tags).

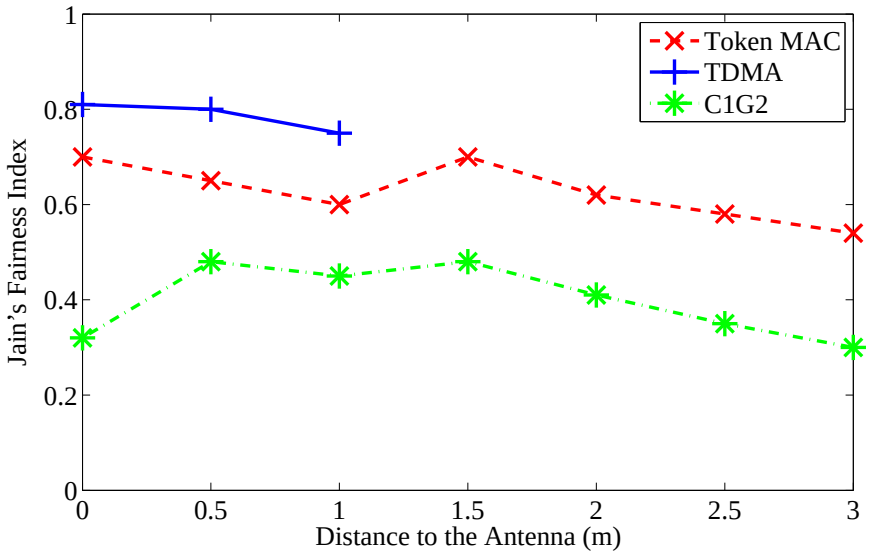

Figure 4.6: Fairness for tags at the same distance (4 tags).

higher total tag rates than C1G2 for all distances evaluated. At 3 m, Token-MAC still enables the reader to access tags at 10 tags/min while C1G2 can only access tags at 2 tags/min.. The reason for the slight increase in tag rate after 0.5 m is the multi-path effect resulting from the ground reflection.

Fig. 4.6 shows the fairness results for the same experiment set. The TDMA approach results in a good fairness performance when the tags are close to the reader due to the individual assigned slots. However, the fairness results are undefined for all distances longer than 1 m, since no tag can be read after this range using the TDMA protocol. The reason is again that the time required for a tag to wait until its slot time requires more energy than the tag has harvested. C1G2 results in low fairness for all distances, since some powerful tags (due to manufacturing differences) win the contention easier than the other tags. We can see that Token-MAC achieves much higher fairness compared to that of C1G2 for all distances evaluated.

4.3.2 Tags at the Different Distance to the Reader

Figs. 4.7 and 4.8 show the total tag rate results and the fairness achieved when three tags are located close to the antenna at 0.05 m, and the distance of the other tag is varied. We see that the tag rate achieved by C1G2 is much lower than both TDMA and Token-MAC for short distances (up to 1.5 m), and is more than 50% lower than Token-MAC for longer distances. From Fig. 4.8, it is clear that C1G2 results in severe unfairness when the tags are located at different distances from the antenna, due to the capture effect. Token-MAC has a lower probability of capture effect than C1G2. TDMA can have better performance in both tag rate and fairness than Token-MAC when the tag is located close to the reader, as TDMA is a protocol that can guarantee the access with no collision. However, since Token-MAC does not have assigned slots, it can achieve better performance

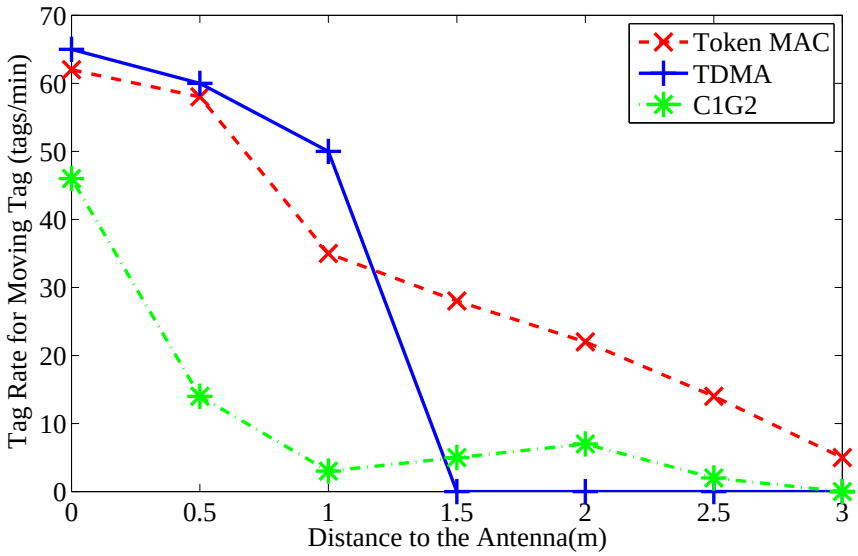

Figure 4.7: Tag rate of a tag that is different distances from the reader, with the remaining 3 tags close to the reader.

than TDMA when tags are farther than 1 m from the antenna. We can see that TDMA provides little access to the tags when the tags are located at a distance greater than 1 m. Token-MAC can provide the best performance among all three protocols evaluated when the tags are located more than 1 m from the reader. This is a common scenario in real life applications such as determining items in a shopping cart, for which Token-MAC can provide much better fairness along with higher tag rates at all distances greater than 1 m.

4.4 Energy Harvesting and Communication Models

We are limited in our test-bed to the four WISP nodes to which we currently have access. Thus, in order to further explore the performance of Token-MAC in relation to C1G2 and the TDMA protocol, we implemented the three protocols

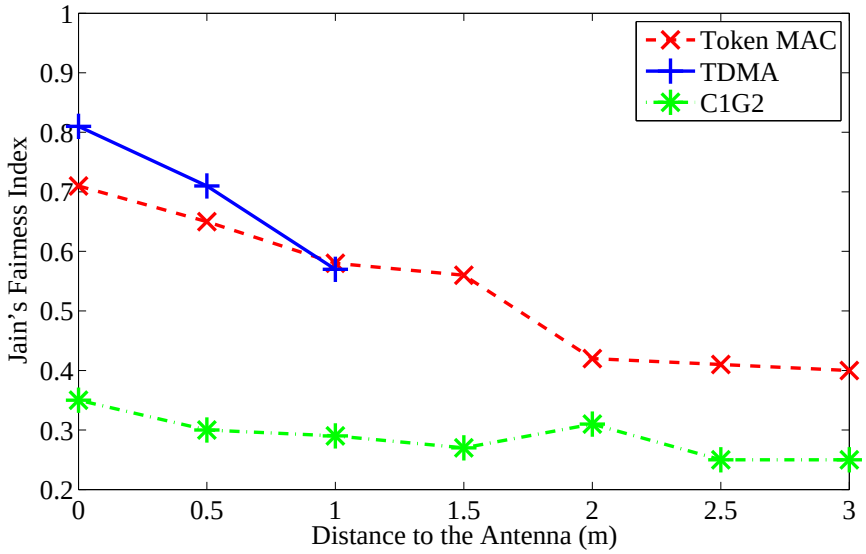

Figure 4.8: Fairness results with 3 tags close to the reader and one tag at different distances from the reader.

in MATLAB to conduct extensive simulation evaluations. However, in order to make the simulations as realistic as possible, we devised energy harvesting and communication models based on the experimental results, which are then used in the simulations.

First, we modeled the physical characteristics of our hardware platforms by measuring the amount of energy harvested by the tags and creating an energy harvesting model. Then we built a communication model based on the energy harvesting model. After incorporating these models into the simulation platform, the three different MAC protocols were simulated and their performances evaluated.

4.4.1 Energy Harvesting Model

For the energy harvesting model, we make the following assumptions. First, we assume that the amount of energy that is sent from the reader in a unit time is a

constant E. Tags at the same distance receive an equal amount of energy, which is E times the path loss. We assume the path loss follows the free-space path loss formula. Also, we assume that the amount of energy that is stored in the capacitor of a tag is the energy-saving efficiency, Q, times the energy that is received by the tag. As we will see, these assumptions are close to the real scenario. The energy that can be stored by the tag is thus

$$E' = E \times Q \times \frac{\lambda}{R^2},$$

where E' is the total amount of energy that is stored by the capacitor on the tag per unit time, R is the distance from the reader to the tag, and λ is a weight parameter. In our simulations, each RFID tag is assigned a different value of λ, within 10% of each other, to model the manufacturing differences in the WISPs.

We assume that a tag consumes E_c amount of energy per unit time when it is active. Also, the capacitor leaks E_l amount of energy per unit time when the tag is not active. Thus, we obtain the amount of energy in the tag capacitor at time t when the tag is inactive

$$E'_t = E'_{t-1} + E \times Q \times \frac{\lambda}{R^2} - E_l, \tag{4.7}$$

and the energy in the tag capacitor at time t when the tag is active

$$E'_t = E'_{t-1} + E \times Q \times \frac{\lambda}{R^2} - E_c, \tag{4.8}$$

Note that the leakage when the tag is active is negligible because $E_c >> E_l$. Fig. 4.9 summarizes the energy harvesting process.

Assuming all tags start with no energy stored in their capacitors, from (7) and (8) we can obtain a tag's current energy level based on the history of the tag's actions. Using this model for the energy stored in the capacitor at time t, and knowing the capacitance C of the capacitor used to store the energy, we can calculate the expected capacitor voltage, V_t, at time t using

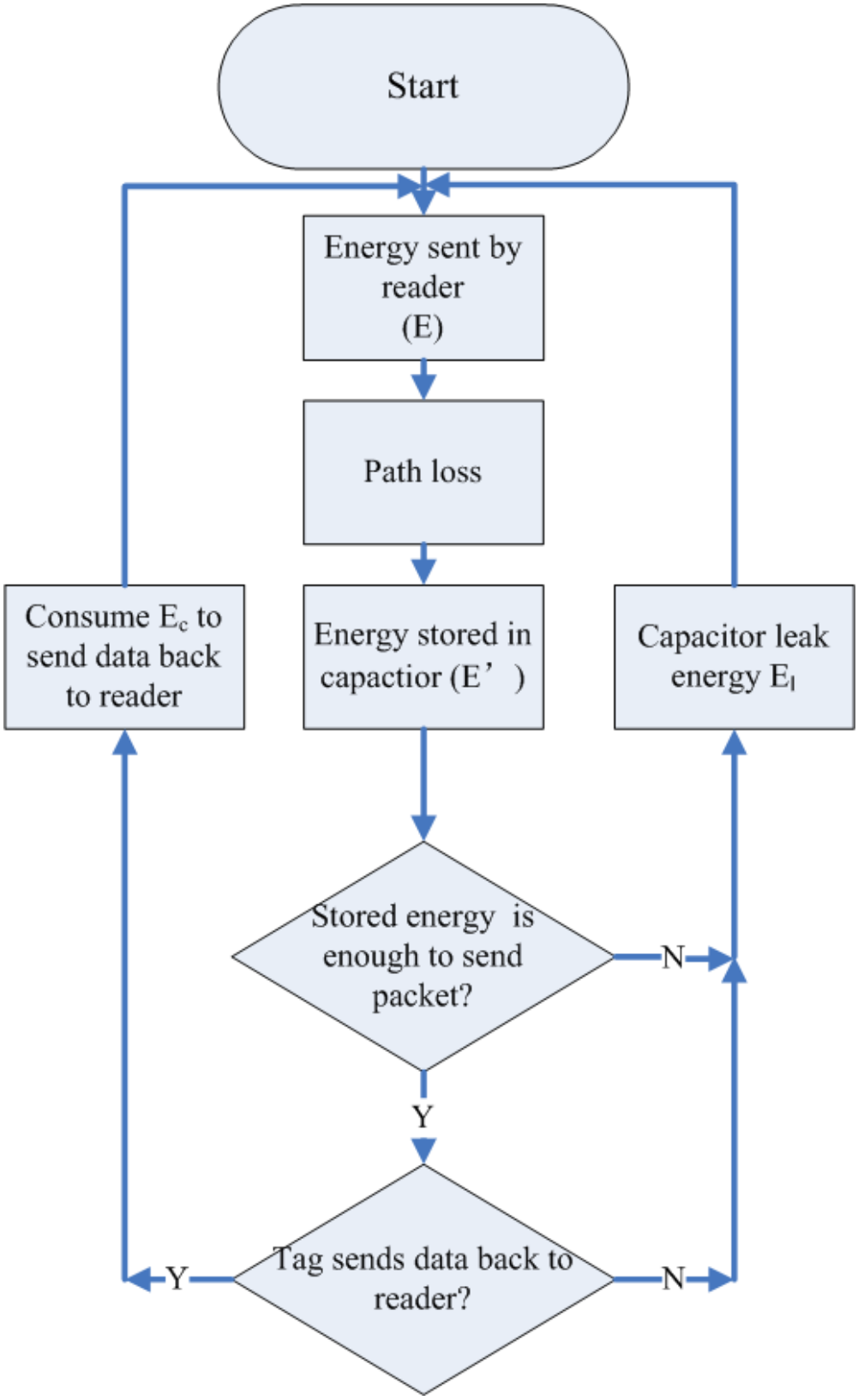

Figure 4.9: Energy harvesting and usage model.

$$E'_t = \frac{1}{2} C V_t^2,$$

or

$$V_t = \sqrt{\frac{2E'_t}{C}}.$$

The parameter values that we need to specify for this model are E, Q, λ, E_l, E_c, and C, which we determine through experiments and the WISP design specifications. Using the derived parameter values, we test the validity of the energy harvesting model through a set of experiments. In these experiments, we place a tag at difference distances to the reader and measured the voltage on the WISP capacitor used to store the energy. We compared the measured voltage levels to the derived energy harvesting model voltage V_t.

Fig. 4.10 shows the voltage levels found by the derived simulation model (V_t) and voltage levels measured in the experiments. We can see that our energy harvesting model matches very well with the experiment results.

4.4.2 Communication Model

We use this energy harvesting model as a fundamental tool to build the communication model. First, we represent the channel using the free space model. Then, we build the transmission model of sending one bit of data based on this free space model. The modulation method is based on the C1G2 protocol, which uses double side-band, amplitude shift keying (DSB-ASK) as the modulation method to modulate a bit of data and send it through the channel.

At the tag, we receive the transmitted signal attenuated by the channel with some additive white noise. We assume that the thermal noise at the receiver end is -87 dbm according to the Johnson-Nyquist noise formula [65], with the parameter values of temperature equaling 300K and bandwidth equaling 100MHz.

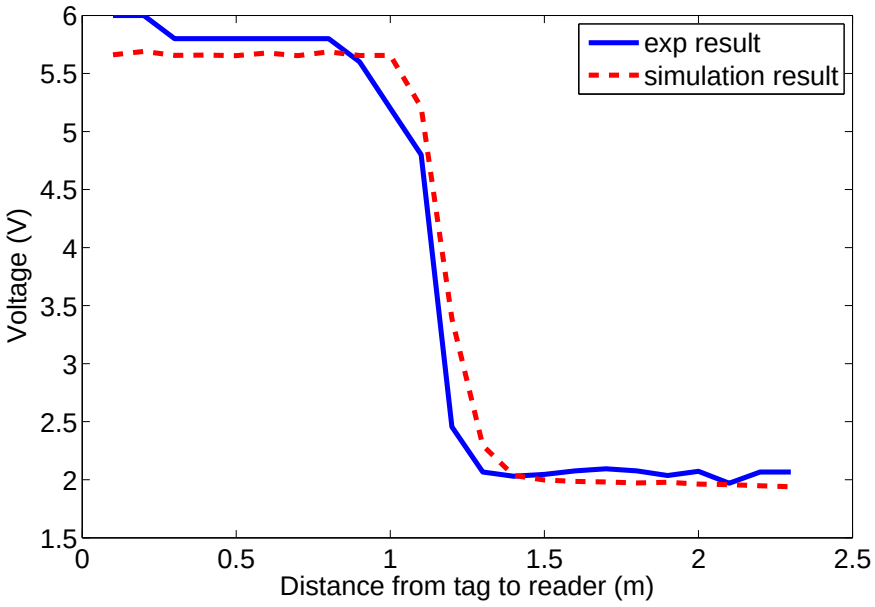

Figure 4.10: Voltage level found by the energy harvesting model compared with the measured voltage on the WISP tags.

Therefore, we find the received signal strength based on the free space model with added white gaussian noise with a power of -87 dbm. We decode the signal with noise to obtain the received bit. Since the transmission power is high and the distance between the reader and the tag is short, the bit error rate turned out to be negligible according to our calculations when the power supply is continuous. Therefore, there are no received bit errors due to the channel in our simulations, and thus the bit rate is limited only by the symbol length from the C1G2 protocol.

The transmission time is also considered in our simulations in order to detect any potential collisions. Thus, we implemented the basic physical layer of the WISPs. Moreover, one tag can receive or transmit when the energy harvesting model indicates that it is active, i.e., energy stored is enough to send a packet according to Fig 4.9. With the physical layer model and the energy harvesting model, we build the the model of sending packets between the reader and the tags. All three protocols are evaluated using this communication model.

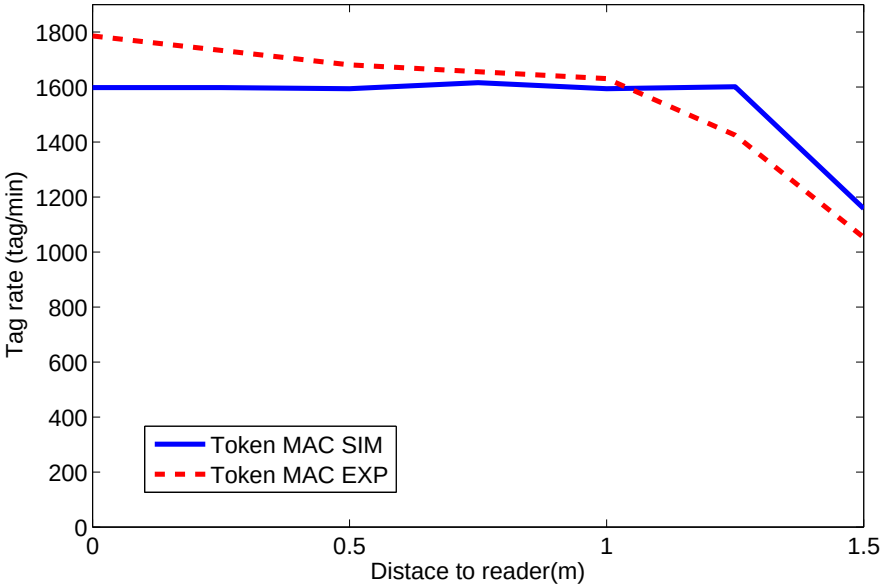

Figure 4.11: Comparison of the Token-MAC protocols' experimental tag rate results with the simulated tag rate results.

4.4.3 Simulation Model Validation

We implemented the Token-MAC, C1G2 and TDMA protocols using our simulation model, and we compared the results with the experimental results in terms of tag rate. Fig. 4.11, Fig. 4.12 and Fig. 4.13 shows the comparisons between the simulation results and the experimental results for the three protocols when one reader accesses one tag.

Our simulation results match the experimental results closely. Thus, we have confidence in our energy harvesting and communication models and use these to explore the behavior of the protocols with a larger number of tags.

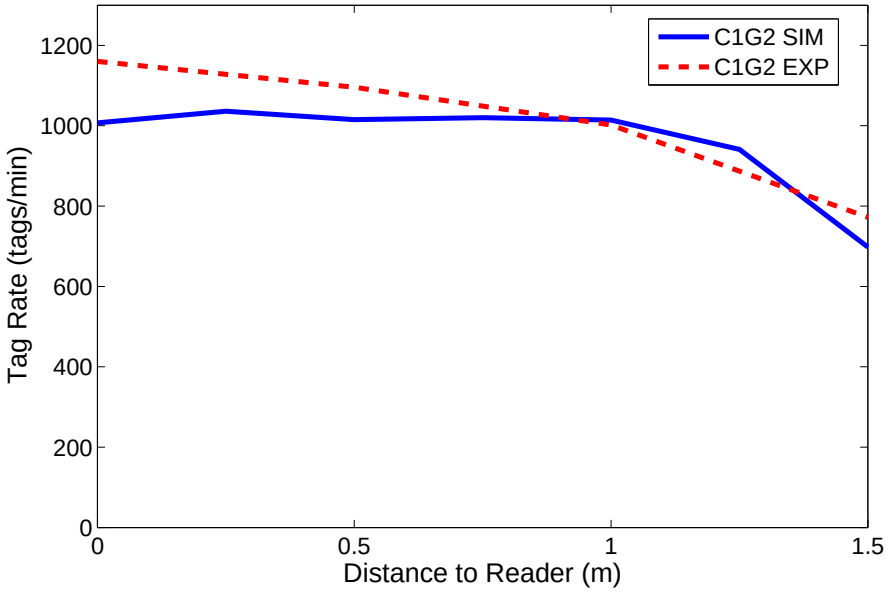

Figure 4.12: Comparison of the C1G2 protocols' experimental tag rate results with the simulated tag rate results.

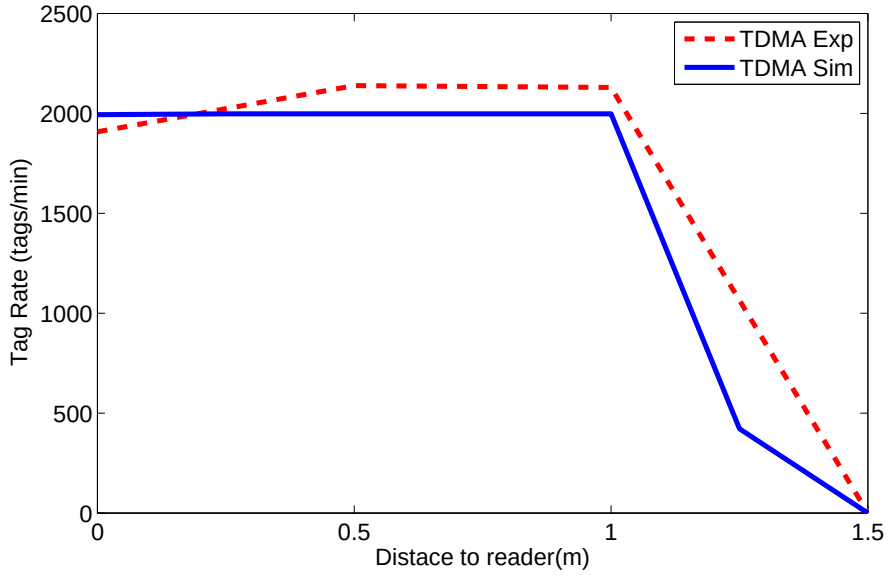

Figure 4.13: Comparison of the TDMA protocols' experimental tag rate results with the simulated tag rate results.

4.5 Simulation Results

Using our simulation framework, we develop two scenarios. In the first set of simulations, we compare the three protocols in an ideal scenario, where a set of tags is placed at the same distance from the reader, and we vary the number of tags as well as the location of the tags. In this set of simulations, we obtain the best possible performance for each protocol in terms of fairness, as there is the least chance that certain tags will capture the channel.

The second set of simulations is aimed at evaluating the performance of each protocol in a more realistic scenario, where a set of tags are randomly deployed between 0 m and x m, where x is the maximum distance of any tag to the reader. In this set of simulations, we vary the maximum distance to the reader as well as the number of tags.

The third and the final set of simulations explores the maximum number of tags that each protocol can support, which is found by adding a tag one at a time to the system until the reader cannot detect the new tag within 1 minute.

4.5.1 Tags at the Same Distance to the Reader

In this first set of simulations, the number of tags is varied from 10 tags to 100 tags, and all tags are deployed the same distance to the reader, which varies from 0.5 m to 3 m. Fig. 4.14,Fig. 4.15 and Fig. 4.16 show the total tag rates achieved by the three protocols investigated for this set of simulations. The results show that Token-MAC performs well when the tag population increases, since the total tag rate achieved does not decrease. When the distance increases, the tag rate drops linearly but still can provide fairly good tag access.

On the other hand, C1G2 performs decently when the distance is short and the tag population is small, since there are not many collisions with a small number of tags. However, clearly the C1G2 protocol does not scale well: the tag rate drops

to almost 0 when the number of tags increases to 100. This result shows that an approximate maximum number of tags that the C1G2 protocol can support is between 90 to 100.

Finally, we can see that TDMA provides very good results when the tags are close to the reader, regardless of the number of tags in the network, and hence TDMA scales well for short distances. However, when the distance increases, TDMA tag rate drops rapidly, as expected from the experimental results. There are only occasional tag reads when the distance between the reader and the tags is greater than 1.5 m.

Note that, in practice, the tag rates achieved are expected to be slightly lower if multiple tags are placed very close to each other, since the power harvesting efficiency of a tag is impacted by other tags in this case. However, this aspect is not feasible to model in the power harvesting model, and thus we do not consider this in the power harvesting model.

Fig. 4.17, Fig. 4.18 and Fig. 4.19 show the fairness results for the three protocols observed for the first set of simulations. From this figure, we see that Token-MAC can provide good fairness performance when the distance is short. Although the fairness decreases with an increase in the distance between the tags and the reader, the fairness with Token-MAC is still much better than the fairness achieved with C1G2 or TDMA. Moreover, the fairness performance of Token-MAC does not change significantly with an increase in the number of tags.

Clearly, the C1G2 protocol performs poorly with respect to fairness. Even with a low number of tags, the C1G2 protocol is unfair to some tags. When the number of tags is as high as 30, the fairness result drops to almost 0. It is

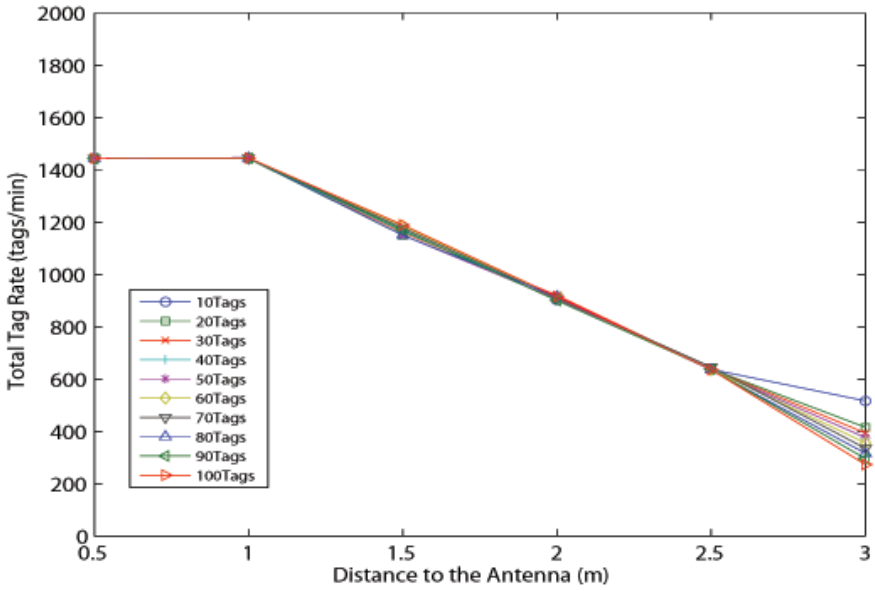

Figure 4.14: Total tag rate of Token-MAC for varying distances to the antenna and number of tags (simulation).

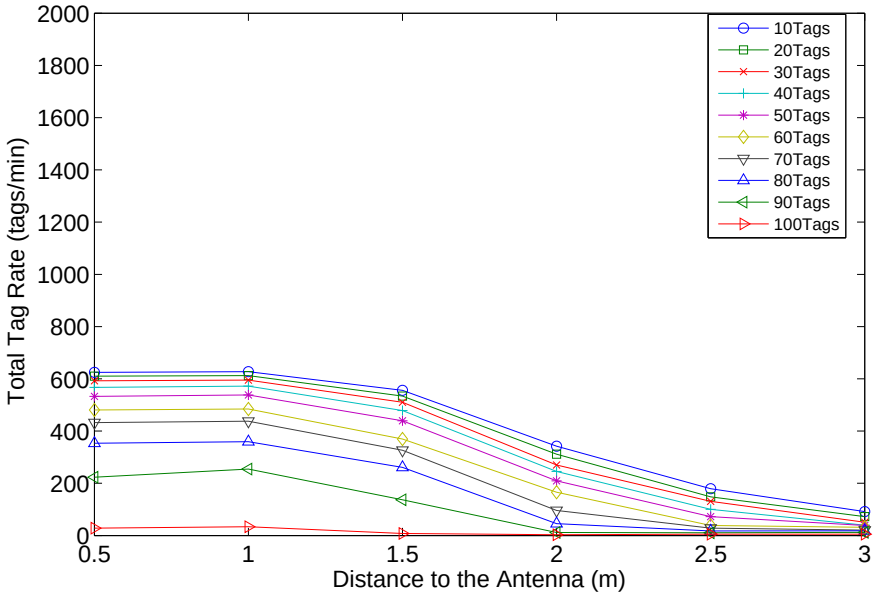

Figure 4.15: Total tag rate of C1G2 for varying distances to the antenna and number of tags (simulation).

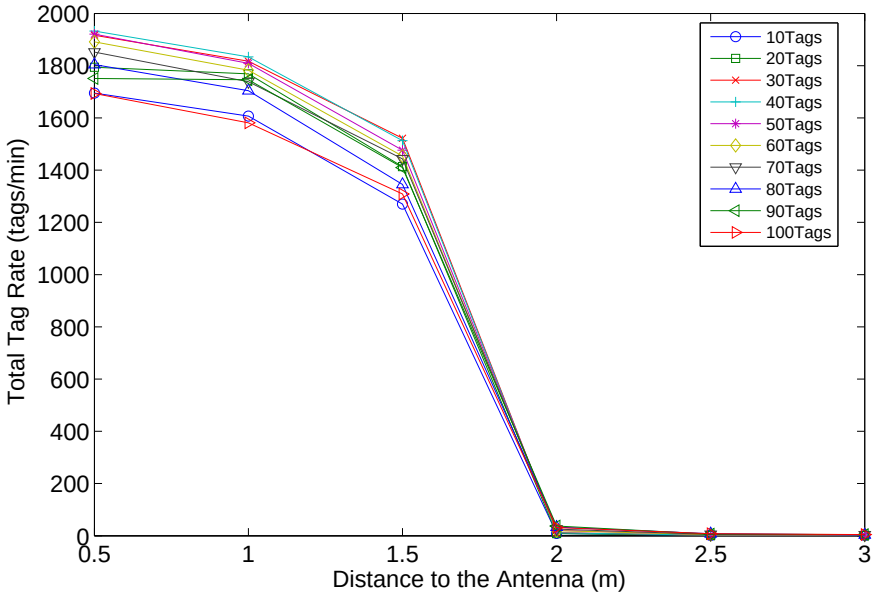

Figure 4.16: Total tag rate of TDMA for varying distances to the antenna and number of tags (simulation).

clear that the C1G2 protocol fails to provide fair access to all tags. On the other hand, TDMA performs well when the distance between the tags and the reader is short. The fairness performance does not change much with an increase in the number of tags. However, when the distance increases beyond 1.5 m, the fairness performance drops to a very low level. The simulations show that the power issue affecting the TDMA performance, not only lowers the performance in terms of tag rate, it also greatly affects the fairness.

Next, we evaluate the time between when a new tag enters the network and when the reader detects this new tag. We begin the simulations with a fixed number of tags located at the same distance from the reader. After the network stabilizes, we add a new tag into the network at the same location and measure the time between when the tag enters and when the reader detects the tag information. This is a crucial metric for networks with mobile tags or with varying channel conditions. The number of tags in the network before the introduction of the new

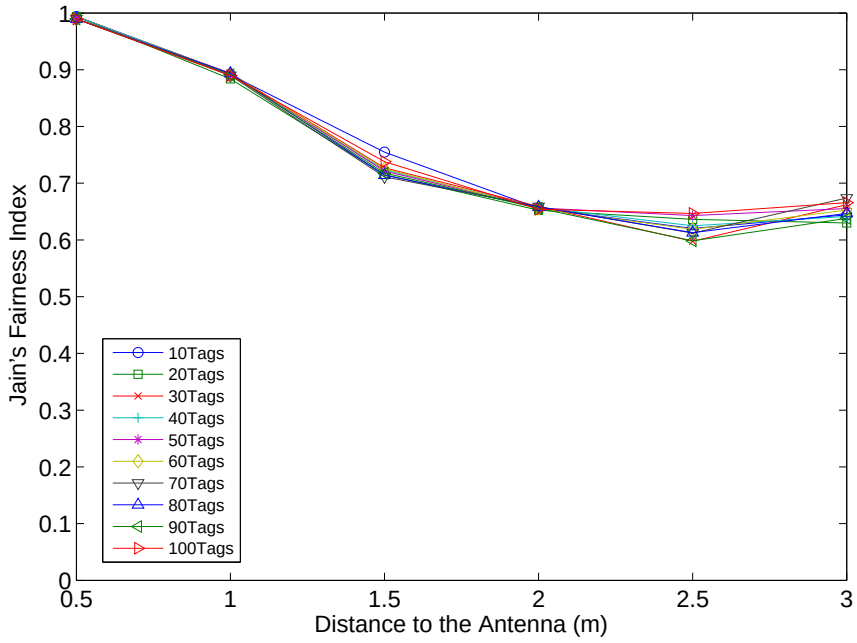

Figure 4.17: Fairness of Token-MAC for varying distances to the antenna and number of tags (simulation).

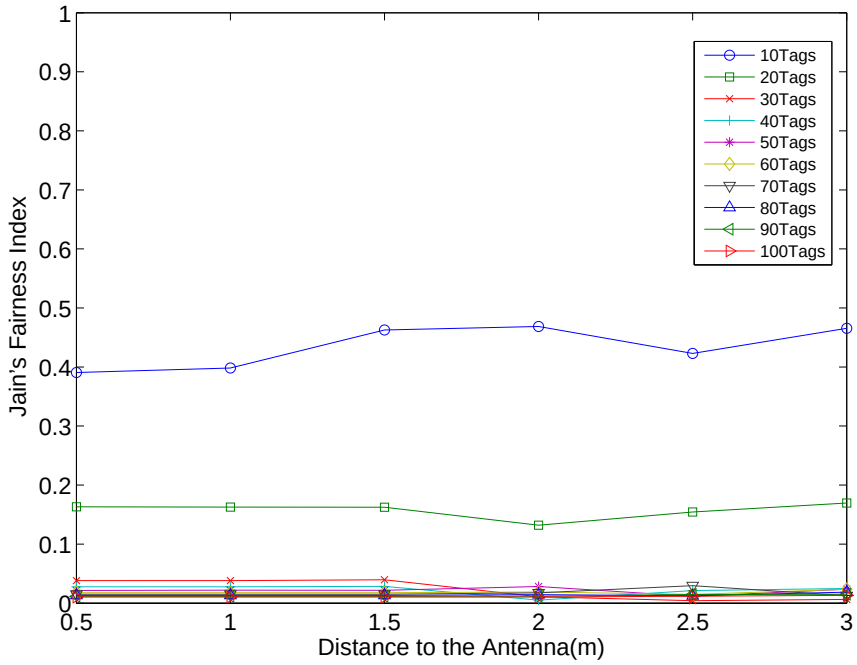

Figure 4.18: Fairness of C1G2 for varying distances to the antenna and number of tags (simulation).

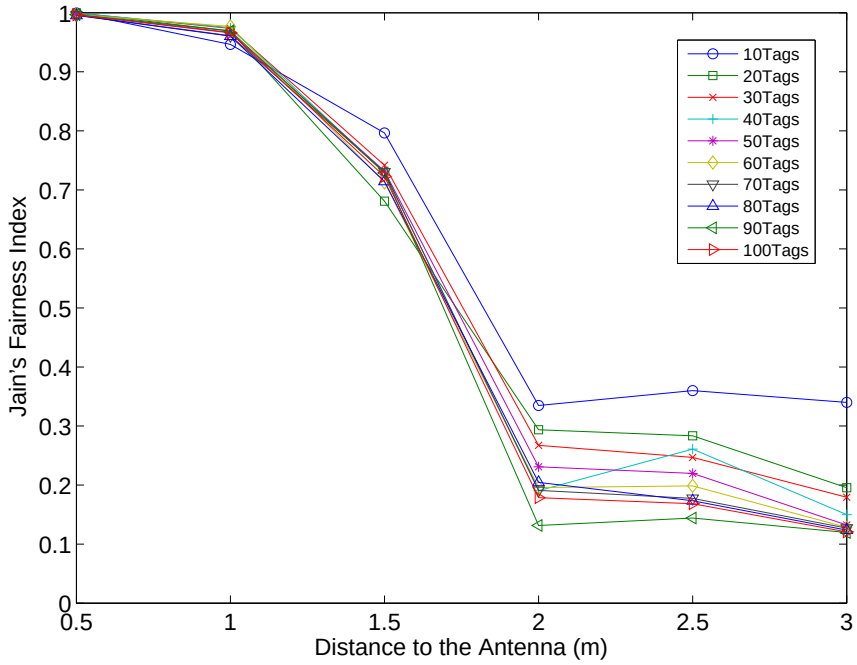

Figure 4.19: Fairness of TDMA for varying distances to the antenna and number of tags (simulation).

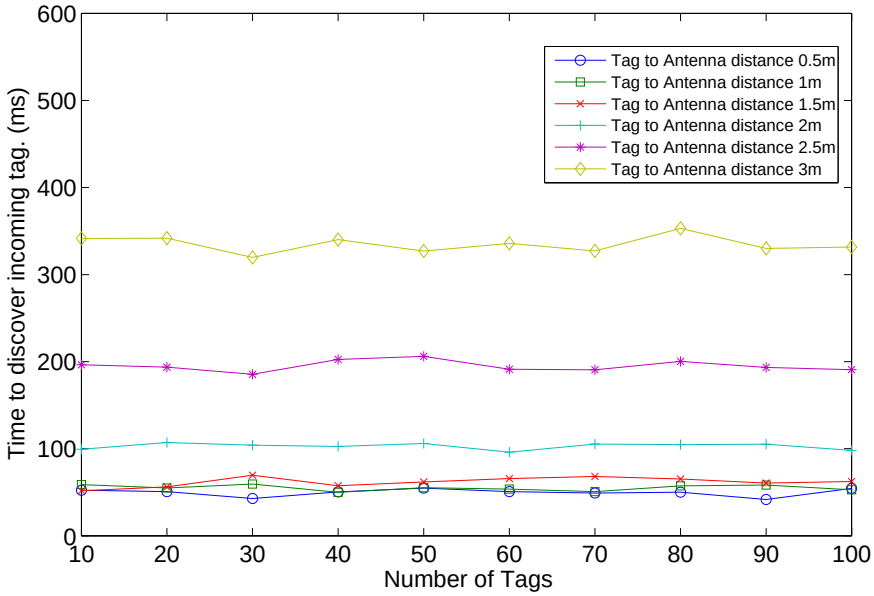

Figure 4.20: Time delay to detect a new tag for varying distances of Token-MAC to the antenna and different number of existing tags (simulation).

tag is varied from 10 tags to 100 tags, and all of the tags are deployed the same distance to the reader, which is varied from 0.5 m to 3 m. The new tag is placed at the same distance as the other tags.

Fig. 4.20,Fig. 4.21 and Fig. 4.22 show the time delay between when a tag enters the network and when it is read by the reader for the three protocols. The y-axis of the Token-MAC protocol and the TDMA plot are set between 0 ms to 600 ms in order to get a clear view of the delay result. The y-axis of the C1G2 is set between 0 s to 60 s according to the simulation results. We see that for the Token-MAC protocol, the delay remains constant when the number of tags increases. This result is due to the random tokens allocated to new nodes, allowing them to access the channel and inform the reader of their presence. This shows the scalability of the Token-MAC, which is an important property for RFID

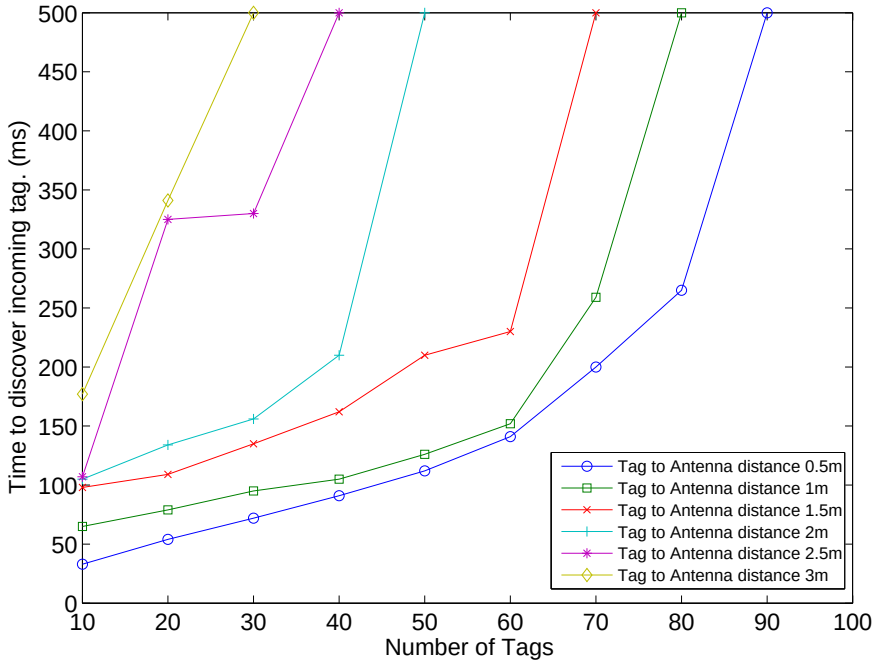

Figure 4.21: Time delay to detect a new tag for varying distances of C1G2 to the antenna and different number of existing tags (simulation).

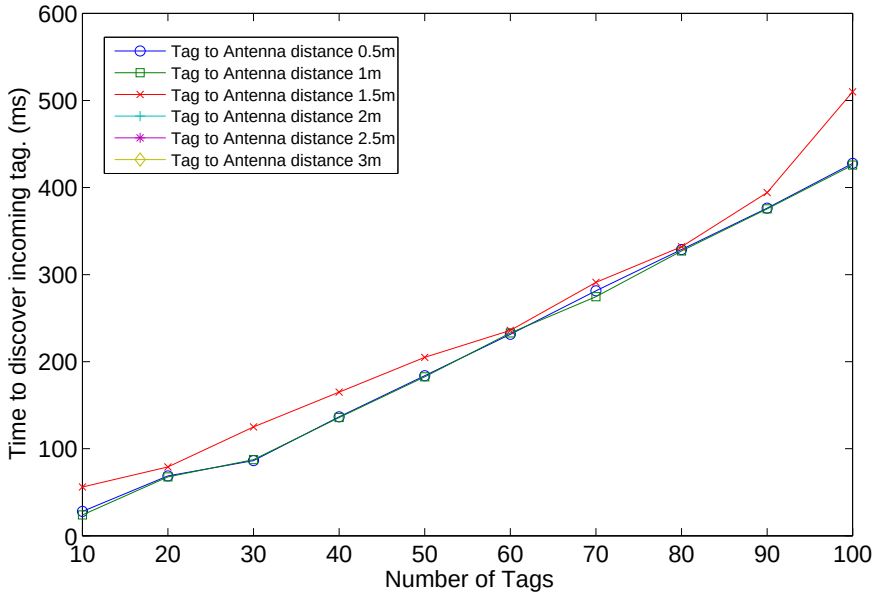

Figure 4.22: Time delay to detect a new tag for varying distances of TDMA to the antenna and different number of existing tags (simulation).

applications. Also, we see that the delay increases as the distance between the tags and the reader increases, since the probability of the reader receiving random packets decreases with an increase in the distance between the reader and the tags.

The results also show that C1G2 needs a very long time to detect an incoming tag when the tag population increases. Also, we notice that even when the distance to the reader is short, an increasing number of tags degrades the delay performance rapidly. When the number of tags increases to 100, the new tag is virtually undetectable to the reader no matter where it is located.

For the TDMA protocol, we can see that when the distance between the tags and the antenna is small, the delay increases linearly with an increase in the number of tags. This is reasonable because the length of an inventory round increases as the number of tags increases. Hence, when the tag population increases, the

new entering tag needs to wait for the next available contention period to be assigned a slot. No results can be shown for the tags that are located at distances greater than 1.5 m, since no reads for the new tag are observed in these cases. This is an expected result, since at these distances, the reader cannot even detect the existing tags.

4.5.2 Tags at Different Distances to the Reader

To evaluate the performance of the three protocols in a more realistic scenario, in the second set of simulations, we place a number of tags at random locations between 0 m to x m, where we vary x, the maximum distance to the reader. This scenario is more realistic in commercial applications, such as in inventory monitoring in a storeroom or in containers. In this set of simulations, the number of tags is increased from 10 to 100 to evaluate the ability of the protocols to scale. Once again, we evaluate the total tag rate, fairness, and the delay to detect a new tag.

Fig. 4.23, Fig. 4.24 and Fig. 4.25 show the total tag rates achieved by the three protocols investigated for the second set of simulations. As we can see in the figure, for this scenario, TDMA has the best performance when the maximum distance of the tags from the reader is less than 1.5 m, but its performance drops sharply after 1.5 m. The Token-MAC protocol performance is stable for all distances, and is much higher compared to that of C1G2. Moreover, Token-MAC achieves much higher tag rates than TDMA for distances larger than 1.5 m. Also, we can see that the tag rate of C1G2 drops very quickly with an increase in the number of tags. On the other hand, TDMA and Token-MAC scale well, changing only slightly with an increase in the number of tags.

Comparing the tag rate results of this set of simulations (Fig. 4.23, Fig. 4.24 and Fig. 4.25) with the previous set (Fig. 4.14,Fig. 4.15 and Fig. 4.16), we

can draw different conclusions for each protocol. For Token-MAC, the tag rate performance decreases about 30% when the tags are located randomly. This is due to the management of the inventory round by the reader. According to the reader operation described in Section 4.2, the reader increases the access probability of those tags that are less likely to be accessed, i.e., those located far from the reader. Thus, the reader decreases the inventory round of those tags that are located close to the reader. This strategy will lead to a more fair network with some loss in tag rate.

For C1G2, we see that the tag rate is higher in the random location scenario. However, we found out that the increase in tag rate shown in Fig. 4.23, Fig. 4.24 and Fig. 4.25 is due to some tags capturing the channel. Those tags that are located close to the reader can easily capture the channel. Thus, these tags can reply with a high tag rate, while the other tags have only a small chance to send their tag information back to the reader.

The performance of TDMA does not change much when the tags are located between 0 to 1.5 m. This is easy to understand, as at these distances, the power supply to all tags is stable. When the distance between the tags and the reader increases, the tag rate decreases. However, compared to previous set, the tag rate results in Fig. 4.23, Fig. 4.24 and Fig. 4.25 do not drop to 0. This is because some of the tags are still located between 0 to 1.5 m, and these tags are still assigned a slot and can send their data back to the reader.

Fig. 4.26, Fig. 4.27 and Fig. 4.28 show the fairness of the three protocols for the random location scenario. We can see that Token-MAC can lead to a high fairness performance in this experiment for all distances evaluated. Similarly, the TDMA protocol results in a good fairness performance when the tags are close to

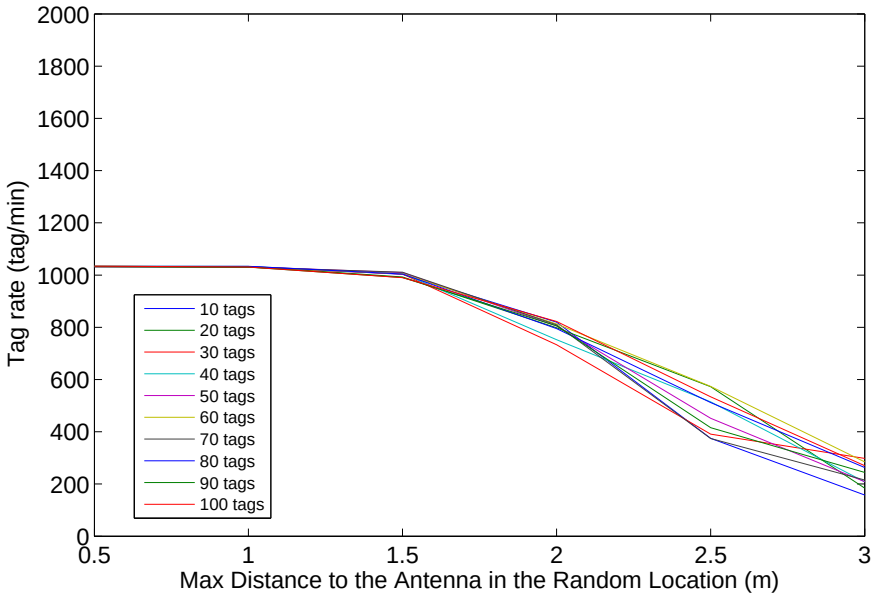

Figure 4.23: Total tag rate of Token-MAC for varying number of tags with tags at random locations (simulation).

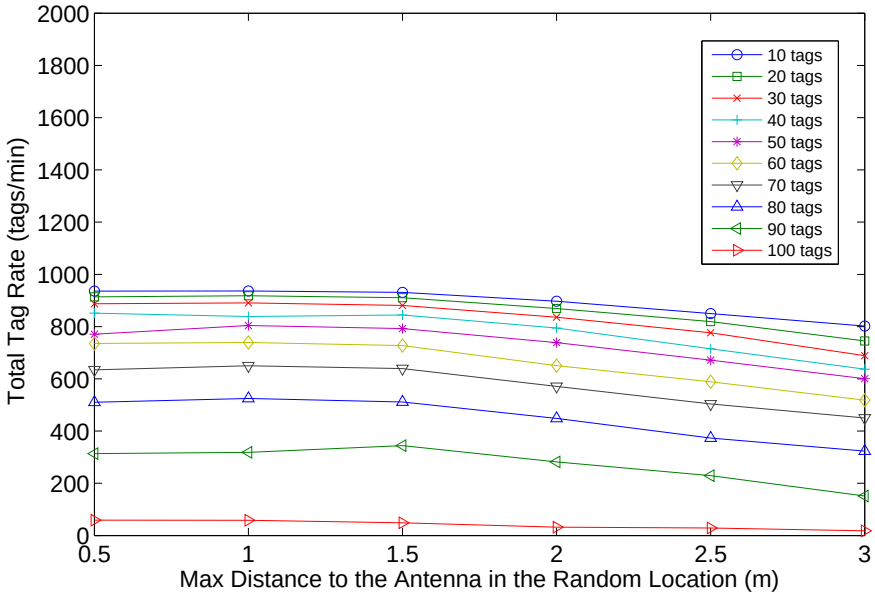

Figure 4.24: Total tag rate of C1G2 for varying number of tags with tags at random locations (simulation).

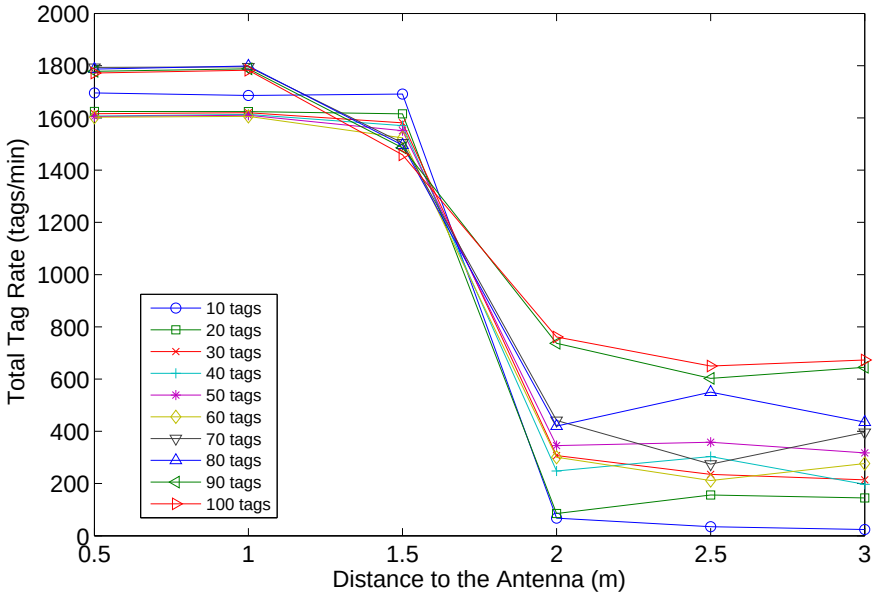

Figure 4.25: Total tag rate of C1G2 for varying number of tags with tags at random locations (simulation).

the reader due to the individual assigned slots. However, the fairness degrades for distances higher than 1.5 m. The reason is again that the time required for a tag to wait until its slot time requires more energy than the tag has for such distances. The TDMA protocol can maintain a fair performance even as the number of tags increases. On the other hand, C1G2 has very poor fairness results for all distances evaluated. The increase in the tag population hurts fairness even more, as the probability of collisions increases with an increase in the number of tags.

Comparing the fairness performance of the protocols when the nodes are at the same distance (Fig. 4.17, Fig. 4.18 and Fig. 4.19) and when they are at random distances (Fig. 4.26, Fig. 4.27 and Fig. 4.28), we see that the fairness of Token-MAC in the ideal scenario is slightly better than that in the more realistic scenario. The reason is that the tags that are close to the reader can more easily send packets to the reader compared with those located far away from the reader. Although access control by the reader can help to increase the fairness, it cannot ensure

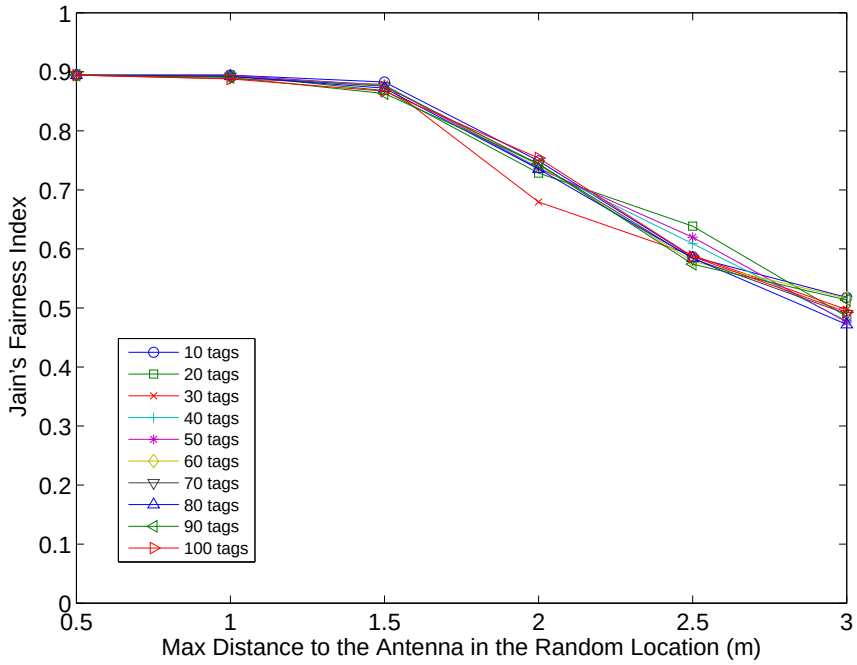

Figure 4.26: Fairness of Token-MAC for varying number of tags with tags at random locations (simulation).

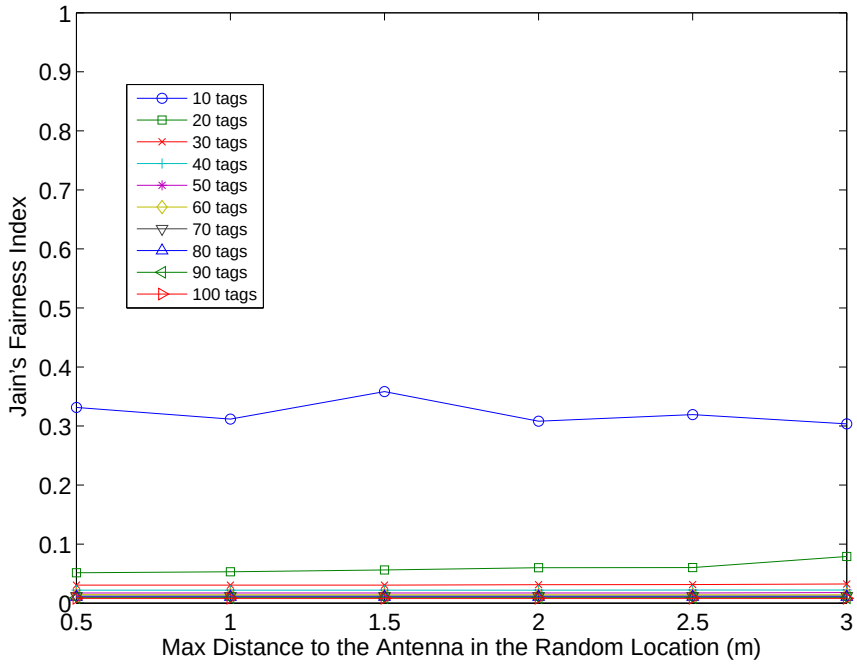

Figure 4.27: Fairness of C1G2 for varying number of tags with tags at random locations (simulation).

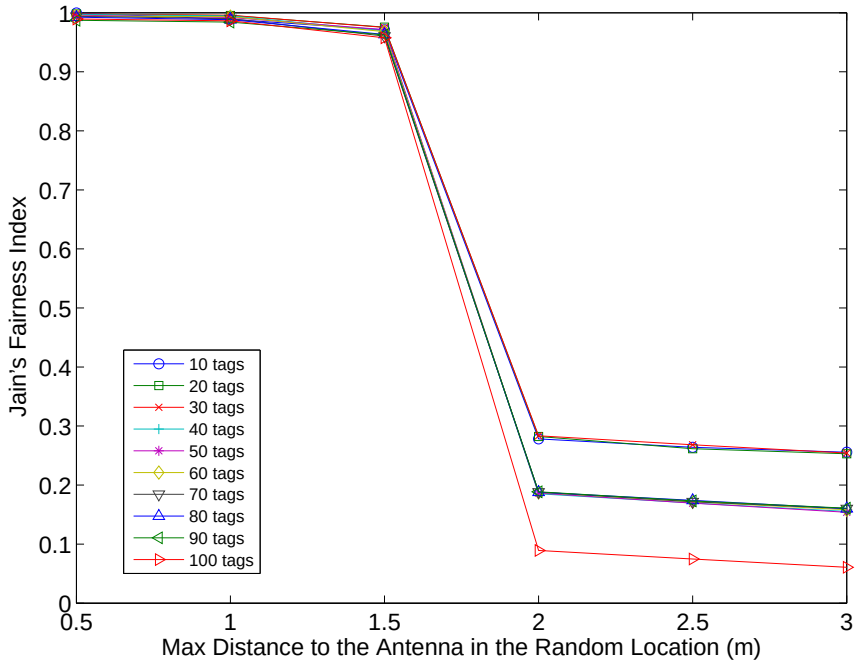

Figure 4.28: Fairness of C1G2 for varying number of tags with tags at random locations (simulation).

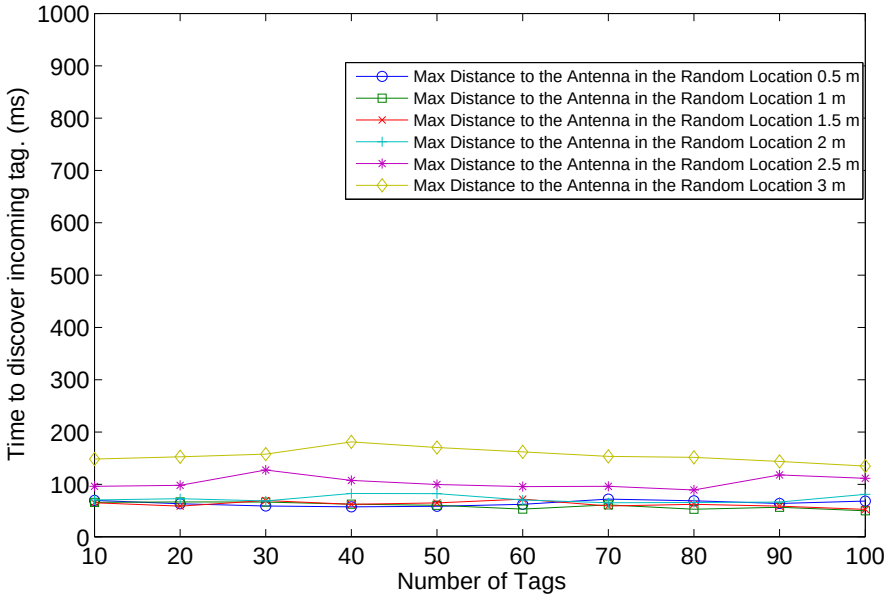

Figure 4.29: Delay to detect a new tag of Token-MAC for varying number of tags with tags at random locations (simulation).

perfect fairness. The fairness performance of C1G2 in the more realistic scenario is also worse than in the ideal scenario due to those tags that are located close to the reader capturing the channel. The fairness performance of TDMA is similar in both scenarios, because TDMA is a slot based protocol.

Fig. 4.29, Fig. 4.30 and Fig. 4.31 show the delay results for detecting entering tags for the three protocols for the second set of simulations. The y-axis of the Token-MAC protocol and the TDMA protocol are set between 0 ms to 600 ms in order to get a clear view of the delay results. The y-axis of C2G2 is set between 0 s to 60 s according to the simulation results. For Token-MAC, we see that the delay to detect an entering tag does not change with an increase in the number of tags. When the maximum possible distance between a tag and the reader increases, the average delay increases due to the probability of receiving a random packet

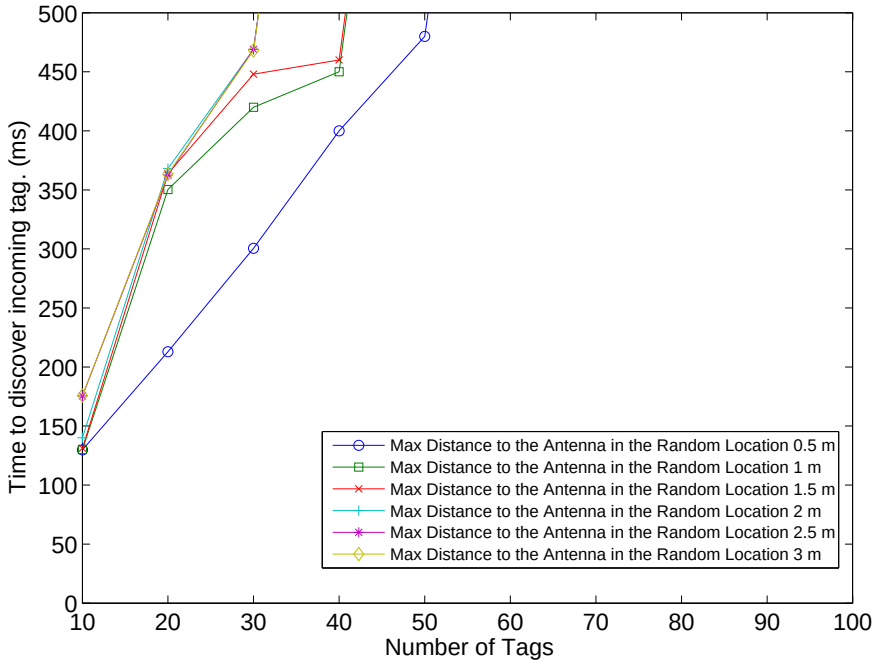

Figure 4.30: Delay to detect a new tag of C1G2 for varying number of tags with tags at random locations (simulation).

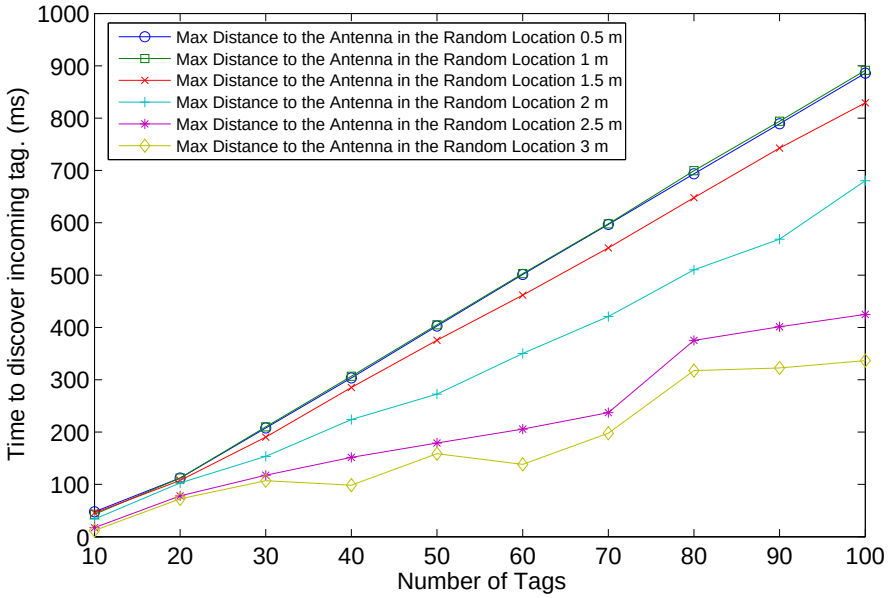

Figure 4.31: Delay to detect a new tag of C1G2 for varying number of tags with tags at random locations (simulation).

decreasing for power harvesting reasons as the random packet is the first packet to be send. We can see that Token-MAC is the protocol that can detect entering tags most quickly compared with the other protocols for all distances and for almost all number of tags evaluated. Moreover, it is the only protocol that is scalable, i.e., only Token-MAC's performance is stable with an increasing number of tags.

The C1G2 protocol performs poorly when the new tag enters, requiring a long time to detect an incoming tag. When the number of tags increases, it is even harder for the C1G2 protocol to detect the entering tag, and when the number of tags is more than 50, the entering tag is undetectable. For TDMA, the delay result is similar to the result in the ideal scenario. We see that the delay to detect the entering tag increases with an increase in the number of tags. Also, we see that the performance of TDMA does not change much when the tags are located between 0 to 1.5 m. However, when the distance increases beyond 1.5 m, a smaller portion of the tags are located in the area where reader can access them using

Table 4.2: Maximum Number of Tags at Different Distances.

	C1G2	TDMA	Token-MAC
Number of Tags @ 0.5 m	75.2	643.6	672
Number of Tags @ 1 m	97.3	645	672
Number of Tags @ 3 m	84.3	0	638.8

TDMA, which decreases the length of the Inventory round. Thus, the delay to detect a new tag, when it can be detected, is decreased as the maximum distance to the reader increases.

4.5.3 Maximum Number of Tags Supported

Our final set of simulations explores the maximum number of tags that each protocol can support. In this set of simulations, we add a tag one at a time to the network until the reader cannot detect the new tag within 1 minute. Three simulation setups are evaluated where all tags are located at 0.5 m, 1 m and 3 m. We run the simulations for each setup 50 times and provide the average of these results.

Table 2 shows the results of these simulations. C1G2 is limited by the collision problem that leads to a low tag support capability. The performance at 0.5 m is lower than other two scenarios due to the capture effect. TDMA can theoretically obtain an infinite capacity at short distance. While it is true that TDMA leads to a very high number of tags supported at 0.5 m and 1 m, the number shown in the table is not a limitation of the protocol, but a function of the maximum Inventory round within 1 minute. However, as the reader cannot access those tags located at 3 m for the TDMA protocol, the maximum number of tags at 3 m for TDMA is 0. Token-MAC can also support a near-infinite capacity at all distances, and the measured maximum number of tags in Token-MAC is also limited by the

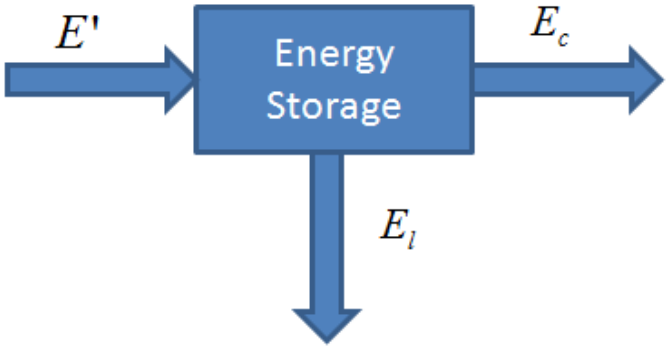

Figure 4.32: General energy harvesting system.

Inventory round. It is clear that Token-MAC provides good capacity. TDMA achieves good capacity for short range, while C1G2 performs poorly with regard to this metric.

The results from these three sets of simulations show that Token-MAC can provide higher tag rates and better fairness than the C1G2 protocol. The TDMA-based protocol achieves better results than Token-MAC for small distances, but Token-MAC outperforms the TDMA protocol in tag rate and fairness for all distances greater than 1.5 m. As for delay for detecting entering tags, C1G2 performs poorly due to the collision issue. TDMA performs well when the number of tags is small, but the delay increases linearly with an increase in the number of tags. Token-MAC performs the best of the three protocols in terms of the delay to detect new tags.

4.6 Discussion

Both the experimental and simulation results show that TDMA performs very well when the distances between the tags and the reader are short. If the distances increase, the performance using TDMA drops dramatically. Here, we provide an explanation for this behavior.

In order to understand the poor performance of TDMA at large distances, we need to understand the energy harvesting system within each tag [64]. A general energy harvesting system can be described as shown in Fig. 4.32, where E' is the energy received from the energy harvester, E_c is the energy consumed to operate the tag, and E_l is the energy leakage from the energy storage device. Generally, the energy can be stored in a capacitor or a rechargeable battery with maximum capacity E_{max}. Also, the tag will stop operating when the energy stored in the energy storage device, E_{stored}, is less than a threshold, $E_{threshold\_off}$. At that time, the consumed energy, E_c, goes to 0 and only leakage E_l will reduce the energy stored in the energy storage device. If the stored energy is greater than or equal to a turn-on threshold, $E_{threshold\_on}$, the tag will begin operation.

In an RFID system, the parameters E_c and E_l are determined by the RFID chip on the tag and thus these two values are fixed. The parameters $E_{threshold\_on}$ and $E_{threshold\_off}$ are based on the energy harvesting system and the power regulator, and thus, are also determined. However, the value of E' changes based on the transmitted power from the reader and the distance of the tag to the reader. For a fixed transmitter power, when the tag is located close to the reader, E' will be high, but as the distance between the tag and the reader increases, E' drops rapidly. Thus, the location of the tag with respect to the reader will change the system's working state.

According to Fig. 4.10, we see that there is a big drop in the capacitor voltage around 1.3 m. When the tag is located close to the reader, E' will be high enough to surpass the E_c+E_l+$E_{threashold\_on}$, so there is always sufficient energy to keep the tag in operation. However, when the tag is deployed far from the reader (e.g., greater than 1.3 m, as shown in Fig. 4.10), E' is greatly reduced, and E' will always be lower than the E_c+E_l+$E_{threashold\_off}$. Thus, there will not be sufficient energy to continuously run the tag. In this case, for the TDMA protocol, the tags will lose synchronization at some point during the Inventory round when

they cease operating due to lack of energy. As shown by the protocol operation in Fig. 4.4, it is possible for one tag to wake up at the contention period and obtain an assigned slot. However, if this tag cannot remain alive until its assigned slot, it cannot respond to the reader. This severely impacts the performance of the TDMA protocol in terms of both tag rate and fairness. It is possible that an optimized TDMA protocol may lead to better performance when the tags are in the range of 0 m to 1 m, but regardless of the specific design of the TDMA protocol, the tags will often lose synchronization for distances greater than 1.3 m, which causes problems for the TDMA protocol in RFID systems. This issue with synchronization is unavoidable due to the hardware limitations of the tags and the energy harvesting system.

For Token-MAC, the tag may not get a continuous power supply according to the previous analysis when the tag is located at distances greater than 1.3 m. However, there is no synchronization needed for Token-MAC. Even if the tag is temporarily inactive before its own query round, it is possible for the tag to reply to the reader in its own round. If the tag can accumulate enough energy before its query round, it can utilize this energy to send a packet back to the reader, which is possible as the tag does not consume or leak a lot of energy in other tags' query rounds. Thus, even if tags are located at distances greater than 1.3 m, Token-MAC does not suffer from the loss of synchronization that causes TDMA to have a reduction in tag rate and fairness after 1.3 m.

4.7 Conclusions

In this chapter, we propose and evaluate Token-MAC, a MAC protocol to improve the fairness and throughput performance of RFID systems compared with existing protocols. We compare the performance of Token-MAC with the standard C1G2 protocol as well as a TDMA protocol using both small-scale implementation

experiments and larger-scale simulations.

We first performed physical experiments using a testbed that consisted of programmable Intel WISP passive RFID tags. Then, we developed simulation models both for energy harvesting and the communication channel. These simulation models are validated with the experimental results and are used to evaluate the three methods investigated with larger network sizes.

The results of the experiments and the simulations show that Token-MAC can provide higher tag rates, better fairness, and much shorter delay to detect an entering tag compared with C1G2. Although the TDMA protocol provides better performance than Token-MAC for small distances, Token-MAC outperforms the TDMA protocol in terms of both fairness and tag rate for all distances greater than 1 m. In terms of delay to detect an entering tag, which is a crucial metric for mobile applications, Token-MAC performs better than TDMA for long distances or for large numbers of tags. We also evaluate the maximum number of tags each protocol can support at different tag-to-reader distances. In terms of this metric, the TDMA protocol performs slightly worse than Token-MAC, up to 1m, after which the TDMA protocol cannot read any tags. On the other hand, Token-MAC is shown to read the highest number of tags for all distances.

5 Range Extension for Passive Radio Wake-up Systems

5.1 Introduction

Wireless Sensor Networks (WSNs) are composed of a number of sensor nodes that can sense the physical environment (e.g., temperature, air quality, sound, pressure), process the sensed data, and send the processed data to other nodes or to the data sink(s) in the network. There are many potential applications for WSNs, including smart grid monitoring, emergency response, military surveillance, home security, and environment monitoring. As typically the sensor nodes are powered by batteries, WSNs are highly energy constrained. Additionally, in some cases the batteries attached to the sensor nodes are difficult or even impossible to replace. Thus, minimizing the energy dissipation of a sensor node is a key problem in WSN research.

Duty cycling, where the sensor node is periodically set to the sleep mode, is one of the most commonly used methods to reduce the energy dissipation of a sensor node. As communication between two nodes can only be achieved when both the transmitter and the receiver nodes are awake, the duty cycles of all the nodes must either be time synchronized so the nodes all wake up at the same time, or idle listening is required until both the transmitter and receiver are awake

simultaneously. However, both time synchronization and idle listening increase the complexity of the MAC protocol and waste additional energy. Furthermore, in order to reduce the energy dissipation of the nodes, the sensor nodes tend to be kept in the sleep mode for the majority of the time, which increases the delay for packet delivery. In the case of a mobile sink, the sensor node may be in the sleep mode when the sink comes by to collect data, and thus the sink may miss collecting that node's data. Thus, duty cycling may not be suitable for some delay sensitive applications.

Using a wake-up radio, a low power, secondary radio that is only used to wake up the primary radio for communication, is another solution for prolonging the lifetime of a WSN. Using a wake-up radio, the sensor node is only woken up when communication is necessary. The cost for this approach is the additional hardware needed on the devices, including a wake-up radio receiver (WuRx) and a wake-up radio transmitter (WuTx). Each sensor node with a WuRx has two working modes: sleeping mode and active mode. Most of the time, the sensors are kept in an ultra-low power sleep mode, where they cannot communicate with other nodes nor perform any computation. The sensor node may wake up periodically to sense the environment and go back to sleep after the data is collected and stored in local memory. Only when a surrounding node's WuTx sends a trigger signal to start data communication and the WuRx receives this signal, will the WuRx trigger the sensor node to enter the active mode, at which point it can communicate with other nodes in the network.

Two classes of wake-up radio devices have been developed: active wake-up radios and passive wake-up radios. An active wake-up radio receiver requires a power supply, which commonly is the battery of the sensor node. Most active wake-up receivers provide good performance in terms of wake-up delay and wake-up distance. On the other hand, passive wake-up radio devices are powered by energy harvested from the WuTx signals (and hence do not require any energy

from the sensor node's battery), which reduces the energy consumption of the sensor node but results in a shorter wake-up range than the active wake-up approach. As passive WuRxs utilize the energy harvested from the RF signals sent by the WuTx, this approach extends the lifetime of the sensor network compared to using active wake-up radios and using duty cycling.

However, there are several challenges for passive wake-up radio sensor networks. First, due to the limitations and efficiency losses in the energy harvesting process, passive wake-up radio sensor nodes operate over a shorter communication range and present longer wake-up delay than active wake-up radios. Additionally, the performance of a passive WuRx may be affected by environmental conditions, such as heavy rain, which may decrease the energy received by the WuRx, possibly making some sensor nodes inaccessible. Furthermore, in order to achieve a reasonable wake-up distance, the WuTx needs to be designed to have a high energy transmission efficiency. As a result, it is difficult to build a multi-hop WSN where each node is equipped with both a WuTx and a passive WuRx.

In our previous work, we developed one of the first implementations of a passive wake-up radio sensor node. This node, called a WISP-Mote [99], combined an Intel passive RFID device (a WISP) with a Tmote Sky mote. We determined the performance of the WISP-Mote through field experiments, and we described the advantages of using WISP-Motes compared with duty cycling through simulations based on the field test measurements. The WISP-Mote is able to provide both broadcast-based wake-up (waking up all nodes in range of the WuTx) and ID-based wake-up (waking up a particular node by sending the ID of that node in the wake-up signal).

Clearly, one way to extend the range of a passive wake-up radio sensor node is to provide improved energy harvesting efficiency. Following this reasoning, we combined a novel energy harvesting circuit we developed [68] with our WISP-Mote to create a new device that we call an EH-WISP-Mote (Enhanced-WISP-Mote).

In this chapter, we provide field experiments that show the EH-WISP-Mote can, indeed, improve the wake-up range and reduce the wake-up delay compared with the WISP-Mote. However, the EH-WISP-Mote contains extra hardware that is necessary for ID-based wake-up, to decode a particular ID in the wake-up signal, that is not required for broadcast-based wake-up.

Hence, we also describe the design of a novel wake-up radio sensor node, which we call REACH-Mote (Range EnhAnCing energy Harvester-Mote), composed of the energy harvesting circuit [68] and an ultra low power wake-up pulse generator that uses a Maxim Integrated chip [69] as the WuRx, and a Tmote Sky mote as the wireless sensor node. We implemented the REACH-Mote and characterized its performance in terms of wake-up delay over a range of distances. The field test results show that REACH-Mote can achieve a feasible wake-up range of about $11.2m$, which is almost double that of any known passive wake-up radio.

In order to further improve the wake-up range performance, we enhance the design of the REACH-Mote to create REACH^2-Mote, with an improved wake-up range achieved by applying an improved energy harvesting module and a supply voltage regulator. We perform a thorough evaluation of the performance of REACH^2-Mote, through both field tests of the hardware and through simulations. We compare the performance of REACH^2-Mote with that of REACH-Mote as well as with another passive wake-up radio called the WISP-Mote [70]. The field test results show that the REACH^2-Mote can achieve an extended wake-up range of $13.4m$, which represents a 19% increase compared to the wake-up range of REACH-Mote and a 220% increase compared to the wake-up range of WISP-Mote. Based on the physical characterization of the REACH^2-Mote and the WISP-Mote, we developed a simulation model of the performance of the REACH^2-Mote and the WISP-Mote. Additionally, we model a conventional duty cycling approach and an active wake-up radio approach [71]. Using these models, we perform simulations under a number of different network scenarios with a mobile sink (e.g., a

data mule [72]) that traverses the network to collect data from the sensor nodes. The simulation results show that REACH^2-Mote can significantly extend the network lifetime, while achieving a high packet delivery rate and low latency for the scenarios we tested.

The remainder of this chapter is organized as follows. The description of the hardware design of the EH-WISP-Mote, 1^{st} generation REACH-Mote is provided in Section 5.2, and the description of the hardware design of the 2^{nd} generation REACH^2-Mote is provided in Section 5.3. Section 5.4 presents results from field experiments using three passive wake-up radio designs (WISP-Mote, REACH-Mote and REACH^2-Mote). Simulation results under different network scenarios using REACH^2-Mote, WISP-Mote, an active wake-up approach and a duty-cycling approach are provided in Section 5.5, and conclusions are drawn in Section 5.6.

5.2 REACH-Mote

A passive wake-up radio receiver (WuRx) does not use any energy from the sensor node's battery, instead, it utilizes the energy harvested from the signal sent by the wake-up radio transmitter (WuTx). Thus, in order to achieve a long range passive wake-up, the WuRx must include a high efficiency energy harvester. Also, the wake-up circuit that triggers the MCU of the sensor node should operate using as little energy as possible to further extend the wake-up range. Thus, an efficient passive WuRx should be composed of a high efficiency energy harvester, a low power wake-up trigger generator, and a wireless sensor node. Using these components, we created a node called the REACH-Mote, as shown in Fig. 5.1 [67]. The REACH-Mote operates as follows:

- By default, the REACH-Mote is in the sleep mode, i.e., the MCU on the Tmote Sky, which is an MSP430F1611, is put to LPM3 sleep mode [90] and the radio on the Tmote Sky is turned off.

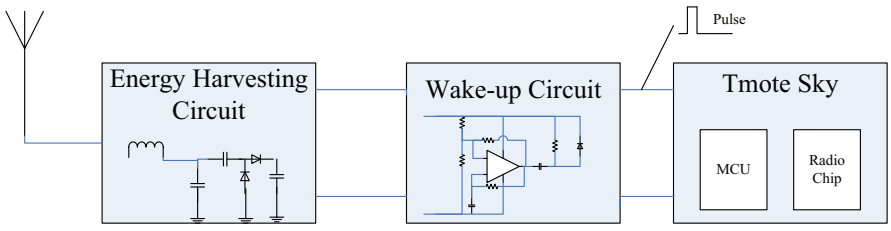

Figure 5.1: REACH-Mote main system components.

- When a wake-up signal is sent by the WuTx of a nearby mote or base station, the energy harvesting circuit receives the energy and outputs a DC voltage.
- The wake-up circuit generates a pulse once the DC voltage is higher than $1.5V$, and this will trigger the sensor mote.
- The trigger forces the MCU on the sensor mote to be woken up, and then the MCU turns on the radio, i.e., the CC2420 [91] on the Tmote Sky.
- After waking up, if the mote has data to send, data transfer commences.
- If the mote does not have data to send, or after the data transmission is complete, the mote goes directly back to sleep mode (i.e., the MCU is set to LPM3 and the radio is turned off).

The flow chart of the REACH-Mote operation is shown in Fig. 5.2

5.2.1 Energy Harvesting Circuit Design

The RF energy harvesting circuit enhances the wake-up ability of the REACH-Mote, as a more efficient energy harvester increases the wake-up distance. In this section, we describe the general design of the energy harvesting circuit and interfacing principles, as well as motivate the choice of specific circuit components.

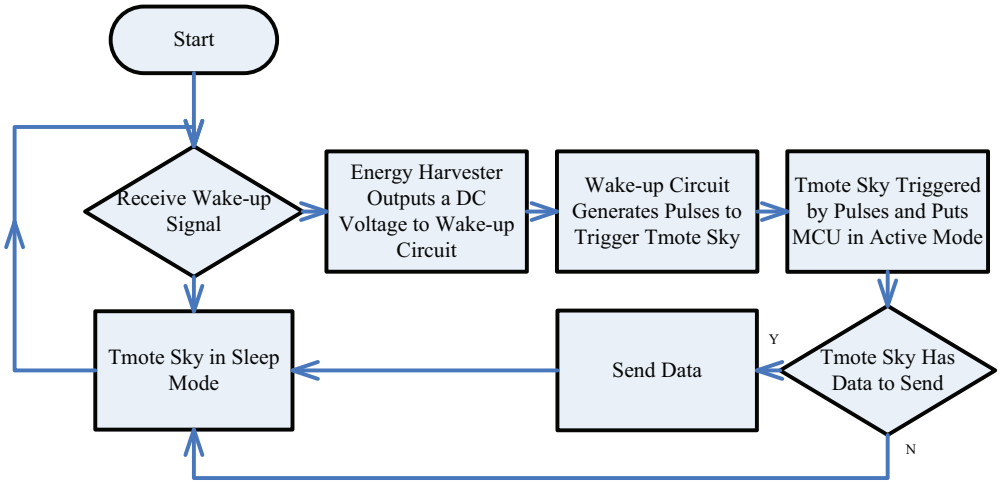

Figure 5.2: REACH-Mote operation flow chart.

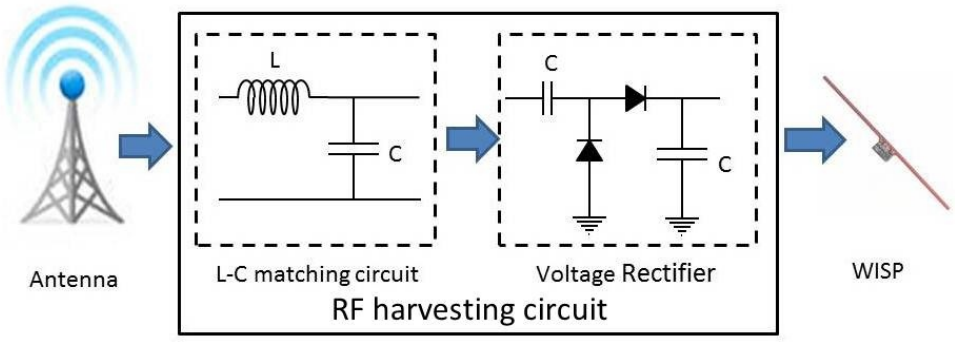

Figure 5.3: Architectural view of the REACH-Mote circuit and connections.

Selection of Circuit Components

The overall aim of our design is to maximize the energy conversion from the front-end antenna to the sensor node. To achieve this, as shown in Fig. 5.3, we carefully tune a matching circuit to balance the input impedance seen from the antenna side with the circuit load (i.e., the WuRx and Tmote Sky combination), as well as use a voltage rectifier that also functions as a multiplier. The multiplier is based on the classical Dickson's voltage multiplier circuit (Fig. 5.4), which has a number of stages connected in parallel, each stage being a series combination of a diode and a capacitor. The advantage here is that because the capacitors appear in parallel with respect to each other, the effective circuit impedance is reduced. Hence, this makes the task of matching the antenna side to the load side simpler.

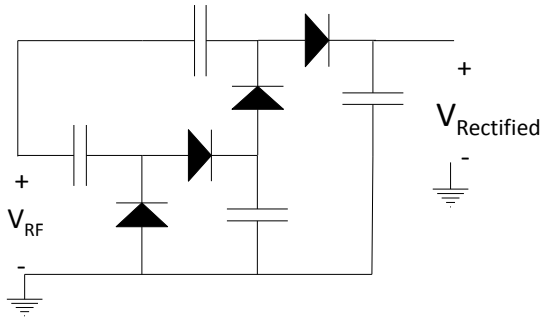

Figure 5.4: Dickson diode based multiplier.

As the peak voltage of the AC signal obtained at the antenna is generally much smaller than the diode threshold [92], diodes with the lowest possible turn-on voltage are preferable. Moreover, since the energy harvesting circuit operates in the high MHz range, diodes with a very fast switching time need to be used. Schottky diodes use a metal-semiconductor junction instead of a semiconductor-semiconductor junction. This allows the junction to operate much faster, and gives a forward voltage drop of as low as $0.15V$. We employ diodes from Avago Technologies, HSMS$-$2852 that have a turn-on voltage of $150mV$, measured at

$0.1mA$, because this specific diode is suitable for operating in the low power region, typically considered as the range of power between $-20dBm$ and $0dBm$.

The selection of the number of multiplier stages has a major influence on the output voltage of the energy harvesting circuit. While the output voltage is directly proportional to the number of stages used in the energy harvesting circuit, it also reduces progressively the current drawn by the load, which in turn impacts the overall charging time. We set the number of stages to 10 as this ensures sufficient output voltage of the circuit to drive the REACH-Mote at $915MHz$.

Optimization Framework and Fabrication

The selection of the precise values for the matching circuit is undertaken through an optimization framework, where a fixed input RF power is injected via the Agilent N5181 MXG RF signal generator, and the resulting changes in the output voltage values are measured through the Agilent 34401A multimeter, while sweeping the input frequency of the circuit. After we determine the frequency at which the output voltage value reaches a maxima, we add the capacitor and inductor components on the matching circuit as series and parallel, respectively, to change the frequency of the peak response and draw it closer to $915MHz$, which is the RF frequency of the WuTx.

Table 5.1: Components Used to Build the Energy Harvester

Component	Value	Component	Value
Series Capacitor	0.1 pF	Stage capacitor	36 pF
Parallel Capacitor	1.0 pF	Diode	HSMS-2852

In order to ensure that energy transmission from the antenna to the circuit occurs with minimal waste of energy, we use a fine granularity in the component value selection, i.e., the capacitor value is varied from $0.1pF$ to $10pF$ with $0.1pF$

Table 5.2: Parameters Used in PCB Fabrication for Dual-Stage Circuit Design

Component	Value
Laminate thickness	62 mil FR-4
Number of Layers	2-layer, one serves as a ground plane
Copper thickness	1.7 mil
Trace width	20 mil with 12 mil gap
Dielectric constant	4.6
Through-hole size	29 mil

step size. Similarly, the value of the inductor is changed from $1nH$ to $10nH$ with $1nH$ step size.

After selection of the series components, we repeat a similar procedure to find the proper component values for the parallel connections of the matching network. These iterations finally result in the peak voltage being attained at a frequency very close to $915MHz$. Fig. 5.5 shows the final fabricated PCB of our energy harvesting module. The PCB is fabricated with FR-4 epoxy glass substrate and has two layers, one of which serves as a ground plane. We select components with values and ratings of their performance parameter as close as possible to the ones obtained from the simulation. This data is summarized in Table 5.1 and Table 5.2.

5.2.2 Wake-up Circuit

Even with the high efficiency energy harvester circuit, the energy received from the radio is limited. Thus, the wake-up circuit of the WuRx must meet the following design requirements:

- The wake-up circuit must consume as low energy as possible, in order to achieve a long wake-up range.

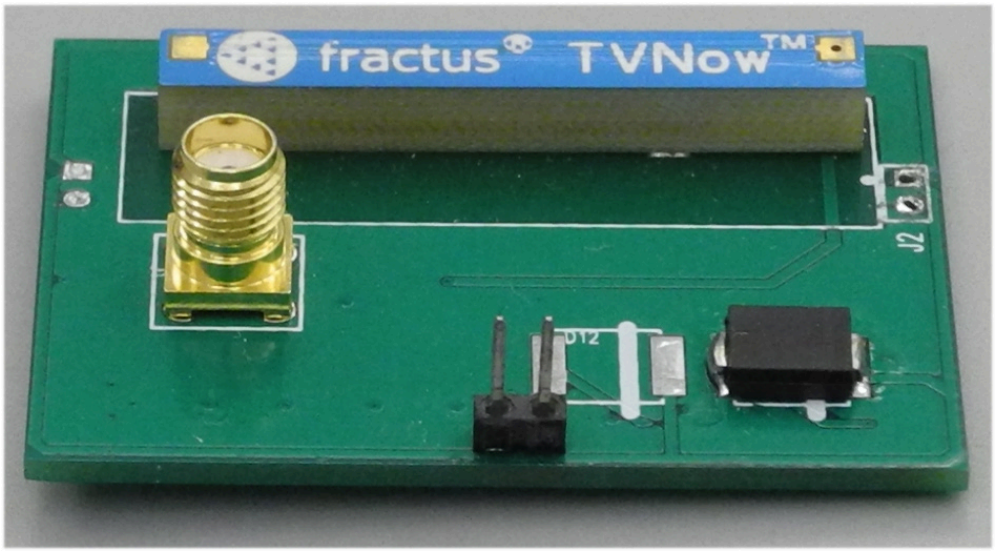

Figure 5.5: Photo of the energy harvesting circuit on the REACH-Mote.

- The wake-up circuit must generate a rising edge of 1.8V to trigger the Tmote Sky to wake up from the sleep mode.
- The trigger circuit must work on a variable support voltage, as the voltage level output by the energy harvesting circuit is not stable.

Fig. 5.6 shows the wake-up circuit of the REACH-Mote. This circuit is an adaptation of a normal relaxation oscillator with a differentiator and diode clamp on the output to generate the pulse. The pulse width can be adjusted by varying the value of the capacitor C_p and the resister R_p. The period of the pulse is determined by the value of C_1 and R_1. In this design, we applied $C_p = 1nf$, $R_p = 270k\Omega$, $C_1 = 130nF$, and $R_1 = 8.2M\Omega$ to generate a pulse of $100\mu s$ width with a period of $1s$. Using these values, the wake-up circuit requires only $1\mu A$ with a supply voltage of $1.5V$ to $5V$. Thus, with different input voltages from the energy harvester, the voltage output of the wake-up circuit can trigger the MCU on the sensor node. Note that this energy is drawn from the energy harvester

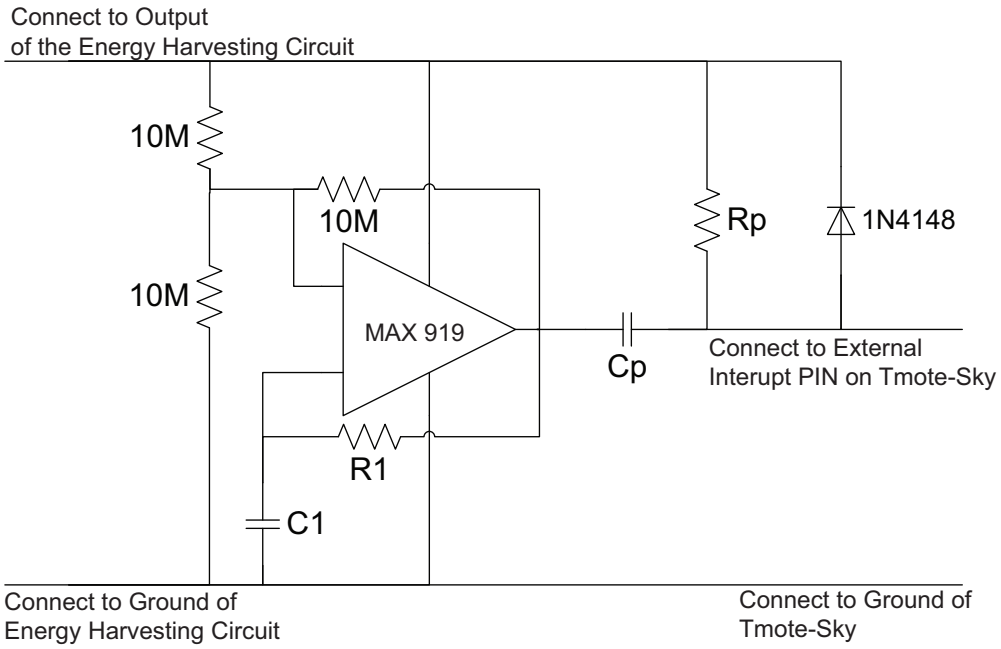

Figure 5.6: Wake-up circuit of the REACH-Mote.

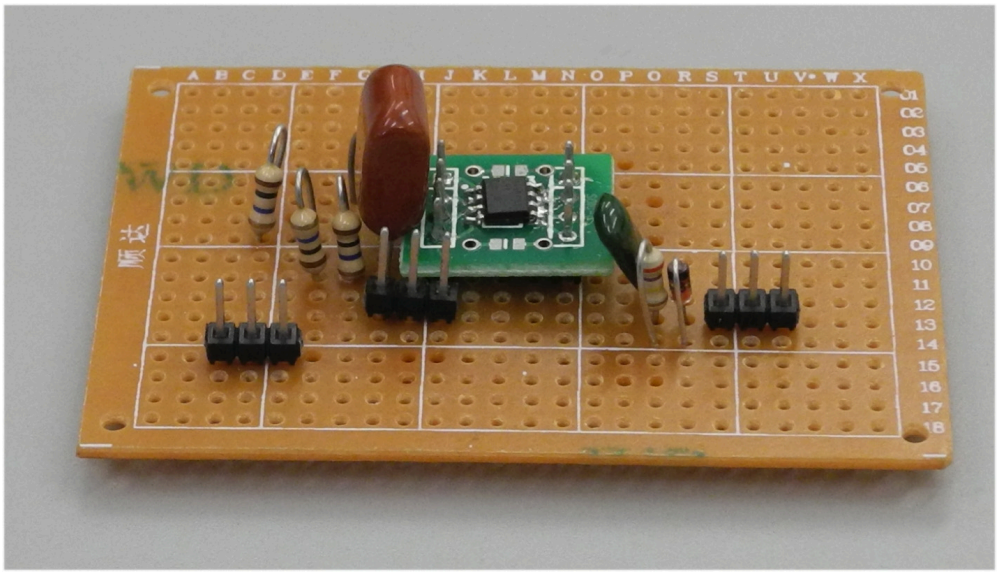

Figure 5.7: Photo of the wake-up circuit on the REACH-Mote.

circuit and not from the node's battery. Fig. 5.7 shows a photo of the wake-up circuit.

5.2.3 Design of EH-WISP-Mote

As there is an existing passive wake-up sensor node, namely WISP-Mote [70], we use our energy harvesting circuit to improve the performance of WISP-Mote. We connected the energy harvesting circuit with the WISP-Mote to build an EH-WISP-Mote (Energy Harvesting-WISP-Mote), in order to extend the wake-up range of the WISP-Mote. The output of the energy harvester is connected directly to the Vcc pin, i.e., the power supply pin, of the WISP, and the ground pin of the energy harvester is connected to the ground pin of the WISP. Thus, the energy harvesting circuit is connected in parallel to the WISP to provide additional energy harvesting capability, hence extending the wake-up range, while retaining the ability to perform ID-based wake-up.

5.2.4 Integration of the REACH-Mote

We combine the RF energy harvesting circuit and the wake-up circuit as well as the Tmote Sky to build the REACH-Mote (Range EnhAnCing energy Harvester-Mote) passive wake-up radio sensor node [67]. When a wake-up signal is sent by the WuTx, the energy harvesting circuit outputs a DC voltage. The wake-up circuit starts to generate the pulse once the DC voltage is higher than $1.5V$, and this will trigger the mote and put the mote's MCU into active mode in $5ms$ [93]. After waking up, the Tmote Sky starts the data transmission and goes back to sleep after the data transmission is complete. The energy harvesting circuit is a passive component that does not consume energy from the node's battery. The wake-up circuit is powered by the energy harvesting circuit, so the wake-up circuit also does not drain energy from the battery. Thus, all of the energy

provided by the REACH-Mote battery is used for sensing, data processing and data communication, and no energy is wasted on unnecessary communication overhead.

5.3 REACH^2-Mote

REACH^2-Mote incorporates some design enhancements to improve the wake-up range compared with that of the REACH-Mote. In particular, two approaches have been utilized to improve the efficiency of the wake-up design: improving the output of the energy harvester circuit and lowering the voltage required to trigger the MCU on the Tmote Sky to wake up.

For the first approach, in order to improve the output of the energy harvester circuit, we note that the energy harvester circuit in the REACH-Mote works as the battery supply for the wake-up circuit. Thus, increasing the number of energy harvesters and connecting them serially can increase the output voltage of the energy harvester, which can increase the voltage of the wake-up circuit and potentially extend the wake-up range.

For the second approach, reducing the voltage required to wake up the MCU, we exploited the fact that the Tmote Sky can work using different voltage values. Typically, the Tmote Sky is powered by two AA batteries that provide a 3V power supply. The MCU on the Tmote Sky, the TI MSP430 F1611, requires a 1.5V rising edge to be triggered with the 3V battery supply. However, a lower supply voltage can potentially decrease the requirement for the trigger signal. We designed a voltage regulator and a switch controlled by the Digital I/O of the Tmote Sky to change the supply voltage of the Tmote Sky between 3V and 2.5V. By applying this approach, the Tmote Sky can sleep at 2.5V voltage supply with a lower voltage trigger wake-up requirement. After the MCU of the Tmote Sky is woken up, the Tmote Sky then switches the supply voltage to 3V to obtain the

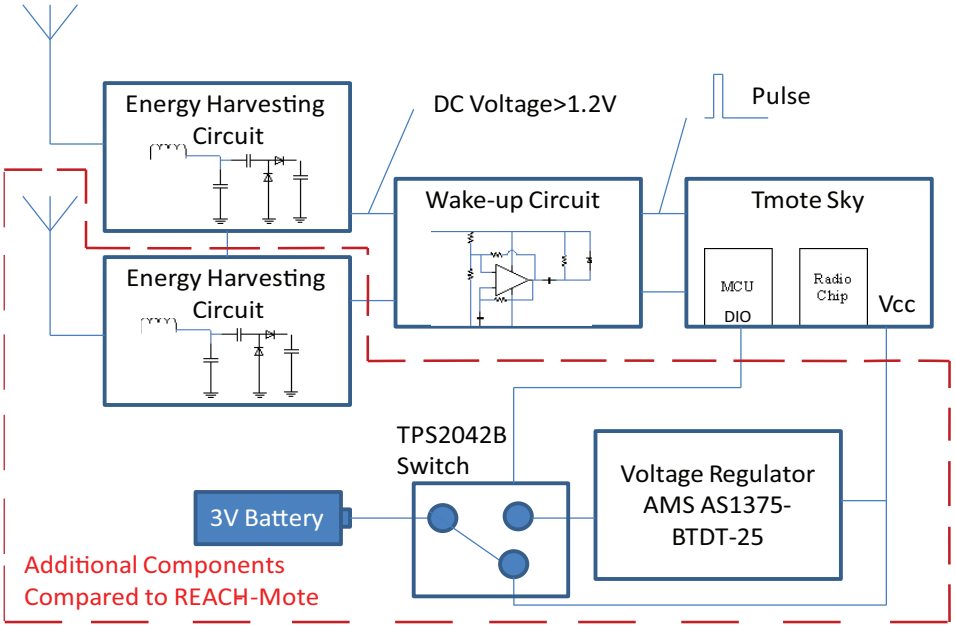

Figure 5.8: Block diagram of the REACH^2-Mote components.

best communication performance for the sensor node.

5.3.1 Operation of the REACH^2-Mote

Fig. 5.8 shows the system diagram of the REACH^2-Mote. The REACH^2-Mote operates following the flow chart shown in Fig. 5.9. In the following, we describe the operation principles for REACH^2-Mote.

- The REACH^2-Mote remains in the sleep mode before the WuTx transmits the wake-up signal, i.e., the MCU on the Tmote Sky, which is an MSP430F1611, is put to LPM3 sleep mode [90] and the radio on the Tmote Sky is turned off.

- The voltage regulator maintains the battery supply voltage of the REACH^2-Mote at $2.5V$.

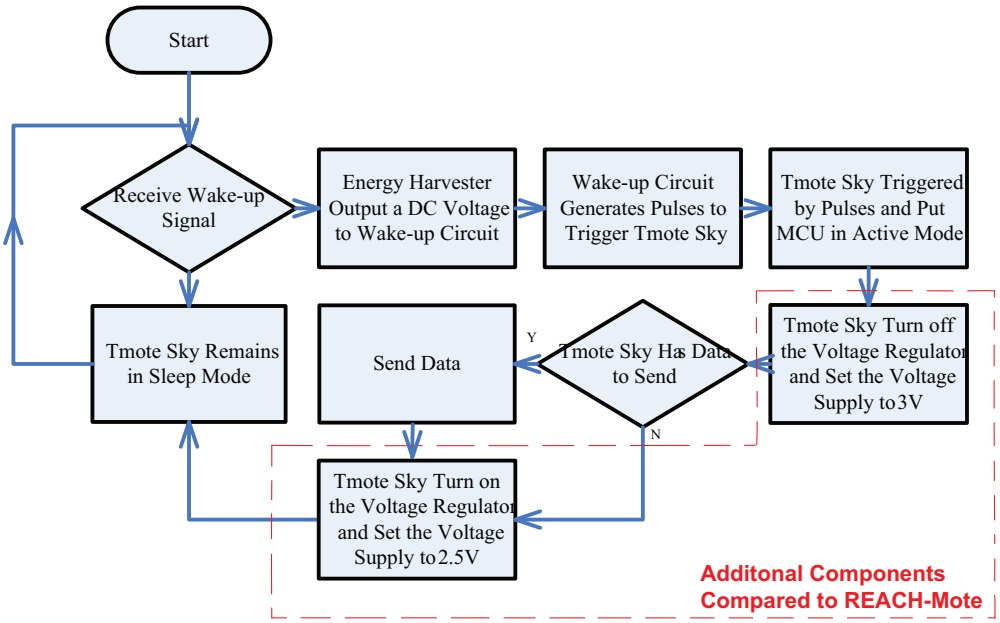

Figure 5.9: Flow chart of the REACH^2-Mote operation.

- When a wake-up signal is sent by a nearby WuTx, the energy harvesting circuit receives the energy and outputs a DC voltage.
- The wake-up circuit generates a pulse once the DC voltage is higher than $1.2V$ and this will trigger a wake-up of the MCU on the sensor mote. Note that the voltage requirement of wake-up has been lowered from $1.5V$ to $1.2V$ because the supply voltage of the MCU is set at $2.5V$.
- The MCU changes the Digital I/O (DIO) pin on the voltage regulator and switches the power supply of the sensor node back to $3V$.
- The MCU turns on the radio, i.e., the CC2420 radio on the Tmote Sky. As the supply voltage is $3V$ at this time, the CC2420 can achieve a reasonable communication range.
- After turning on the radio, data transfer is started if the mote has data to send.

- If the mote does not have data to send, or after the data transmission is complete, the MCU switches the supply voltage back to $2.5V$ and the mote goes back to the sleep mode (i.e., the MCU is set to LPM3 and the radio is turned off).

The improved energy harvester circuit and the adaptation of the power supply voltage for the Tmote Sky enable the REACH^2-Mote to extend the wake-up range compared with the REACH-Mote, as shown in Section 6.3.

5.3.2 Energy Analysis of the REACH^2-Mote

A voltage regulator will require some energy from the node's battery. However, the lowered supply voltage also decreases the energy cost of the MCU during the sleep state. Thus, a well selected voltage regulator is important to extend the lifetime of the sensor node. The voltage regulator used in the REACH^2-Mote must meet the following requirements.

- The input voltage of the voltage regulator circuit is $3V$ so that the input of the voltage regulator can share the same battery supply with the Tmote Sky in active mode.
- The output voltage of the voltage regulator is $2.5V$.
- The quiescent current of the voltage regulator should be as low as possible.

According to these criteria, we select the AMS AS1375-BTDT-25 [94] as the voltage regulator, as this chip only requires a quiescent current of $1\mu A$. We also added a TI TPS2042B [95] to switch the supply voltage between $2.5V$ and $3V$. Also, the switch consumes $1\mu A$ continuously. As the sleeping current of the Tmote Sky is about $11.2\mu A$, the energy cost of the sleeping REACH^2-Mote is $33\mu W$ ($28\mu W$ for the sleeping mote, $2.5\mu W$ for the switch and $2.5\mu W$ for

the voltage regulator) compared to the $33.6\mu W$ sleeping energy cost of a normal Tmote Sky powered by a $3V$ battery. Thus, with the new voltage regulator and switch system, the energy cost of the sensor node is lowered by 1.7% and the wake-up voltage requirement of the REACH^2-Mote is decreased. Although the voltage regulator and the switch consume energy from the battery, this approach reduces the overall battery consumption of the mote. Hence, we consider this approach as a hybrid-passive WuRx approach.

5.4 Experiments and Field Tests

We performed field tests to evaluate the performance of the REACH-Mote and REACH^2-Mote. We use the field test results for the REACH^2-Mote to build a simulation model to evaluate the performance of REACH^2-Mote in detailed application scenarios.

5.4.1 Experiments and Field Tests for REACH-Mote

We evaluated the wake-up delay and wake-up distance performance of the REACH-Mote through field tests and compared its performance with that of an existing passive wake-up sensor node, namely WISP-Mote [70].

Experiments and Field Test Setup

We ran several experiments in an open-space environment (an empty gym). The WISP-Mote is capable of both addressable wake-up and broadcast wake-up, but the REACH-Mote is only capable of broadcast wake-up. Hence, we only evaluate the performance of the WISP-Mote utilizing broadcast wake-up for this test for a fair comparison. In our experiments, we tested the single-hop wake-up scenario, assuming a base station with a WuTx transmits the wake-up signal to collect

Figure 5.10: Field test set-up.

data on the REACH-Mote and WISP-Mote. The base station is composed of a WuTx, a Tmote Sky and a laptop. The WuTx is composed of a Powercast wireless transmitter [96] and an Impinj R1000 RFID reader [88] controlled by the laptop. After the WuTx transmits the wake-up signal and wakes the sensor node (REACH-Mote and WISP-Mote), the Tmote Sky on the sensor node transmits a short ACK packet indicating the successful wake-up to the base station. We evaluate the period between the start of the wake-up signal transmission and the reception of the ACK packet. As there are no collisions occurring in this scenario, this period represents the wake-up delay.

We placed the transmitter (WuTx) antenna $60cm$ above the ground and varied the location of the REACH-Mote and WISP-Mote (WuRx) in both the horizontal and vertical directions to evaluate their performances. If the mote does not respond within $100s$, we assume that it cannot be woken up at that particular

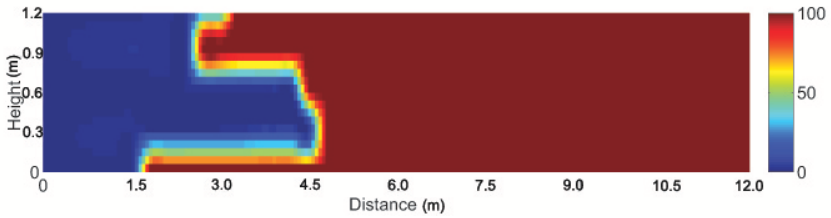

Figure 5.11: Wake-up delay (in seconds) for WuTx: combination of RFID Reader and Powercast; WuRx: WISP-Mote. The delay limit of 100 seconds is used to represent the locations where wake-up is not possible.

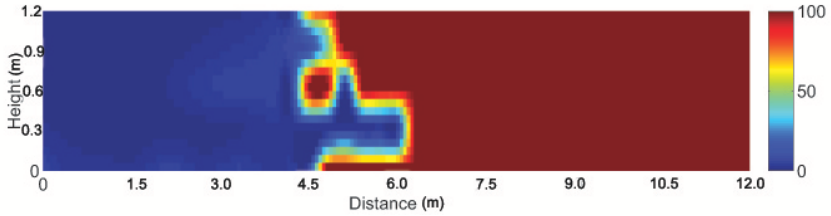

Figure 5.12: Wake-up delay (in seconds) for WuTx: combination of RFID Reader and Powercast; WuRx: EH-WISP-Mote. The delay limit of 100 seconds is used to represent the locations where wake-up is not possible.

location. Fig. 5.10 shows the field test setup.

Experiments and Field Test Results

The tests are repeated with $60cm$ increments in the horizontal direction (x-direction) starting from $3cm$ from the WuTx and $30cm$ increments in the vertical direction (z-direction), with 0 corresponding to the ground level. After each measurement, the Tmote Sky is reset and the energy harvesting circuit is discharged. Each data point in the figures represents the average of five tests.

As seen in Figs. 5.11, 5.12 and 5.13, the REACH-Mote can achieve a $11.2m$ wake-up range, more than double the distance compared to that of the WISP-

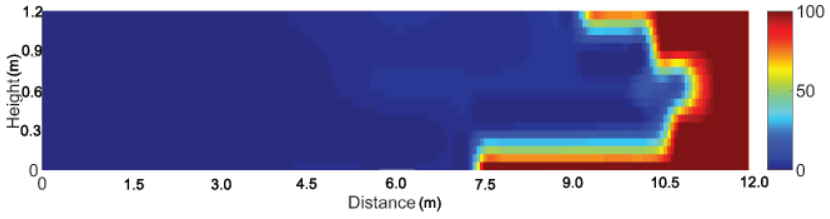

Figure 5.13: Wake-up delay (in seconds) for WuTx: combination of RFID Reader and Powercast; WuRx: REACH-Mote. The delay limit of 100 seconds is used to represent the locations where wake-up is not possible.

Mote, which achieves a $5.1m$ wake-up range. This is due to the ultra low energy consumption of the proposed wake-up circuit and an optimized energy harvesting circuit. EH-WISP-MOTE result in a $6.4m$ wake-up range, which shows the benefit of adding the energy harvesting circuit for passive wake-up. Furthermore, the longest range is achieved at $60cm$ height, which is the same height as the wake-up transmitter.

5.4.2 Experiments and Field Tests for REACH^2-Mote

Here, we provide the experimental results for the REACH^2-Mote. As we see from the previous results that the $60cm$ height achieves the best results vertically (z-direction), the REACH^2-Mote tests are performed only at this height. For these experiments, the experiments are performed while varying both the x-direction and the y-direction. Also, three sets of tests are performed during different days, with one being a rainy day to evaluate the performance of REACH^2-Mote under different environmental conditions. Although these tests are performed indoors, the rainy day increases the moisture of the air, which will decrease the performance of the REACH^2-Mote somewhat. Each set of tests is performed 3 times, and the average values of the wake-up delays are calculated. The tests are repeated with $30cm$ increments in the x-direction starting from $3cm$ from the WuTx and $0.9m$

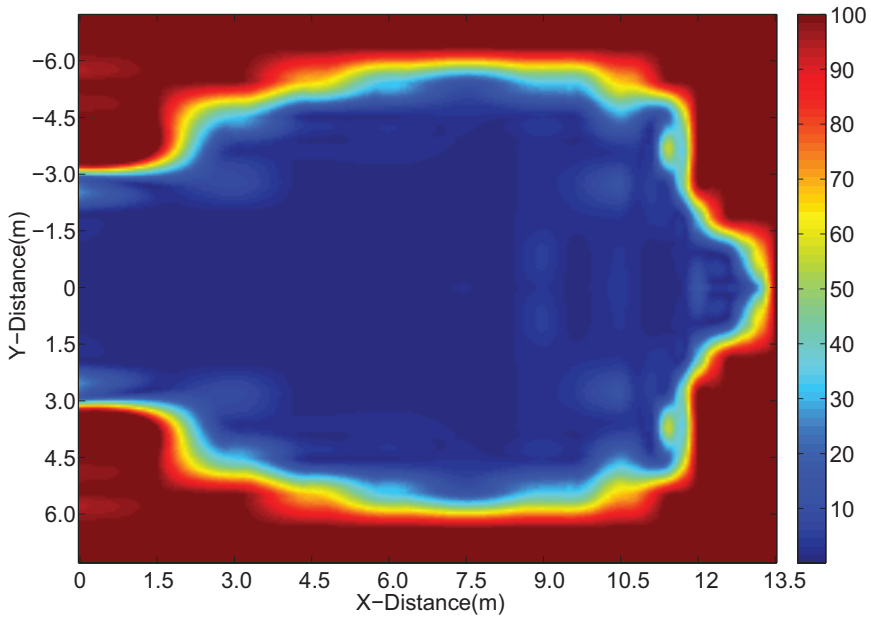

Figure 5.14: Wake-up delay (in seconds) for WuTx: combination of RFID Reader and Powercast; WuRx: REACH^2-Mote. The test is performed in the X and Y directions with the height set at $z = 60cm$. The delay limit of 100 seconds is used to represent the locations where wake-up is not possible.

increments in the y-direction. The other settings in these tests are the same as the tests for the REACH-Mote and the WISP-Mote.

Fig. 5.14 shows the results of wake-up coverage for the REACH^2-Mote. These results show the average of three tests. Test 1 and Test 2 are performed on a clear day, while Test 3 shows the results on a rainy day. We see that REACH^2-Mote can achieve a wake-up distance of $13.4m$, which represents a 19% improvement compared to the REACH-Mote. In the experiments, we find that the rainy day achieves a $13.1m$ wake-up distance, which shows that the high moisture in the air does little to degrade the performance of the REACH^2-Mote.

In the Y-direction, as the WuTx on the base station is composed of a directional

antenna, the result show that REACH^2-Mote can be woken up at $\pm 5.7m$ in the y-direction. These results will be used in the modeling for the simulation in order to further evaluate the performance of the REACH^2-Mote in different network scenarios.

5.5 Simulation Results

Due to the prototype phase of the hardware, we cannot build many REACH^2-Motes to perform a full scale test in a large network. In order to evaluate the performance of the REACH^2-Mote in a network scenario with multiple REACH^2-Motes, we build an energy harvesting model of the REACH^2-Mote based on the field test results. Also, we build a communication model for REACH^2-Mote and WISP-Mote as well as for an active wake-up scenario and for a duty cycling approach. In this way, we can compare the performance of these different approaches for a range of network scenarios. Additionally, we build a simulation scenario for a particular application, air pollution monitoring, and evaluate the performance of these approaches for this application.

5.5.1 Models Created for the Simulation

In order to perform the simulations, we modeled the energy harvesting process of the REACH^2-Mote by measuring the wake-up delay. We assume that the sensor node will be woken up when the energy harvester receives enough energy to trigger the MCU. After that, we build a communication model for the communication between the sensor nodes and the base station(s).

Energy Harvesting Model

An energy harvesting model is developed to indicate the amount of energy harvested for the wake-up based on the locations of the WuTx and the WuRx. For the energy harvesting model, we make the following assumptions. First, we assume that the amount of energy that is harvested from the transmitter at a fixed location (x, y) in a unit time is constant. We denote this location-specific constant value with $E_h(x, y)$. We assume that a wake-up circuit consumes E_c amount of energy when it wakes up the MCU on the sensor node. Also, the capacitor leaks E_l amount of energy per unit time when the wake-up circuit is not active. Thus, the amount of energy in a REACH^2-Mote capacitor at time t when it is not sending a wake-up trigger to the MCU is

$$E_t = E_{t-1} + E_h(x, y) - E_l, \tag{5.1}$$

and the energy in the capacitor at time t when the REACH^2-Mote is woken up is

$$E_t = E_{t-1} + E_h(x, y) - E_c. \tag{5.2}$$

Note that the leakage when the wake-up circuit is active is negligible because $E_c >> E_l$. The values E_c and E_l are measured through field tests. To do this, we charged the capacitor and turned on the wake-up circuit, and then measured the voltage change on the capacitor to calculate E_c. Then we turned off the wake-up circuit and measured the leakage E_l.

Assuming there is no energy stored at the beginning of the simulation, we can calculate the energy stored in the capacitor of the WuRx. We measured the voltage value on the capacitor (C_w) when it is just sufficient to trigger a wake-up. Then we calculate the energy based on the following equation.

$$E'_t = \frac{1}{2} C_w V'^2_t. \tag{5.3}$$

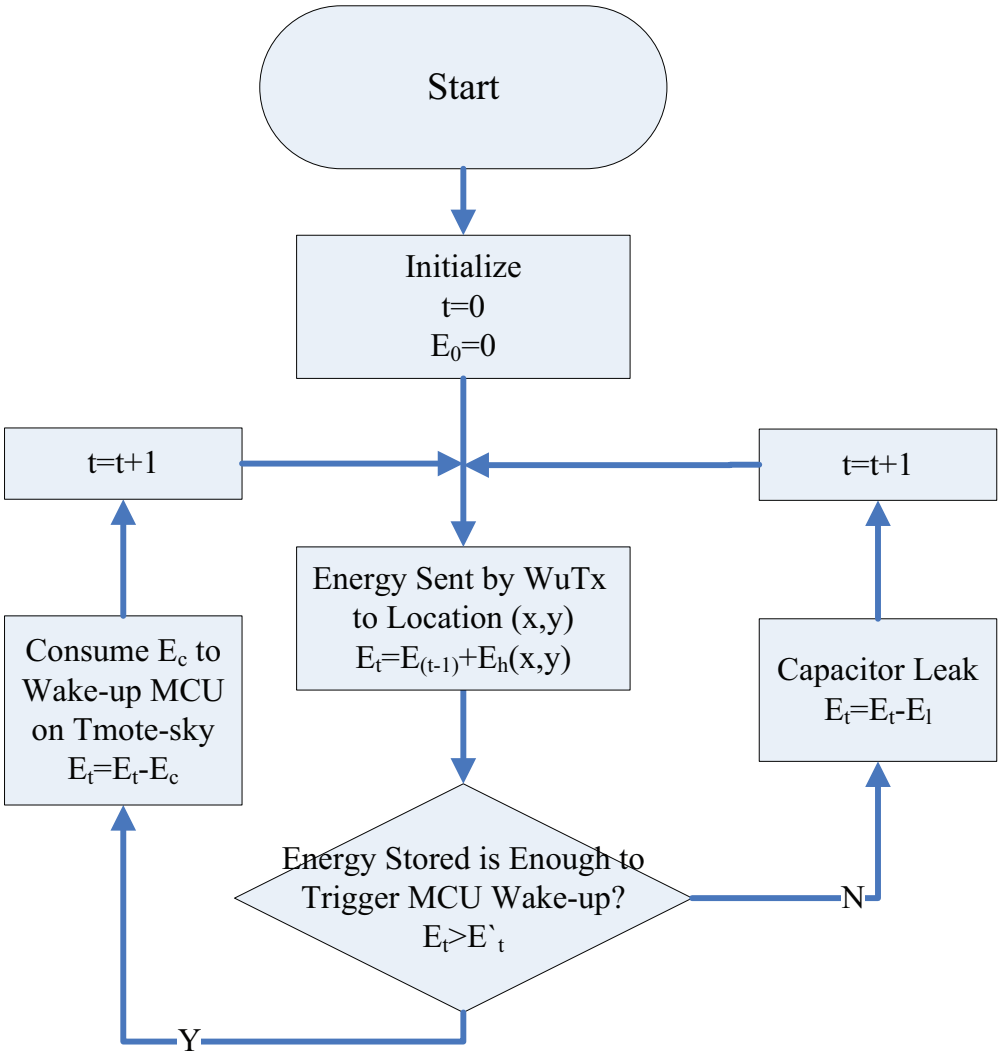

Figure 5.15: Energy harvesting model for the simulations.

Let $T_d(x, y)$ define the wake-up delay when the REACH^2-Mote is deployed at location (x,y) relative to the base station. With the assumption of constant energy harvesting at one location,

$$E_h(x, y) = E'_t/T_d(x, y). \tag{5.4}$$

Note that as E'_t is the energy that is barely sufficient to trigger a wake-up, this represents the threshold energy to turn on the wake-up circuit.

Fig. 5.15 shows the energy harvesting model we are using in the simulation framework.

Communication Model

To compare the performance of the REACH^2-Mote, WISP-Mote, an active wake-up approach and duty cycling approach, we build communication models for these approaches. Note that the approach of the active wake-up is based on the work described in [71], as it is the only active wake-up with $-72dBm$ sensitivity, i.e., long wake-up range. The communication is modeled based on time slots, where each time slot is $10ms$.

For REACH^2-Mote we build the communication model based on the energy harvesting model. When a sensor node is woken up, it performs carrier sensing using its communication radio. The node will sense the channel immediately after it wakes up. If the channel is clear, the sensor node will transmit its data to the base station. The base station will provide an ACK once it successfully receives the data. If the channel is busy, the sensor node will back off for a random number of time slots. If the transmission is not successful, i.e., an ACK is not received from the base station, the sensor node will back off for another random number of time slots and re-transmit the data.

For WISP-Mote, we build the wake-up model based on the wake-up probability model given in [70]. When the node is located in the wake-up range of the WuTx, the node has a given probability to wake up. After the node is woken up, it acts the same as the REACH^2-Mote.

For active wake-up, we assume that the sensor node is woken up as soon as the base station moves into the wake-up range of the sensor node. After that, the sensor node performs carrier sensing in the same way as for the REACH^2-Mote and the WISP-Mote.

For the duty cycling approach, the base station transmits a beacon packet once every 8 time slots and waits for a response for the remaining 7 slots. If there is no response from a sensor in these 7 slots, the base station transmits the beacon packet again. The sensor node remains in the sleeping mode until a preset timer wakes it up. The timer is set based on the ratio of active/sleep mode, which represents different duty cycle values. After the sensor node is woken up by the timer, it starts to listen for the channel for 8 time slots in order to guarantee not missing the beacon signal if a base station is nearby. If the sensor node receives the beacon packet, it will randomly select one of the next 7 slots to transmit data to the base station. Otherwise, it will reset the wake-up timer and return to the sleep mode. If the transmission to the base station is not successful due to collisions, the sensor node will back off for a random number of time slots and pick another random slot in the 7 slots to re-transmit the data.

For all four approaches, the sensor node will receive an ACK packet after a successful transmission. The ACK packet notifies the sensor node that the base station is still within its communication range and that no collisions occurred during the data transmission. Thus, the sensor node can continue to transmit other packets stored in its buffer. After emptying its buffer, or if the base station goes out of communication range and no longer sends ACK packets, the sensor node will not receive the ACK for a period of time and it will return to the sleep mode.

5.5.2 Simulation Setup

To evaluate the performances of the investigated approaches, we consider two categories of application scenarios: one with a low data rate requirement and one with a high data rate requirement. In the low data rate requirement scenarios, the sensor nodes generate packets with a relatively long interval. This category simulates the sensing tasks that do not require continuous monitoring, such as

air pollution control, temperature and moisture monitoring, where a measurement/reading might be taken only once an hour or even once a day. On the other hand a high data rate requirement sensing task generates packets much more frequently and performs continuous sensing observations such as for hazard monitoring.

The simulations are performed in Matlab and utilize the following simulation setup.

- The sensor nodes are deployed randomly in an area of $200m \times 200m$.
- There are one or multiple mobile base stations that move with a random direction mobility model with a speed of $10m/s$ [97].
- The nodes generate packets according to the designated packet generation rate periodically and store these packets in their buffers. The sensor nodes can have finite buffer size or infinite buffer size depending on the scenario. For finite buffer size, the oldest packet is dropped when the buffer is full.
- For the wake-up scenarios, once the base station is within the wake-up range of the sensor nodes, they wake up according to the model described in Section 5.5.1.
- For the duty cycling approach, the sensor node wakes up according to its internal timer.
- After the sensor nodes wake up, they apply the communication model described in Section 5.5.1.
- Each simulation run lasts for 6 hours with a time step of $10ms$.

In each category, both low data rate and high data rate, 4 sets of simulations are performed as detailed below.

1. Set 1: 100 sensor nodes in the $200m \times 200m$ area. There is one mobile base station collecting data. The sensor nodes have infinite buffer size. The packet generation rate changes from 0.02 pkt/min to 0.2 pkt/min for category 1 and 0.2 pkt/min to 2 pkt/min for category 2.

2. Set 2: the same as Set 1 except that the buffer size is 10 pkt instead of unlimited.

3. Set 3: varying the number of sensor nodes from 100 to 1000. In these simulations, the packet generation rate is set to 0.02 pkt/min for category 1 and 0.2 pkt/min for category 2.

4. Set 4: varying the number of base stations from 1 to 4. The packet generation rate is 0.02 pkt/min for category 1 and 0.2 pkt/min for category 2 with unlimited buffer. The number of sensor nodes is 100.

We also implemented an air pollution monitoring scenario in simulation to evaluate the performance of these approaches in a real application. In this scenario, 100 sensor nodes are deployed along the road. Each node will collect air pollution information once every hour. The base station moves along the designed route to collect air pollution data once a day. The route is 10 kilometer long, and the simulation runs for 2 days.

5.5.3 Simulation Results

In all of the simulations, we collect data for five performance metrics to evaluate the performance of the different approaches.

- Average buffer size represents the memory requirement needed to store the packets that have not been sent. The lower the average buffer size is, the less memory is required on the sensor node.

- Average collisions per packet represents the collisions that occur during the communication with the base station. The higher the number of collisions, the higher the re-transmission rate, which will cost additional energy.
- Average packet delay measures the delay between when a packet is generated and when the packet is received by the base station. A high packet delay is caused by missed wake-ups, short wake-up range or high collisions in data transmission.
- Energy consumption per packet represents the energy efficiency in data transmission. Packet re-transmission, unnecessary wake-up for the wake-up approaches and unnecessary idle listening for the duty-cycling approach will increase this value. A lower energy consumption per packet represents a better energy-efficiency.
- Packet delivery rate (PDR) calculates the ratio between the number of packets generated by the sensor node and the number of packets delivered to the base station.

Set 1 Simulation Results

Fig. 5.16 shows the performance of each approach with varying packet generation rates from 0.02 pkt/min to 0.2 pkt/min (category 1). In this set of simulations, there are 100 nodes deployed in the area and there is 1 base station moving within the target area to collect the data. The buffer size is assumed to be unlimited for sensor nodes in this set of simulations. We can see that none of the approaches requires much buffer space, as the packet generation rate is relatively low. The buffer requirements for REACH^2-Mote are lower than for WISP-Mote as the longer wake-up range increases the possibility of packet delivery. 0.1% duty cycling, WISP-Mote and REACH^2-Mote achieve a low collision rate. Among

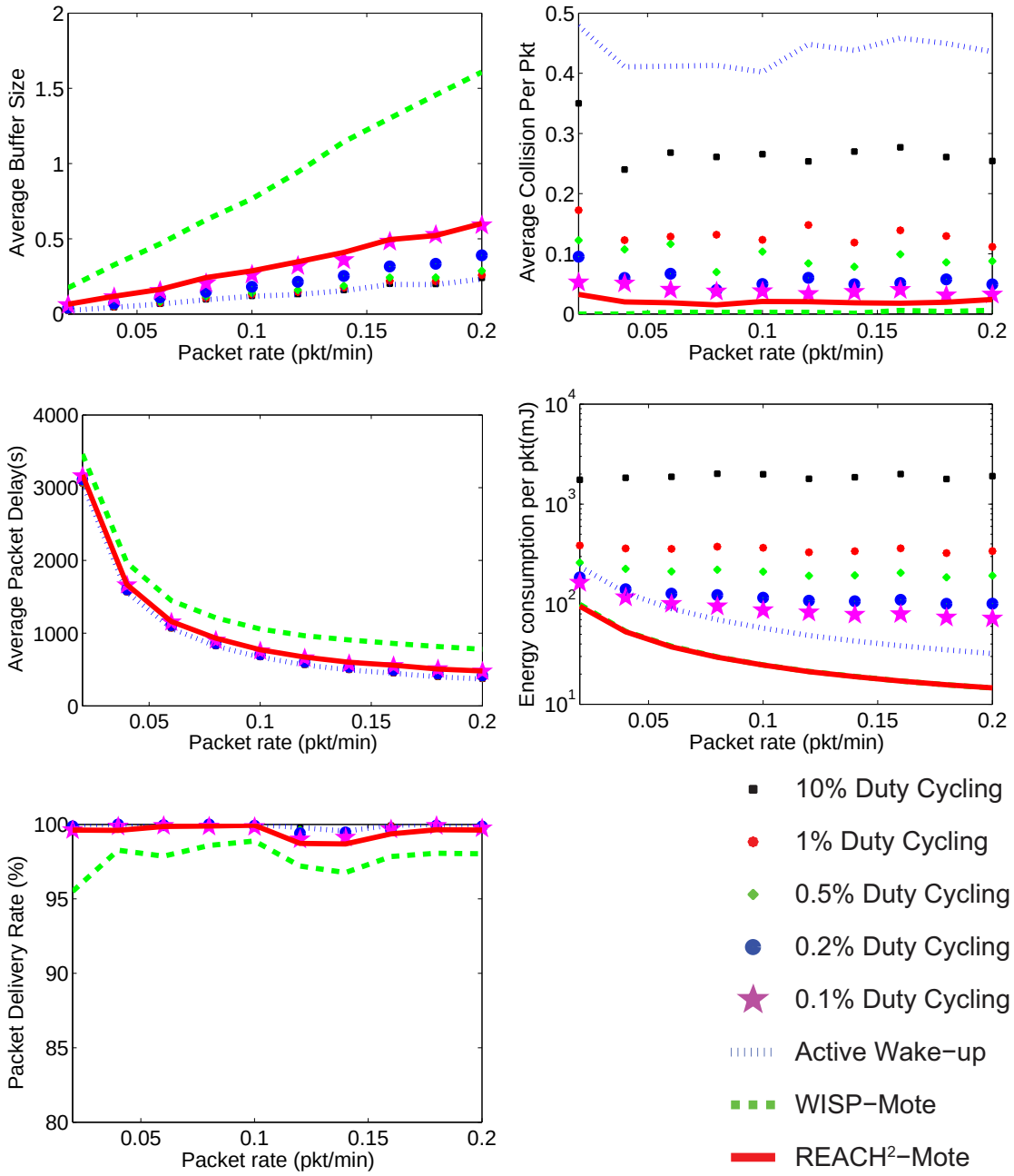

Figure 5.16: Simulation results for different packet generation rates from 0.02 pkt/min to 0.2 pkt/min. (100 sensor nodes, 1 base station, unlimited buffer)

these, WISP-Mote is a little less than the others as the WISP-Mote provides a low wake-up range, which decrease the probability of waking up multiple sensor nodes at the same time to transmit data. 10% duty cycling provides the best delay performance and REACH^2-Mote and active wake-up perform almost the same as the 10% duty cycling approach. REACH^2-Mote and WISP-Mote result in the best energy consumption performances, as both approaches are passive wake-up sensor nodes. The active wake-up approach doubles the energy consumption compared to the passive wake-up approaches. The 10% duty cycling results in the worst energy efficiency, as expected since it wastes a lot of energy on unnecessary idle listening. Although WISP-Mote performs well in terms of energy efficiency, it results in the worst buffer requirement and delay result, as the wake-up range of the WISP-Mote is short.

Fig. 5.17 shows the simulation results when the packet generation rate is varied from 0.2 pkt/min to 2 pkt/min (category 2). This simulation aims to evaluate the performance of each approach when the sensor nodes require high data transmission rate. Results show that all approaches, except REACH^2-Mote and the active wake-up approach, require higher buffer occupancies, as increasing the packet generation rate leads to a lower packet delivery rate and more packets are stored in the buffer for these approaches. Referring to the average packet delay and packet delivery ratio results, we find that the REACH^2-Mote and active wake-up approach can deliver most of their packets, so that the REACH^2-Mote and active wake-up approach increase little when the packet generation rate increases. As we do not implement addressable wake-up for the active wake-up approach, the active wake-up leads to a high collision rate due to the large wake-up range, i.e., more nodes being woken up simultaneously. Note that for these results, when the packet generation rate is 2 pkt/min, the results show the performance for each approach in a heavy data rate scenario. Compared to duty cycling and the active wake-up approach, the passive wake-up approaches result in a huge advantage in

energy cost (50% less than the active wake-up approach and 90% less than the 0.1% duty cycling approach) with high packet delivery rate and low packet delay. Also, passive wake-up requires less memory for the buffer compared with the other approaches.

Set 2 Simulation Results

Fig. 5.18 shows the simulation results for the limited buffer case for low packet generation rate scenarios and Fig. 5.19 shows that of high packet generation rate scenarios. The packet generation rate varies from 0.02 pkt/min to 0.2 pkt/min (category 1) and from 0.2 pkt/min to 2 pkt/min (category 2). For the packet generation rate from 0.02 to 0.2 pkt/min, the results are similar to the unlimited buffer results, as the low packet generation rate does not require much storage in memory. The buffer constraint effect is more visible as the packet generation rate increases. All approaches, except the active wake-up approach and 10% duty cycling, achieve lower packet delivery rate performance with a limited buffer in this scenario. REACH^2-Mote can still provide a decent performance in terms of packet delivery rate while requiring only 40% of the energy necessary for the active wake-up approach and 0.7% of the energy necessary for the 10% duty cycling case.

For the simulation results when the packet generation rate is 0.02 pkt/min and 2 pkt/min for the limited buffer scenario, REACH-^{2}-Mote outperforms all the other approaches in terms of energy efficiency. Active wake-up performs the best in terms of packet delivery ratio and latency with about double the energy consumption compared to REACH^2-Mote. A high duty cycling approach performs well in terms of packet delivery ratio and latency. However, duty cycling requires much more energy than the different wake-up approaches.

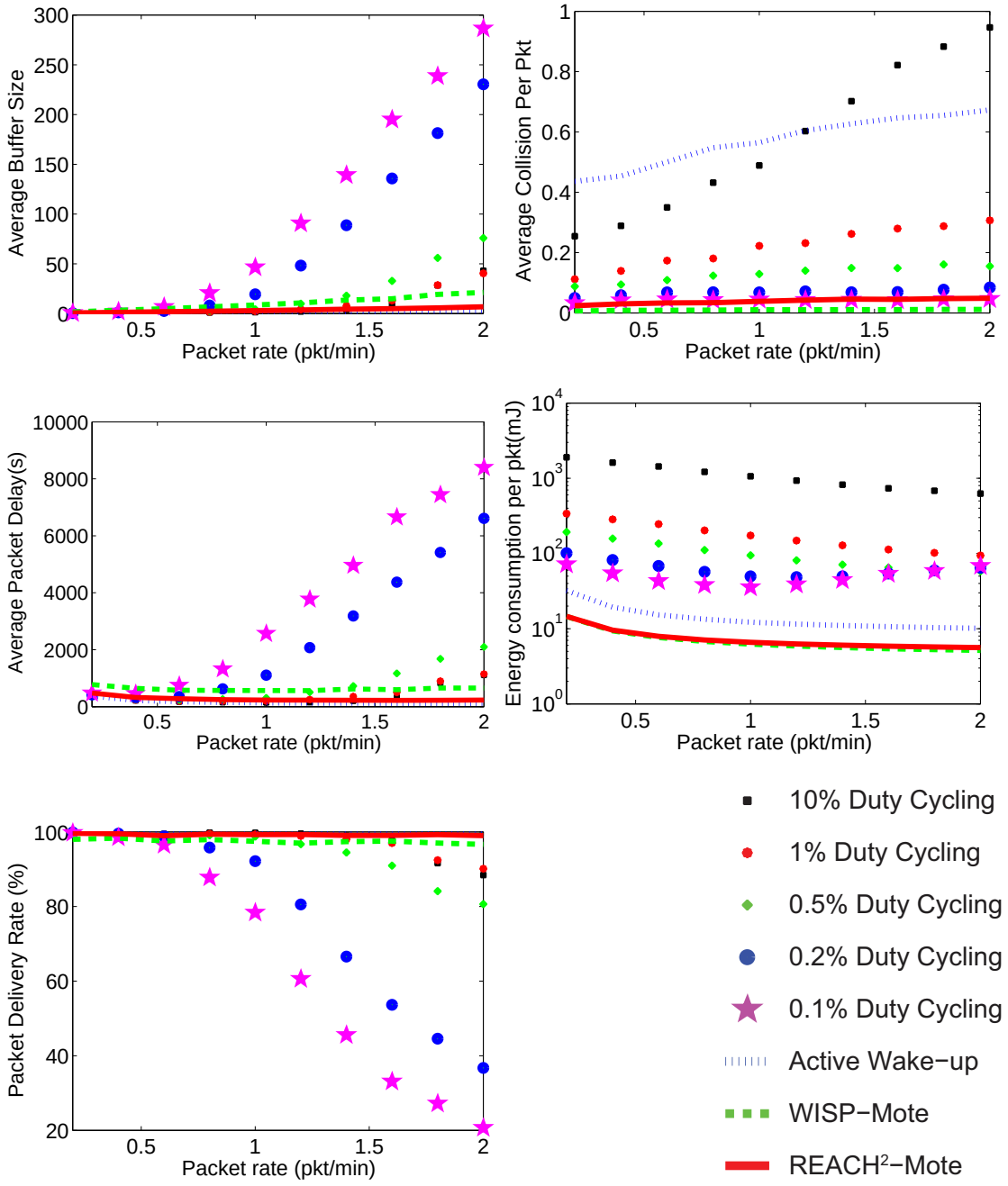

Figure 5.17: Simulation results for different packet generation rates from 0.2 pkt/min to 2 pkt/min. (100 sensor nodes, 1 base station, unlimited buffer)

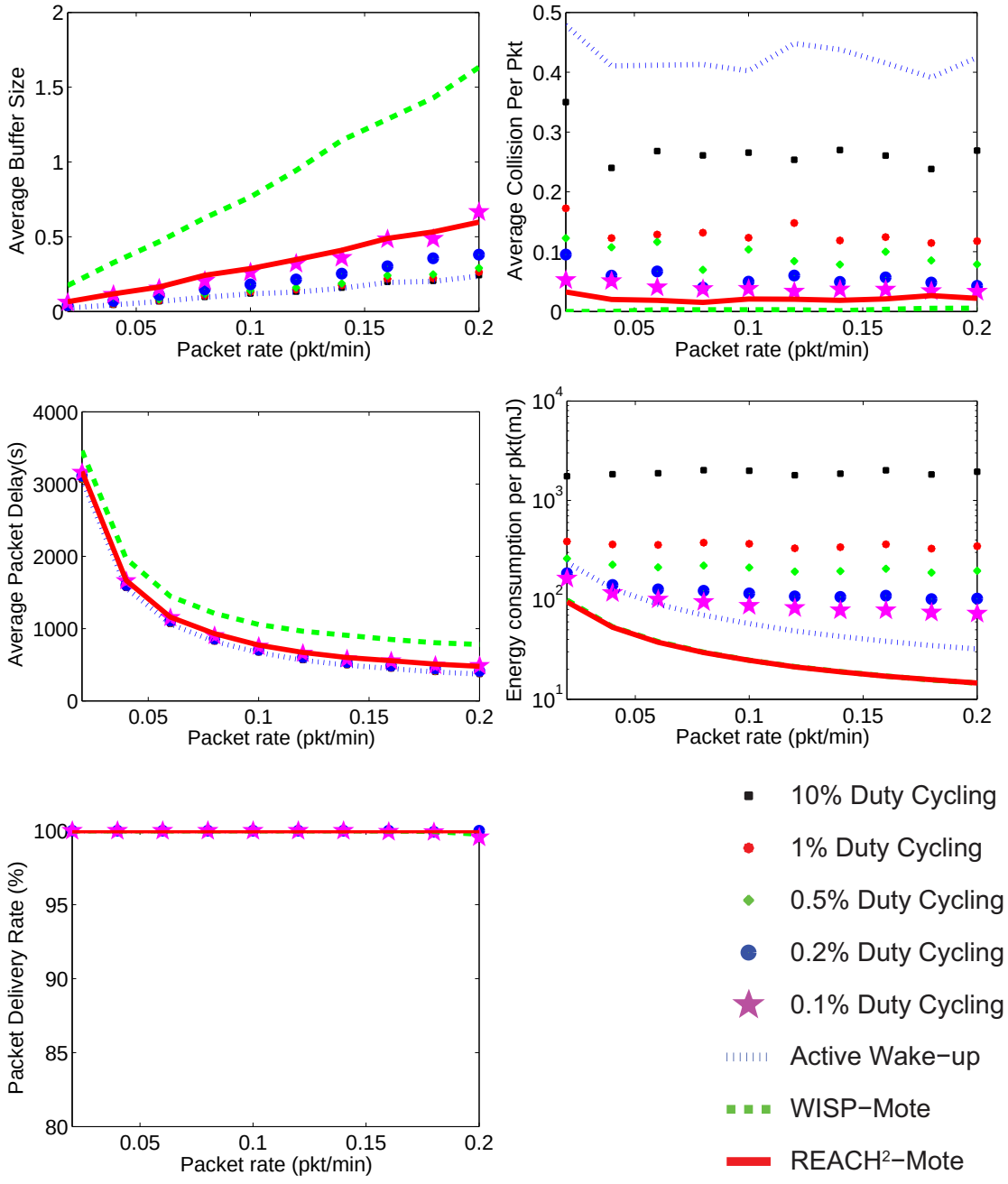

Figure 5.18: Simulation results for different packet generation rates from 0.02 pkt/min to 0.2 pkt/min. (100 sensor nodes, 1 base station, limited buffer)

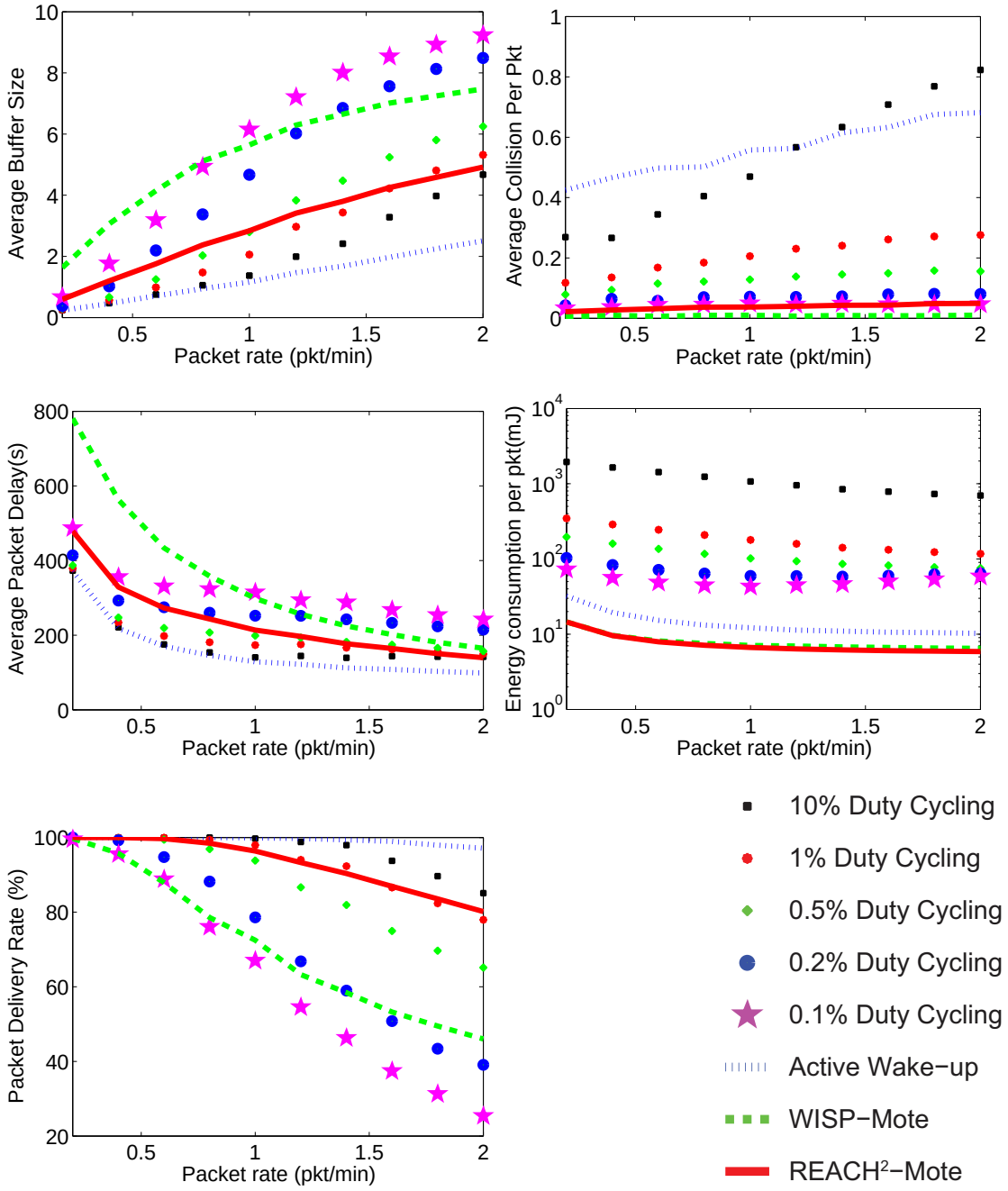

Figure 5.19: Simulation results for different packet generation rates from 0.2 pkt/min to 2 pkt/min. (100 sensor nodes, 1 base station, limited buffer)

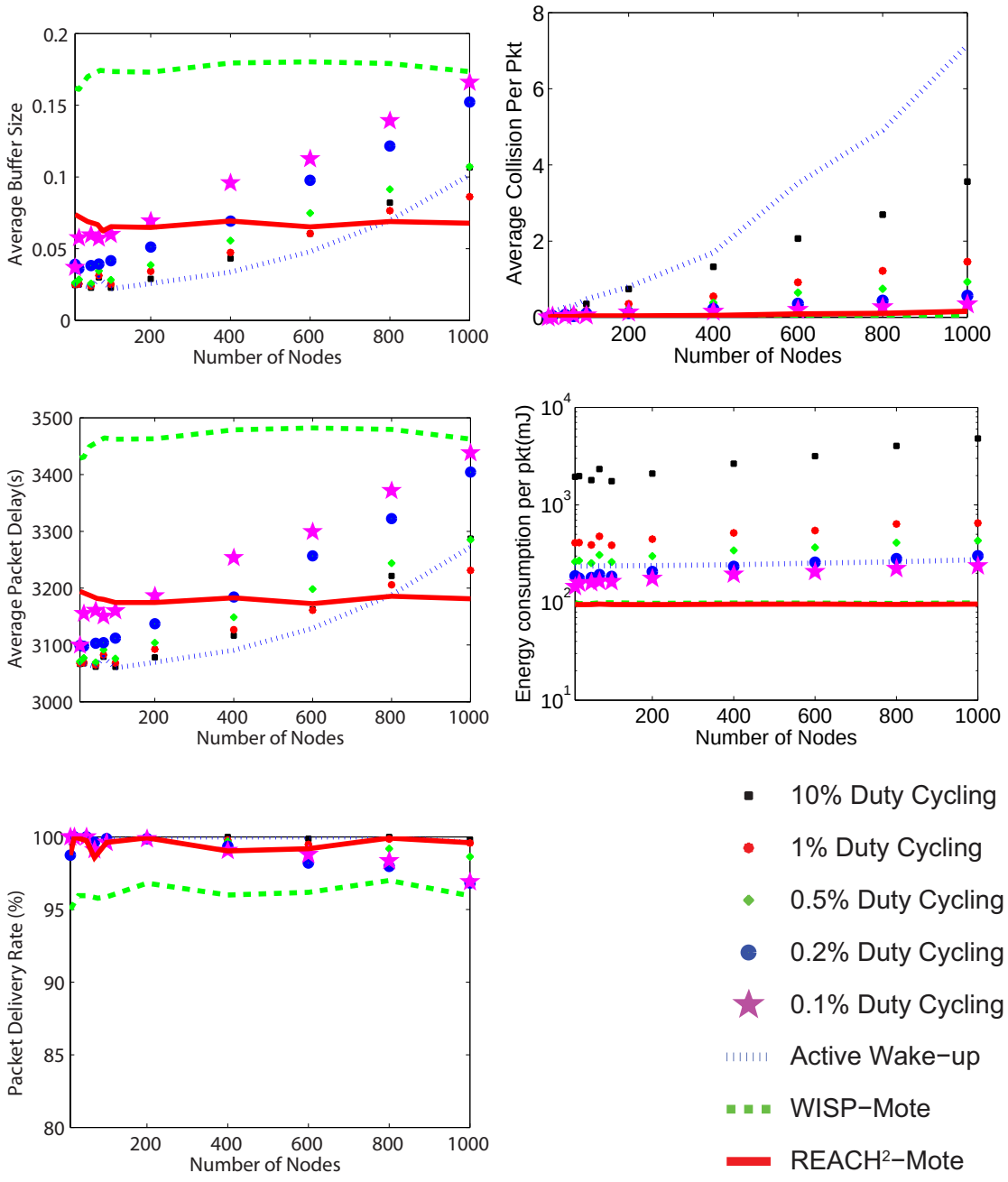

Figure 5.20: Simulation results as the number of nodes varies from 10 to 1000. (0.02 pkt/min, 1 base station, unlimited buffer)

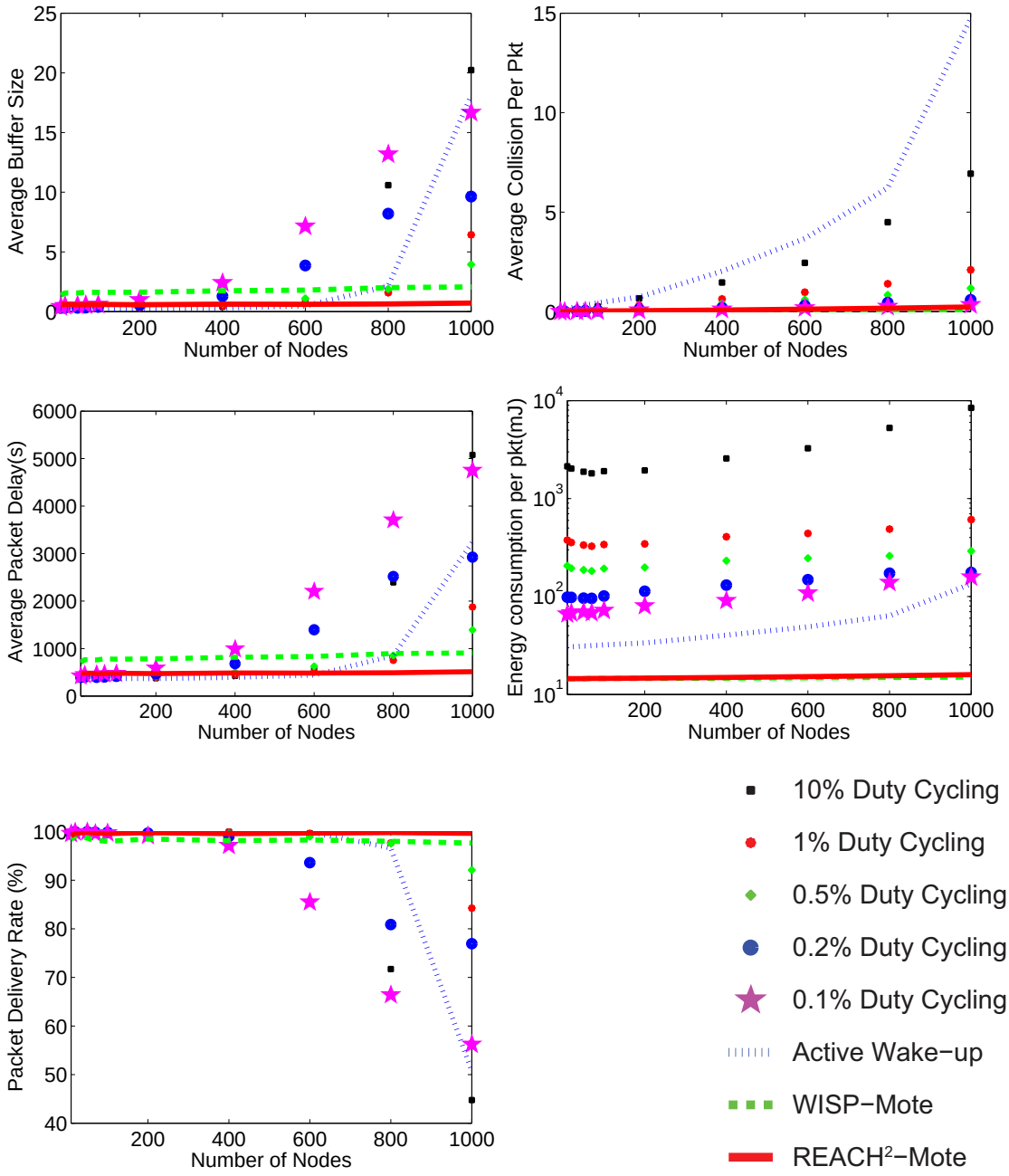

Figure 5.21: Simulation results as the number of nodes varies from 10 to 1000. (0.2 pkt/min, 1 base station, unlimited buffer)

Set 3 Simulation Results

Fig. 5.20 and Fig. 5.21 show the results of the performance of each approach for varying the number of sensor nodes in the network. These two sets of simulations evaluate the scalability of each approach. For the low packet generation rate, all approaches have decent packet delivery rate performance. For buffer size, packet delay and average collision performance, duty cycling and active wake-up decrease their performance dramatically with the increase in the number of sensor nodes. On the other hand, the results for REACH^2-Mote and WISP-Mote increase little with the increase in the number of sensor nodes, which shows a better scalability advantage over the other approaches. For the high packet generation rate case, the collision rate increases for duty cycling and active wake-up, while the packet delivery rate decreases. The WISP-Mote and REACH^2-Mote maintain a decent packet delivery rate with the increasing number of sensor nodes. Reviewing all the results in this simulation set, we find that for a lower packet generation rate (0.02 pkt/min), REACH^2-Mote results in the best performance in all metrics we evaluated compared to the other approaches. Especially for the energy consumption result, REACH^2-Mote requires only 30% of the energy required for active wake-up and 40% of the energy required for 0.1% duty cycling. For the higher packet generation rate scenario (2 pkt/min), REACH^2-Mote can save even more energy compared to the other approaches, while performing similar to or better than the other approaches for the other metrics. WISP-Mote results in the best collision result as the low wake-up range of WISP-Mote causes fewer nodes to wake up simultaneously. However, WISP-Mote also results in the worst latency performance due to the short wake-up range.

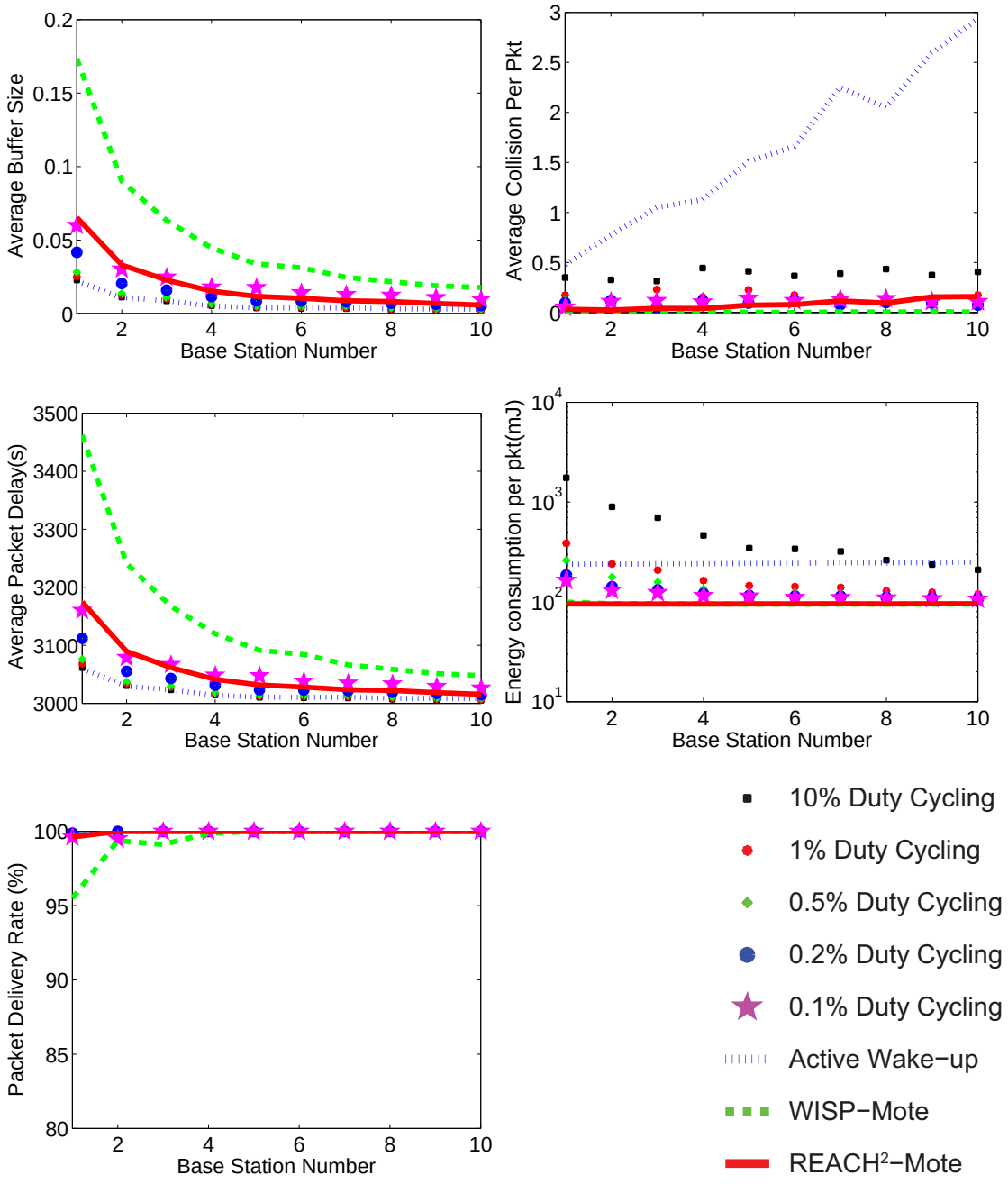

Figure 5.22: Simulation results as the number of base stations varies from 1 to 10. (0.02 pkt/min, 100 sensor nodes, unlimited buffer)

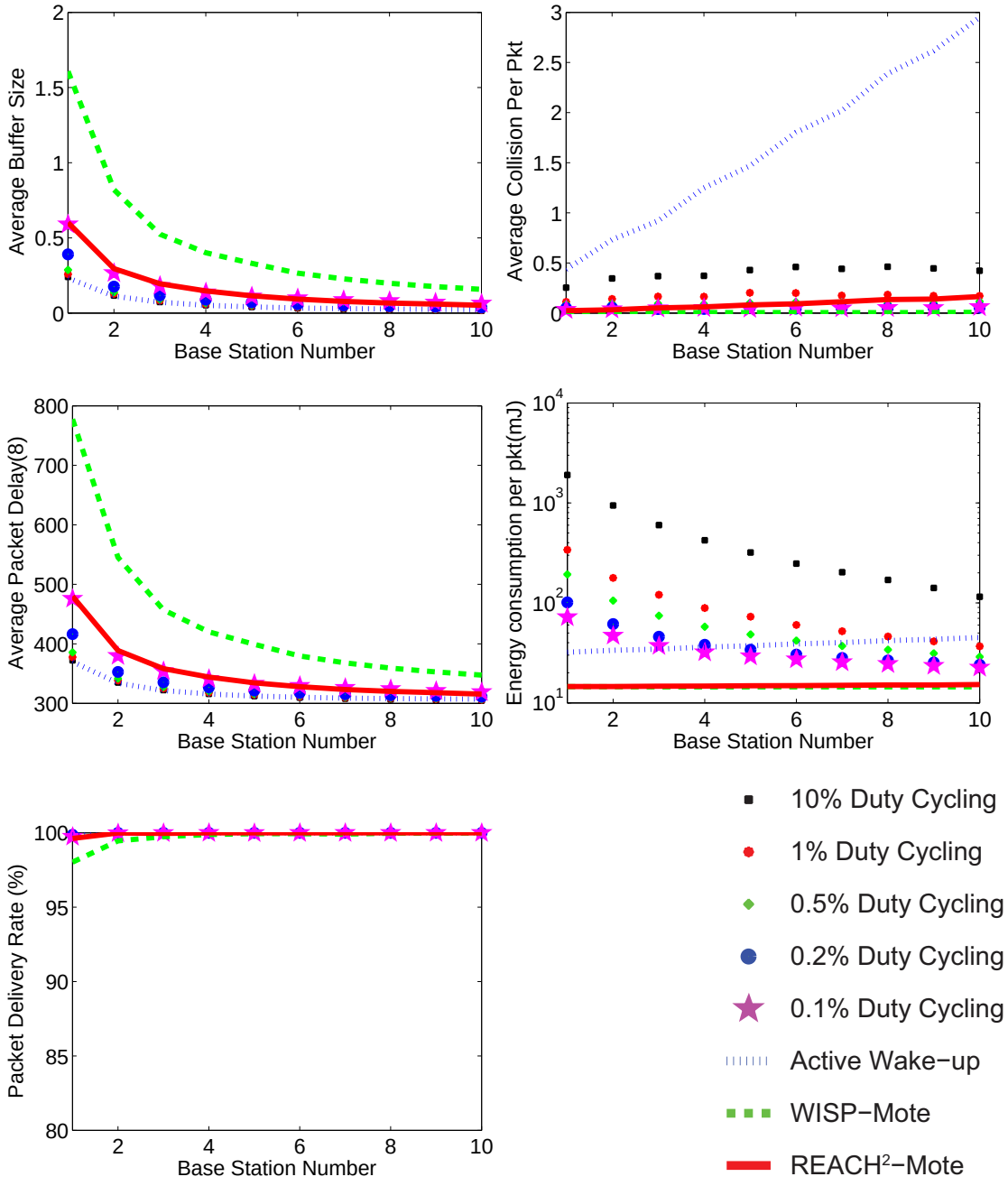

Figure 5.23: Simulation results as the number of base stations varies from 1 to 10. (0.2 pkt/min, 100 sensor nodes, unlimited buffer)

Set 4 Simulation Results

Fig. 5.22 and Fig. 5.23 show the results of the performance of each approach with increasing the number of base stations. The results show that increasing the number of base stations can increase the performance for each approach. Even with a high packet generation rate, all approaches can result in a good packet delivery rate. The REACH^2-Mote and WISP-Mote result in the best energy efficiency performance compared to the other approaches.

Air Pollution Monitoring Scenario

Fig. 5.24 shows the simulation results for the air pollution monitoring scenario, in which the base station moves along the designed route to collect air pollution data from 100 sensor nodes once a day. The results show that all approaches require limited buffer, as the packet generation rate is low. Also, the average collision rate is very low for all approaches as this scenario represents a sparse network. The packet delay is mainly caused by the interval between the visits of the base station so that all approaches lead to high packet delays. The low duty cycling approach leads to higher delay compared to the other approaches, as some nodes miss the base station when it comes by. The results show that the REACH^2-Mote, WISP-Mote and active wake-up require much less energy compared to the duty cycling approach. As the data rate of this scenario is relatively low, a duty cycling approach wastes much of its energy on idle listening, especially for the 10% duty cycling. The energy cost of the REACH^2-Mote ($108mJ$) is only 41% of that required for active wake-up ($263mJ$). Also, all wake-up approaches perform well in terms of PDR. 10% duty cycling is the only approach that results in good PDR among all the duty cycling approaches, as a lower duty cycle leads to a higher probability of missing an opportunity to communicate with the base station.

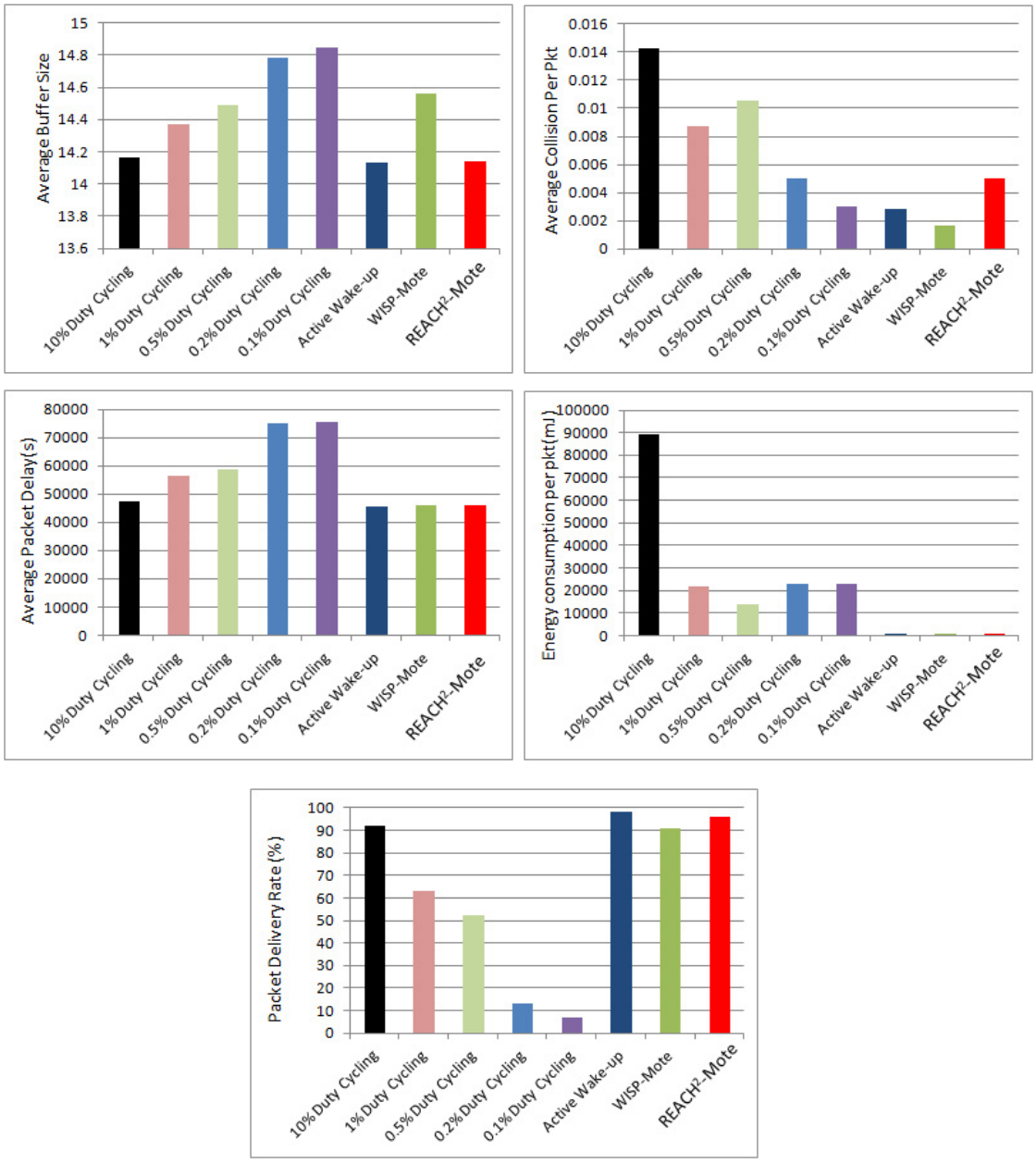

Figure 5.24: Simulation results for the air pollution monitoring scenario.

Conclusions on Simulation Results

These 4 sets of simulations show that the REACH^2-Mote and WISP-Mote provide the best energy performance compared with all the other approaches. These two approaches can save quite a bit of energy compared to the 0.1% duty cycling approach. Considering the 0.1% duty cycling performs worst among all duty cycling approaches in terms of buffer size, latency and packet delivery rate, REACH^2-Mote and WISP-Mote outperform duty cycling in most metrics evaluated. Compared to the active wake-up approach, REACH^2-Mote and WISP-Mote result in huge energy savings. REACH^2-Mote can also provide better collision performance with comparable performance in terms of buffer size and packet delivery rate compared to active wake-up. As REACH^2-Mote and WISP-Mote are both passive wake-up sensor nodes, they result in very close energy consumption performance. However, as WISP-Mote provides a shorter wake-up range, REACH^2-Mote outperforms WISP-Mote in terms of buffer size requirement, latency and packet delivery rate.

The pollution monitoring scenario analysis shows us that the duty cycling approach is not suitable for a low collection rate scenario. All wake-up approaches perform well in this scenario, but the REACH^2-Mote results in the highest energy efficiency.

5.6 Conclusions

In this chapter, we presented the design and evaluation of the REACH^2-Mote passive wake-up radio sensor node, which utilizes energy harvesting and an efficient wake-up circuit for extended wake-up range. We evaluated our implementation of the REACH^2-Mote through field tests and compared its performance with that of the 1^{st} generation REACH-Mote and the WISP-Mote, an existing passive wake-up sensor node. The field test results show that REACH^2-Mote can extend the

wake-up range to $13.4m$ compared to a $11.2m$ wake-up range for the REACH-Mote and a $5.1m$ wake-up range for the WISP-Mote. As the communication range of the Tmote Sky is $30m$, the REACH^2-Mote can achieve a wake-up range that is almost half of the communication range of the Tmote Sky. Thus, the REACH^2-Mote is a passive wake-up sensor node that can be deployed in real wireless sensor networks. Also, as the WuRx of the REACH^2-Mote requires less battery energy while waiting for a wake-up signal from the WuTx compared to a Tmote-Sky, more battery energy on the REACH^2-Mote can be used for either sensing the data or transmitting the data to base station, eliminating most of the overhead in communications.

In order to evaluate the performance of REACH^2-Mote in a network, we modeled the hardware of the REACH^2-Mote and evaluated its performance through simulations. We compared the results with that of a network employing WISP-Motes, an implemented active wake-up approach, and a duty cycling approach. The results show that the REACH^2-Mote outperforms the other approaches in energy efficiency, while performing comparable to the other approaches in terms of packet latency and packet delivery performance with higher scalability.

6 Multi-hop Passive Radio Wake-up for Wireless Sensor Networks

6.1 Introduction

A wireless sensor network (WSN) is composed of a set of sensor nodes, also known as motes, that monitor physical or environmental conditions, such as temperature, sound, or video. The sensor nodes form an ad-hoc network to transmit data to one or more data sinks in the network. A wireless sensor node is typically composed of various types of sensors to collect data, one or more processing units to handle the data collected, memory to store the data before transmission, a power source (frequently a battery), and a transceiver for wireless communications. Since most sensor nodes are battery powered, limited battery capacity can constrain the overall lifetime of the sensor network.

There are several methods proposed in the literature to extend the network lifetime of a WSN. Duty cycling is one of the most widely studied approaches, which schedules data reception, data transmission, and inactive sleeping periods at regular intervals. During its sleep periods, a node neither transmits nor receives data. This approach requires synchronization of adjacent sensor nodes, as

successful communication depends on the transmitting and receiving sides to be active simultaneously. These synchronization activities incur overhead and result in idle listening, since the nodes regularly switch to the reception mode whether or not there is a communication destined to them. Both the overhead incurred and the resulting idle listening consume battery energy, reducing the lifetime of the node and hence the WSN.

Another approach to extending network lifetime is to use wake-up radios, which do not suffer from the idle listening of duty cycling radios, by utilizing an on-demand RF wake-up radio hardware. A sensor node with an RF wake-up radio receiver (WuRx) is kept in an ultra-low-power sleep mode, neither transmitting nor receiving data. A wake-up transmitter (WuTx) sends a trigger signal to begin data transmission. When the WuRx receives the trigger signal, it wakes up the mote from the sleep mode, bringing it into the active mode. Then, the mote begins data transmission. This on-demand wake-up eliminates the energy waste caused by the unnecessary idle listening and synchronization of duty cycling, albeit with the cost of additional wake-up hardware.

There are two types of wake-up receivers. Active wake-up receivers utilize energy from a battery. They have the advantage of better wake-up performance in terms of wake-up range and wake-up delay. However, active wake-up receivers consume energy from batteries, which are also used to power sensors and to transmit data. On the other hand, passive wake-up receivers are powered by energy harvested from the WuTx. A passive WuRx has the advantage of not using any energy from the battery. One caveat of this system is the limitation of the wake-up range due to the limitations in the WuRx's ability to harvest enough energy to generate an interrupt for the MCU on the sensor node. Furthermore, as passive WuRxs are powered by harvested energy, the WuTx is generally designed to transmit as much energy as possible, in order to achieve a reasonably long wake-up range. This makes it difficult to build a multi-hop WSN featuring motes

equipped with both a passive WuRx and a WuTx. Thus, passive wake-up sensor nodes are often used in applications with a mobile data sink that can transmit the large energy required for the WuTx. For example, applications such as air pollution monitoring in a city or meter data collection for a smart grid application require sensor nodes to collect data periodically, but this data must only be communicated when a mobile sink (e.g., a data mule [113]) arrives to collect the data.

In our previous work [98], we proposed a high efficiency passive wake-up radio receiver called REACH-Mote, which utilizes an energy harvesting module and an ultra-low-power wake-up pulse generator to increase the passive wake-up range. We characterized the performance of the REACH-Mote and compared the performance of the REACH-Mote with other passive wake-up radio approaches, specifically the WISP-Mote [99] and the EH-WISP-Mote [98]. In this chapter, we propose a sensor node equipped with both a passive WuRx and a WuTx. We name this new mote the MH-REACH-Mote (Multi-hop-Range EnhAnCing energy Harvester-Mote). The MH-REACH-Mote can wake up other REACH-Motes and other MH-REACH-Motes, creating a multi-hop passive wake-up network. The MH-REACH-Mote is composed of: a Tmote-Sky sensor node; a passive wake-up receiver identical to REACH-Mote's WuRx; and an RFID reader by AMS as the WuTx [100]. We adjust the duration of the wake-up signal sent by the WuTx to evaluate the achieved wake-up distance versus the corresponding energy cost. These field tests show that an MH-REACH-Mote can wake up other REACH-Motes and MH-REACH-Motes at a reasonable distance using only a small amount of energy, enabling the creation of a multi-hop wake-up network with passive WuRxs. In order to determine the benefit of a multi-hop wake-up network with passive WuRxs, we compare the performance in terms of energy consumption of an MH-REACH-Mote with the performance of a $65\mu W$ active wake-up sensor node [105] as well as the performance of a low power listening

approach used for very low duty-cycle operation [101].

The remainder of this chapter is organized as follows. The description of the hardware design of the MH-REACH-Mote is provided in Section 6.2. Section 6.3 presents results from field experiments. Section 6.4 evaluates the energy performance of different settings of the MH-REACH-Mote and compares the energy performance of the MH-REACH-Mote with an active wake-up sensor node and a low power listening (LPL) approach. Conclusions are drawn in Section 6.5.

6.2 Hardware Implementation of the MH-REACH-Mote and a Multi-hop Passive Wake-up Sensor Network

6.2.1 MH-REACH-Mote

Although any sensor node device with an MCU with low-power modes can be used, we used the Tmote-Sky platform to build the multi-hop wake-up sensor node (MH-REACH-Mote). The Tmote-Sky consumes very low energy while sleeping, which helps to conserve battery power and extend the node's lifetime. The Tmote-Sky can be woken up from sleep by a rising/falling edge triggered by the passive WuRx, as described in [98]. In order to achieve multi-hop wake-up, the MH-REACH-Mote must also include a WuTx component that can be triggered by the Tmote-Sky, e.g., through the Tmote-Sky's digital I/O pins to control the WuTx's activity. The entire sensor node requires only one power source, shared by the Tmote-Sky and the WuTx. Due to this approach, it is necessary to use energy judiciously in both the Tmote-Sky and the WuTx to optimize the sensor's lifetime.

Several desired characteristics were considered in the design and creation of a complete sensor node, equipped with both a WuTx and a passive WuRx, including:

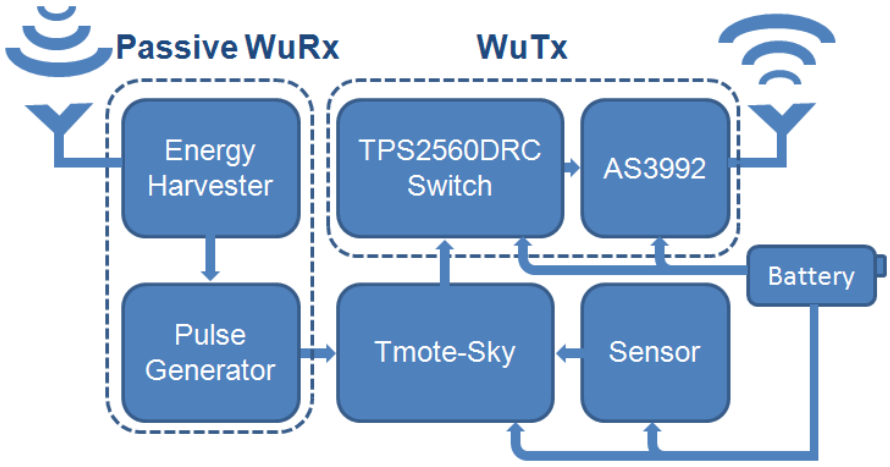

Figure 6.1: Block diagram of the MH-REACH-Mote.

- A sensor node must be able to be reliably woken up from sleep by its WuRx responding to a wake-up signal.
- A $3V$ battery must power the entire sensor node. Since the Tmote-Sky uses two AA ($1.5V$) batteries, ideally the WuTx should share this $3V$ source.
- The WuTx must be able to be controlled by the Tmote-Sky.
- The WuTx must be able to wake up other nearby sensor nodes equipped with a passive WuRx.
- The WuTx must be very energy efficient, in order to maximize the wake-up range without significantly decreasing the node's battery level.
- The WuTx may not need to send any address or implement security, but its design ideally will not prohibit a secure, addressable passive wake-up radio system from being implemented in the future.

We selected the AMS *AS*3992 UHF RFID Reader as the WuTx for the sensor node [109], as this is a low power, single chip solution. Moreover, it provides

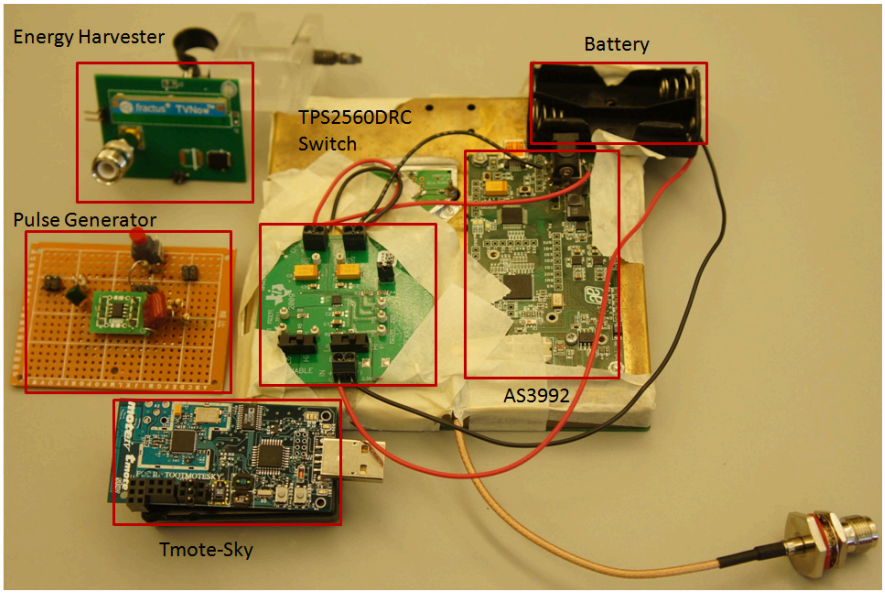

Figure 6.2: Hardware of the MH-REACH-Mote.

the option of building an addressable wake-up radio solution based on an RFID protocol, leaving the door open for the implementation of a secure, addressable passive wake-up radio system. This WuTx is controlled by the Tmote-Sky through a TI $TPS2560DRC$ switch [110]. We combine the Tmote-Sky, the $AS3992$ board, and the REACH-Mote's WuRx [98] to build the new sensor node, MH-REACH-Mote, equipped with both a WuTx and a passive WuRx. Fig. 6.1 shows a block diagram of this MH-REACH-Mote, and Fig. 6.2 shows the hardware components of the MH-REACH-Mote.

6.2.2 Multi-hop Passive Wake-up Sensor Network

Each node in our multi-hop passive wake-up sensor network can function either as a multi-hop node, which sends a wake-up signal to wake-up other nodes, or as an edge node, which does not send a wake-up signal as no other node is located in its wake-up range. Each node must determine periodically whether it is a multi-hop node or an edge node in order to determine whether or not to transmit a wake-up

signal once it is woken up by the sink or by another node in the network.

All nodes in our multi-hop passive wake-up sensor network remain in the sleep mode, with the passive WuRx scanning for a wake-up signal. A mobile sink (or other designated node) provides the initial wake-up in our system. As the sink goes by an area of the network, the WuTx on the sink wakes up all nodes in the vicinity of the sink. Any node that was woken up by the sink sends its data to the sink, and, if it is a multi-hop node, it also transmits a wake-up signal to wake up other nodes in its wake-up range. If it is an edge node, after transmitting its data to the sink, it returns to the sleep state until the next wake-up event.

Specifically, the protocol run by the nodes is as follows:

- When first deployed, an MH-REACH-Mote powers up and goes into the initialization, or *Init*, state.
- In the *Init* state, the MH-REACH-Mote transmits a wake-up signal through its WuTx, attempting to wake up nearby nodes. A timer is set to fire at the end of the wake-up signal transmission period. Simultaneously, the radio on the Tmote-Sky is set to receiving mode, and listens for incoming messages. If a packet is received before the timer fires, the MH-REACH-Mote is defined as a multi-hop node. Otherwise, it is defined as an edge node. Note that although an edge node might not have any other node in its wake-up coverage, it might be in another node's wake-up coverage due to the directorial antennas used.
- Next, the MH-REACH-Mote sets a timer for data sensing and enters into the *sleep* state.
- The MH-REACH-Mote will remain in the *sleep* state until either the timer for sensor data fires, or it receives a wake-up signal from its WuRx.

- When the timer for sensor data fires, the MH-REACH-Mote enters into the *sense* state, and collects and stores the new data in memory. The MH-REACH-Mote then returns back to the *sleep* state.

- When the MH-REACH-Mote receives a wake-up signal from its WuRx, it enters into the *wake-up* state if the MH-REACH-Mote is a multi-hop node. Otherwise, if the MH-REACH-Mote is an edge node, it enters directly into the *transmit* state.

- An MH-REACH-Mote that entered into the *wake-up* state transmits a wake-up signal through its WuTx to wake up other MH-REACH-Motes. Then, the MH-REACH-Mote enters into the *transmit* state.

- An MH-REACH-Mote in the *transmit* state will send its own stored data to the sink. We assume that if a node is woken up, it is in the transmission range of the sink, and hence the communication is direct from the node to the sink. After sending the data, the MH-REACH-Mote returns to the *sleep* state.

- In dynamic topology scenarios, the node can return to the *Init* state periodically to see if it should change its type between multi-hop and edge node.

Fig. 6.3 shows the state diagram of the MH-REACH-Mote operation.

6.3 Experiments

We developed the MH-REACH-Mote prototype that is illustrated in Fig. 6.2. Here, we evaluate the wake-up coverage as well as the energy cost of the MH-REACH-Mote based on field tests of this prototype.

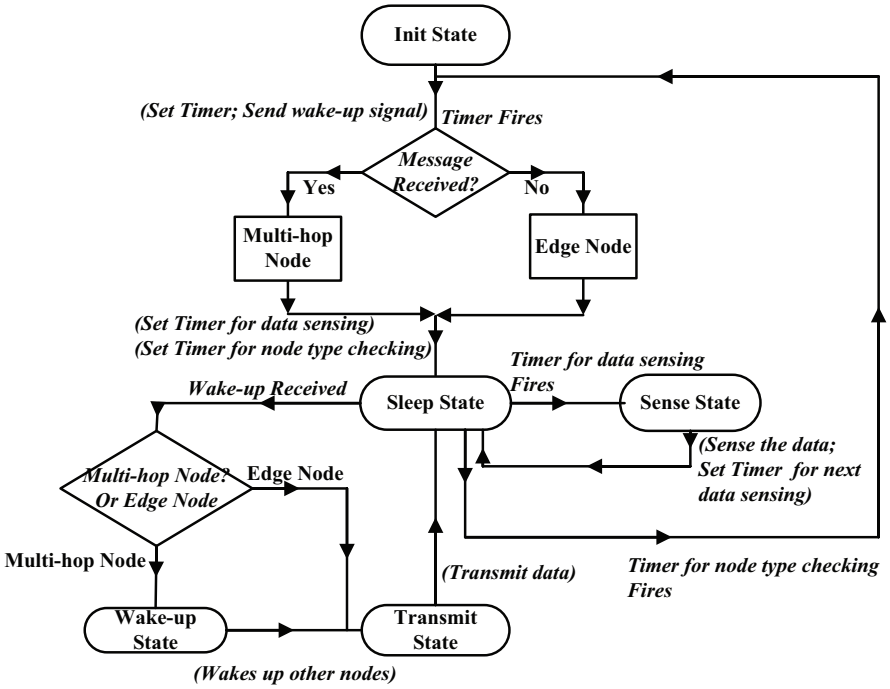

Figure 6.3: State diagram of the MH-REACH-Mote operation.

6.3.1 Characterization of Wake-up Range and Energy Consumption for the MH-REACH-Mote

We performed two sets of field tests to evaluate the wake-up coverage area of the MH-REACH-Mote. In the first set of tests, two MH-REACH-Motes were placed $60cm$ above the ground in an indoor environment. Both the transmitting node and the receiving node were connected to a $S9028PCR$ circular polarity RFID panel antenna with a gain of $9dBiC$ [111], where $dBiC$ (isotropic circular) is the forward gain of an antenna compared to a circularly polarized isotropic antenna [112]. We measured the maximum wake-up range with different durations of wake-up signal transmissions, varying from $30ms$ to $10s$. $30ms$ is the time for a Tmote-Sky to transmit 12 bytes of data. Hence, the MH-REACH-Mote can use the time when it is performing data transmission to simultaneously transmit the wake-up signal.

A longer wake-up signal transmission provides more energy to the receiving

node and does achieve a slightly longer wake-up range. However, this comes at the cost of increased energy consumption at the transmitting node, due to the extended time the wake-up signal is being sent. The purpose of this set of tests was to characterize the relationship between the duration of the wake-up signal transmission and the wake-up range.

Table 6.1 shows the maximum wake-up range and the energy consumed by the MH-REACH-Mote for different wake-up transmission durations in the first set of field tests. The measurements shown correspond to the average of three sets of measurements with a variance less than $15cm$. The results show that the maximum wake-up range is $9.4m$, achieved when the wake-up signal was transmitted for 10 seconds. Even when the MH-REACH-Mote is only turned on for $30ms$, which costs only $0.11J$ energy, the wake-up distance is found to be $8.8m$ by using the WuRx's high efficiency energy harvesting module and high gain directional antenna. Increasing the wake-up signal duration from $30ms$ to $2s$ does not increase the wake-up distance as the AS3992 in the WuTx transmits a high energy pulse along with a Query command in the beginning of the transmission according to the RFID protocol. After the high energy pulse, the AS3992 lowers its energy transmission and waits for a couple of seconds and transmits another pulse. Thus, increasing the signal duration more than 300 times to $10s$, with a cost of $23.54J$, which costs 214 times additional energy compared to a $30ms$ signal, only increases the wake-up range by $60cm$, or about 6%, which may not be a good trade-off for many applications. However, for applications that require the maximum wake-up range, the node lifetime may be traded off to achieve an extended wake-up range.

Table 6.1: Wake-up Range and Energy consumption for different wake-up signal durations

Wake-up Signal Duration	$30ms$	$100ms$	$500ms$	$1s$
Wake-up Range (m)	8.8	8.8	8.8	8.8
Energy Consumption (J)	0.11	0.29	1.35	2.41
Wake-up Signal Duration	$2s$	$3s$	$5s$	$10s$
Wake-up Range (m)	8.8	9.1	9.1	9.4
Energy Consumption (J)	4.66	7.36	12.54	23.54

6.3.2 Performance of MH-REACH-Mote in a Multi-hop Network

We perform the second set of field tests to evaluate the multi-hop performance of the MH-REACH-Mote when it cooperated with a mobile base-station moving along a pre-defined path. This is a realistic scenario such as when a car, which acts as a data mule [113], drives along the road and wakes up the sensor nodes deployed on the side of the road (e.g., on mailboxes, on street signs, etc.). After a sensor node along the side of the road is woken up, it transmits a signal to wake up the other nodes located further away (e.g., on a house or building nearby). Then, all nodes send the data to the data mule.

The base-station we used was a combination of an Impinj RFID reader [114] and a Powercast energy transmitter [115]. Based on our previous work [98], the WuRx on a REACH-Mote can be triggered at a distance of $11.2m$ from the base-station within 120 seconds. In order to ensure a quick wake-up, we deployed the MH-REACH-Mote $10.6m$ from the moving path of the base-station to ensure a stable and quick wake-up within 5 seconds. In this field test, the mobile base-station moves along the path to wake up the first MH-REACH-Mote when it

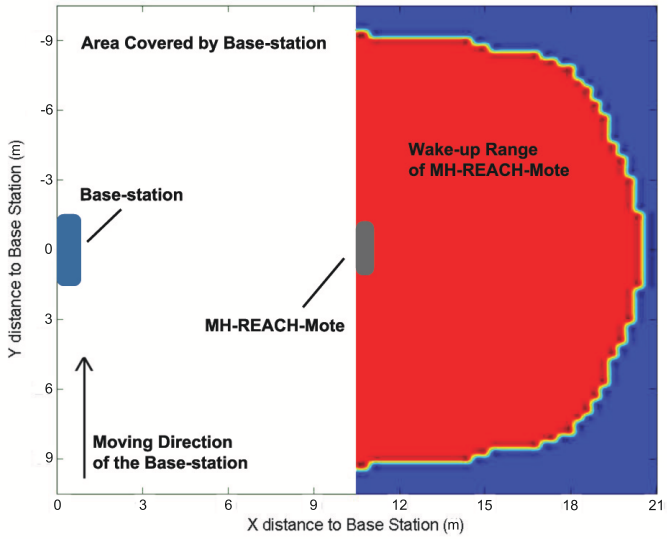

Figure 6.4: Multi-hop wake-up coverage with base-station assistance.

comes close to it. After this MH-REACH-Mote is woken up, it acts as a multi-hop node and wakes up a second, farther MH-REACH-Mote. As the base-station can continuously transmit energy, this can pre-charge the WuRx on the second-hop MH-REACH-Mote before the first-hop MH-REACH-Mote starts transmitting the wake-up signal. Thus, the base-station can potentially improve the wake-up range of the second-hop MH-REACH-Motes.

Fig. 6.4 shows the wake-up range results of the second set of field tests, where the second MH-REACH-Mote is placed in different locations to test the wake-up range of the second-hop. In this test, the mobile base-station moves towards the direction indicated in Fig. 6.4, transmitting a wake-up signal along its path. An MH-REACH-Mote along the moving path of the base-station is woken up by the base-station and transmits a wake-up signal with a constant duration of $30ms$ to wake up a second MH-REACH-Mote. As the wake-up signal received by the WuRx is a combination of the signal transmitted by the MH-REACH-Mote and the base-station, we expect the wake-up range can get extended in this scenario.

We evaluate the performance of wake-up coverage of this 2-hop passive wake-up sensor network. We found that the maximum wake-up range between the first hop MH-REACH-Mote and the second hop MH-REACH-Mote is $10.3m$, which represents a $1.5m$ (17% improvement) increase with the assistance of the base-station compared to the previous result with a $30ms$ wake-up signal. This result is achieved when the base-station and two MH-REACH-Motes are all aligned in a straight line. Additionally, with the assistance of the base-station, the wake-up range is always found to be above $9.4m$. This minimum wake-up range of $9.4m$ corresponds to the case when the base-station is horizontally aligned with the first MH-REACH-Mote, and the second MH-REACH-Mote is vertically aligned with the first one.

6.3.3 Analysis of MH-REACH-Mote Lifetime

In order to evaluate the potential lifetime of the MH-REACH-Mote, we measure the current consumption of the WuTx as well as the Tmote-Sky. We also assume that the MH-REACH-Mote is powered by 2 AA batteries and each battery can provide $1800mAh$. Also, we assume that the nodes are waking up other nodes every 4 hours. Under these assumptions, Table 6.2 shows the node lifetime for the different wake-up ranges. As shown in Table 6.2, since a wake-up range of $8.8m$ only requires the WuTx to be transmitting the wake-up signal for $30ms$, the node can remain operational for more than 5000 days, achieving a lifetime of more than 14 years. However, as the wake-up range requirements increase, the node lifetime decreases dramatically. If a node needs to achieve a wake-up range of $9.4m$, the node lifetime decreases to 134 days, which may still be an acceptable node lifetime for some applications. Note that the energy cost of the data sensing as well as the battery leakage are ignored in evaluation.

Table 6.2: Energy consumption and node lifetime for different wake-up signal durations

Wake-up Signal Duration	$30ms$	$3s$	$10s$
Wake-up distance (m)	8.8	9.1	9.4
Node Lifetime (days)	5376	413	134

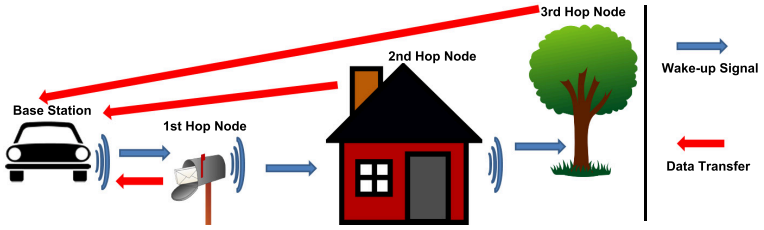

Figure 6.5: Working scenario for MH-REACH-Mote.

6.4 Lifetimes for MH-REACH-Motes, Active Wake-up Motes and a Low Power Listening Approach

In order to determine the benefit of multi-hop passive wake-up in the context of a wireless sensor network, we compare the performance of an MH-REACH-Mote network with that of a network that consists of active wake-up radio motes described in [105] with $65\mu W$ energy consumption as well as a low power listening approach proposed for very low duty-cycles [101]. We assume that nodes in the network are deployed at three different instances as illustrated to be on the mailbox, house and trees along a road, in Figs. 6.5, 6.6 and 6.7. A mobile car, working as a base station, drives along the road to wake up each node and collect data, for example, air pollution data [116].

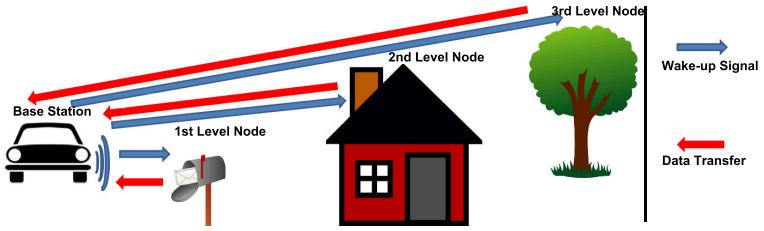

Figure 6.6: Working scenario for active wake-up.

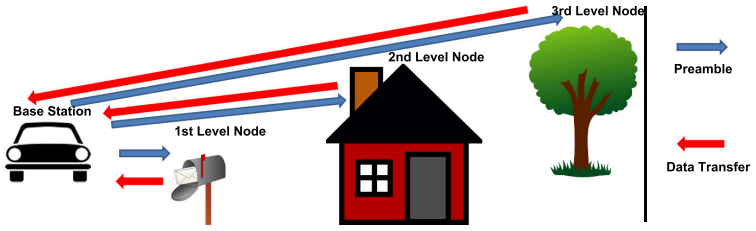

Figure 6.7: Working scenario for low power listening approach.

For the MH-REACH-Mote scenario, all MH-REACH-Motes are in the sleep mode most of the time. The mobile car, working as a data sink, continuously sends a wake-up signal to wake up the MH-REACH-Motes around it while driving along the road. After the first-hop MH-REACH-Motes, located on the mailbox, are woken up, they transmit a wake-up signal to the second-hop, farther MH-REACH-Motes deployed on the house. Then, the second-hop MH-REACH-Motes transmit the wake-up signal to the third-hop MH-REACH-Motes located on nearby trees. After the nodes are woken up, they transmit their data directly back to the mobile car (since the transmission range of the radio ensures that even the nodes in the third level can reach the mobile car directly). Fig. 6.5 shows the working scenario using MH-REACH-Motes.

For the active wake-up radio network scenario, the nodes are also in the sleep mode most of the time. However, during this time in the sleep mode, the active WuRx is dissipating a constant $65\mu W$. The mobile car sends a wake-up signal along the road, which wakes up all three sensor nodes on the mailbox, house and trees. After the sensor nodes are woken up, they send their data to the mobile

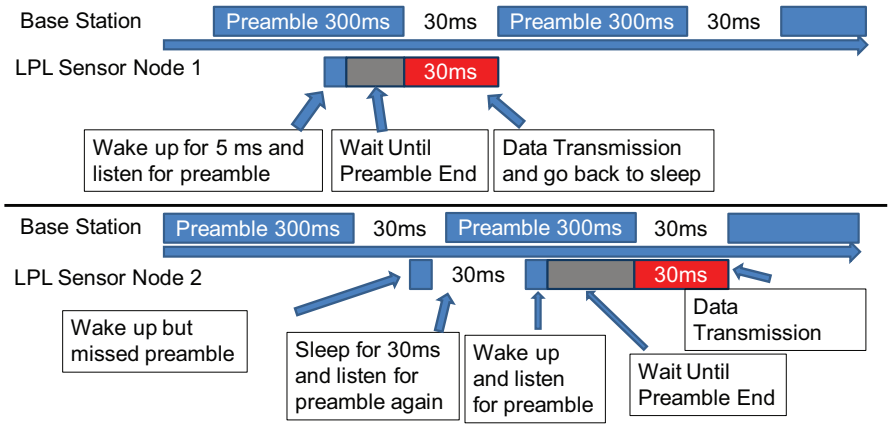

Figure 6.8: Operation of the low power listening protocol.

car. Fig. 6.6 shows the working scenario for this active wake-up.

Fig. 6.8 shows the communication protocol for the low power listening (LPL) scenario we evaluated. The base station continuously sends a long preamble while driving along the road. The preamble lasts for $300ms$, followed by a $30ms$ gap in order for the base station to listen for a response packet sent from the sensor nodes. All nodes are kept in the sleep mode most of the time, and they wake up for $5ms$ periodically according to an internal sleep timer T to listen for the preambles and check if the base station is located within their communication range. If the node wakes up and the base station is located within its communication range, like LPL Sensor Node 1 in Fig. 6.8, the node sends its data to the base station and goes back to sleep. Otherwise, the sensor node goes back to sleep for $30ms$ and listens to the channel again for the possibility that the first listening coincided with the gap between two preambles, as with LPL Sensor Node 2 in Fig. 6.8. If the base station is located within the communication range of the sensor node, this approach can guarantee a wake-up. If the sensor node does not receive a preamble in either of these two listening intervals, the sensor node goes directly back to sleep for a time T.

The value of the sleep timer T should ensure a successful wake-up whenever

the mobile base station is passing by the sensor node. As the Tmote-Sky sensor node can achieve a $125m$ outdoor communication range [117], the speed of the base station determines the maximum period T. The two different speeds of the mobile base station we evaluated are $10m/s$ and $20m/s$. Thus, the sleep timer T should be less than 25 and 12.5 seconds. In our evaluations, we considered the case of 25 and 12.5 seconds, respectively.

For all three of these scenarios, we assume:

- No collisions occur during the data transmission.
- All sensor nodes are located within the communication range of the data sink.
- All sensor nodes in the active wake-up scenario are located within the wake-up range of the data sink.
- All nodes return to the sleep mode once they finish their data transmissions.
- The data sink does not have any energy constraints.
- Each node is powered by 2 AA batteries with $1800mAh$ energy.

Table 6.3 shows the energy consumption of the different components of the MH-REACH-Mote, the active wake-up radio mote [105] [110] and the LPL mote.

Fig. 6.9 shows the network lifetime for different intervals between when the base station collects data. As the TI $TPS2560DRC$ switch on the MH-REACH-Mote's WuTx only leaks $0.1\mu A$ from the battery during the sleeping period [110], the MH-REACH-Mote can achieve much higher energy efficiency compared to the active WuRx approach as the interval between two wake-up events increases. The

Table 6.3: Energy consumption for components of the MH-REACH-Mote, an active wake-up radio mote [105] and an LPL mote [101]

Operation	Average current consumption	Duration
Tmote-Sky transmit 12 byte packet	$18.35mA$	$30ms$
Tmote-Sky in sleep mode	$11.2\mu A$	Continuous
MH-REACH-Mote send wake-up signal	$1.25A$	$30ms$
Current leakage of TI $TPS2560DRC$ switch	$0.1\mu A$	Continuous
Active wake-up	$65\mu W$	Continuous
Low Power Listening	$18.35mA$	$5ms$

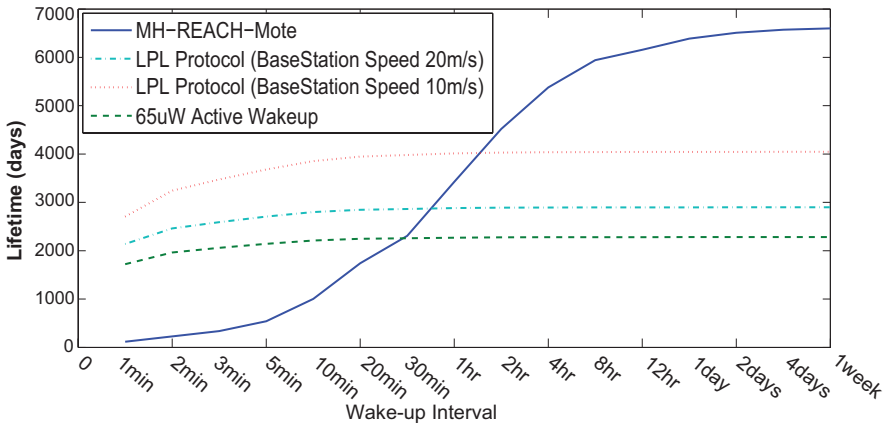

Figure 6.9: Comparison of node lifetime using an MH-REACH-Mote, an active wake-up radio mote [105] and a low power listening sensor node.

MH-REACH-Mote can achieve longer lifetime than active wake-up for average intervals between successive base station data collections of 30 minutes or more, which is a common scenario for a sensor network with regular data collection such as daily or even weekly temperature/moisture data collection and air pollution monitoring.

This observation also applies to the low power listening approach. For every 25 or 12.5 seconds, the sensor node will wake up from sleep state and check if the base station is close by. If the base station is not within the communication range, this process will waste $0.5505mJ$ energy. This low power listening strategy wastes a lot of energy for unnecessary wake-ups especially for longer interval arrival times of the base station. As this low power listening approach does not have continuous energy consumption except for the $11.2\mu A$ current draw in sleep mode, this approach consumes less energy than the $65\mu W$ active wake-up and results in longer lifetimes compared to active wake-up. As this approach periodically wastes energy on listening for the channel, a huge amount of energy is wasted if the communication between base station and sensor node occurs infrequently. Thus, the MH-REACH-Mote can achieve better energy efficiency than this low power listening approach for average intervals between successive base station data collections of 2 hours or more.

Further increasing the interval between successive data collections to a week extends the network lifetime of MH-REACH-Mote to 6600 days, which represents almost three times the network lifetime of the active wake-up radio sensor network and 50% longer lifetime compared to the low power listening approach. As the energy cost of the data sensing as well as the battery leakage are ignored in the calculation, the actual lifetime for nodes in the application could be potentially less than this calculation. Also, we notice that the increasing rate of the node lifetime goes down with an increase in the wake-up interval for longer wake-up intervals. This is because a greater portion of the energy is consumed by the

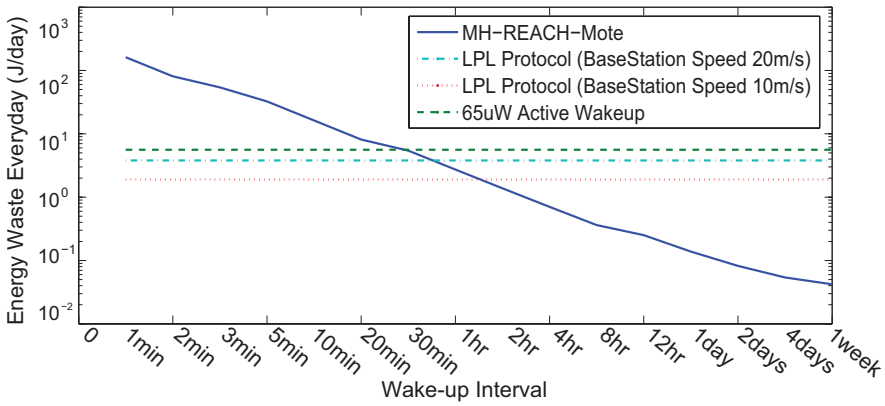

Figure 6.10: Comparison of energy overhead of an MH-REACH-Mote, an active wake-up radio mote [105] and a low power listening sensor node.

Tmote-Sky during the sleep period when the wake-up interval is long.

As the network lifetime is affected by the energy consumption of the Tmote-Sky, we also evaluate the average overhead costs for the different approaches. For the MH-REACH-Mote, the WuTx and the TI $TPS2560DRC$ switch are the main sources of overhead energy consumption. For the $65\mu W$ active wake-up sensor node, the energy cost for the active wake-up circuit (WuRx) dominates the energy overhead cost. For the low power listening sensor node, the unnecessary wake-ups to probe the channel are the key energy overhead. Thus, we evaluate the energy overhead for these three approaches. The results are shown in Fig. 6.10, which does not include the energy cost of the Tmote-Sky in transmitting data and sensing. The results show that the WuTx circuit on the MH-REACH-Mote consumes less energy than that of the active wake-up receiver for successive data collections of 30 minutes and longer. the low power listening sensor node wastes less energy than the active wake-up receiver. However, it costs more energy than the MH-REACH-Mote for intervals of 1 hour and longer. Also, we find that increasing the moving speed of the base station increases the energy waste for the low power listening approach. If the interval between successive data collections is

a week, the average energy cost of the MH-REACH-Mote's WuTx circuit decreases to as low as $0.04J/day$, which is about 140 times less than that of the active wake-up radio mote and about 45 times less than that of the low power listening mote.

6.5 Conclusions

In this chapter, we proposed the MH-REACH-Mote to build a multi-hop passive wake-up sensor network. Experimental results show that the MH-REACH-Mote can achieve a reasonable wake-up range of $9.4m$. Also, with the assistance of the base-station, an MH-REACH-Mote can achieve a $10.3m$ wake-up range with low energy consumption, which makes the MH-REACH-Mote a robust candidate for applications with long idle intervals between data transmission. Note that the wake-up receiver on the MH-REACH-Mote is designed based on the WuRx on the REACH-Mote. The evaluation in Chapter 5 shows that the REACH^2-Mote results in better wake-up distance than the REACH-Mote. Using the WuRx from the REACH^2-Mote for the MH-REACH-Mote could further improve the wake-up distance. As future work, we plan to design a new network protocol for a WSN composed of MH-REACH-Motes and evaluate the performance of this multi-hop passive wake-up network.

7 Conclusions and Future Work

7.1 Conclusions

In this thesis, we explored the coverage and performance challenges in RFID systems and wireless sensor networks, and we proposed various solutions to address these challenges. The technology proposed here leads to improvements in the performance of RFID systems and WSNs. The contributions of the research are summarized below.

1. We developed an RFID system with EDGE devices that cooperate with the RFID reader to extend the range with wireless technology. The EDGE devices are used to relay packets from RFID tags, which can be powered but not accessed directly by the RFID reader. We implemented the EDGE device and characterized its performance. This design can cooperate with a standard RFID reader and greatly increases the coverage.

2. We created a Token-MAC protocol to improve the performance of throughput, fairness and delay in RFID systems. Token-MAC utilizes tokens managed by the RFID reader and by the tags themselves to decrease the probability of collision and thus increase the throughput. Also, Token-MAC

can achieve better fairness and delay performance compared to the standard C1G2 protocol and a TDMA approach. We implemented Token-MAC, C1G2 and a TDMA approach and evaluated their performances through field tests. Also, we model the performances of these three protocols to create models that are used for simulation studies.

3. We designed two new passive wake-up radio enabled sensor nodes (REACH-Mote and REACH^2-Mote) for wireless sensor networks that can achieve long wake-up ranges. Also, we improved an existing RFID based wake-up sensor node and built an EH-WISP-Mote. We implemented both approaches in hardware and performed field tests. The performances of the REACH-Mote, REACH^2-Mote and the EH-WISP-Mote are evaluated. The experimental results show that the REACH^2-Mote can achieve long range passive radio wake-up. We also model the hardware performance of the WISP-Mote, REACH-Mote and REACH^2-Mote and evaluate the performance of these three approach in simulations. The result shows that REACH^2-Mote outperformed all other approach in energy efficiency.

4. We developed MH-REACH-Mote,a multiple-hop passive wake-up radio sensor node. By enabling the node-to-node wake-up, the MH-REACH-Mote can wake up other MH-REACH-Motes for long wake-up range with the assistance of base station. We evaluate the performance of MH-REACH-Mote in field tests as well as perform an energy analysis. The results shows that MH-REACH-Mote is an ideal solution for sensor networks with long idle intervals between data transmission.

7.2 Future Work

In order to further improve the performance of RFID systems and wireless sensor networks, several directions can be pursued as future research.

1. For RFID systems with EDGE devices, optimization of the location of the EDGE devices with multiple RFID antennas/readers can further improve performance of the system. As most RFID systems are composed of more than one RFID antenna, effectively deploying the EDGE devices to achieve maximum coverage area is important.

2. For wake-up radio enabled sensor nodes, address based wake-up is an important research area. Both REACH-Mote and REACH^2-Mote support only broadcast wake-up, while address based (ID based) passive wake-up can reduce false alarms and further reduce energy cost. However, design of a low energy cost address check for sensor nodes is difficult. Further research can be performed to develop low power, long range address based wake-up receivers.

3. Wireless energy harvesting to support the sensor can be explored for passive wake-up sensor nodes. The sensor node can be kept in sleep mode until it is awakened by a trigger signal transmitted by a wake-up radio transmitter. After waking up, the energy harvester circuit on the wake-up radio receiver can switch from performing the wake-up function to charging the node. As passive wake-up sensor nodes are equipped with an energy harvester circuit, utilizing this hardware to charge the battery/supercapcitor of the sensor nodes after the wake-up can further extend the network lifetime.

Bibliography

[1] E. Welbourne, L. Battle, G. Cole, K. Gould, K. Rector, S. Raymer, M. Balazinska, G. Borriello, "Building the Internet of Things Using RFID: The RFID Ecosystem Experience," Internet Computing, IEEE , vol.13, no.3, pp.48,55, May-June 2009

[2] M. Billinghurst, T. Starner, "Wearable devices: new ways to manage information," Computer , vol.32, no.1, pp.57,64, Jan 1999

[3] C. Otto, A. Milenkovi, C. Sanders, E. Jovanov, "System architecture of a wireless body area sensor network for ubiquitous health monitoring" J. Mob. Multimed. 1, 4 (January 2005), 307-326

[4] J. Lee, K.-S. Park, S. Hong, W.-D. Cho, "Object Tracking Based on RFID Coverage Visual Compensation in Wireless Sensor Network," Proceedings of the 2007 IEEE International Symposium on Circuits and Systems, May 2007, pp. 1597-1600.

[5] R. Want, "An introduction to RFID technology," Pervasive Computing, IEEE , vol.5, no.1, pp.25,33, Jan.-March 2006.

[6] H. Cho; Y. Baek, "Design and implementation of an active RFID system platform," Applications and the Internet Workshops, 2006. SAINT Workshops 2006.

[7] H. Vogt, "Multiple object identification with passive RFID tags," 2002 IEEE International Conference on Systems, Man and Cybernetics, 2002.

[8] P. V. Nikitin, K. V S. Rao, S. Lazar, "An Overview of Near Field UHF RFID," IEEE International Conference on RFID, 2007.

[9] R. Glidden, C. Bockorick, S. Cooper, C. Diorio, D. Dressler, V. Gutnik, C. Hagen, D. Hara, T. Hass, T. Humes, J. Hyde, R. Oliver, O. Onen, A. Pesavento, K. Sundstrom, M. Thomas, "Design of ultra-low-cost UHF RFID tags for supply chain applications," Communications Magazine, IEEE , vol.42, no.8, pp.140,151, Aug. 2004

[10] http://www.atlasrfidstore.com

[11] http://en.wikipedia.org/wiki/E-ZPass

[12] P. V. Nikitin, K. V S. Rao, "Performance limitations of passive UHF RFID systems," Antennas and Propagation Society International Symposium 2006, IEEE

[13] A. P. Sample, D. J. Yeager, P. S. Powledge, A. V. Mamishev, J. R. Smith, "Design of an RFID-Based Battery-Free Programmable Sensing Platform," IEEE Transactions on Instrumentation and Measurement, Nov. 2008.

[14] G. J. Pottie, "Wireless sensor networks," Information Theory Workshop, 1998.

[15] K. Romer, F. Mattern, "The design space of wireless sensor networks," Wireless Communications, IEEE, 2004.

[16] M. A. Hussain, P. Khan, S. Kwak kyung, "WSN research activities for military application," 11th International Conference on Advanced Communication Technology (ICACT), 2009.

[17] M. P. Durisic, Z. Tafa, G. Dimic, V. Milutinovic, "A survey of military applications of wireless sensor networks," Mediterranean Conference on Embedded Computing (MECO), 2012.

[18] G. Werner-Allen, J. Johnson, M. Ruiz, J. Lees, M. Welsh, "Monitoring volcanic eruptions with a wireless sensor network," Proceeedings of the Second European Workshop on Wireless Sensor Networks, 2005.

[19] L. Jun, Y. Chao, W. Cong, "Perceptual System of the Dangerous Goods in Transit Escort Based on WSN," International Conference on Internet Computing & Information Services (ICICIS), 2011.

[20] W. Chung, S. Lee, S. Toh, "WSN based mobile u-healthcare system with ECG, blood pressure measurement function," Engineering in Medicine and Biology Society, 2008.

[21] Y. Wang, L. Li, B. Wang, L. Wang, "A Body Sensor Network Platform for In-home Health Monitoring Application," Ubiquitous Information Technologies & Applications, 2009. ICUT '09.

[22] S. Hong, D. Kim, M. Ha, S. Bae, S. J. Park, W. Jung, J. Kim, "SNAIL: an IP-based wireless sensor network approach to the internet of things," Wireless Communications, IEEE, 2010

[23] A. P. Castellani, N. Bui, P. Casari, M. Rossi, Z. Shelby, M. Zorzi, "Architecture and protocols for the Internet of Things: A case study," 8th IEEE International Conference on Pervasive Computing and Communications Workshops (PERCOM Workshops), 2010.

[24] Y. Chen, Q. Zhao, "On the lifetime of wireless sensor networks," Communications Letters, IEEE, 2005.

[25] F. Wang, J. Liu, "Duty-Cycle-Aware Broadcast in Wireless Sensor Networks," INFOCOM 2009, IEEE

[26] R. Jurdak, P. Baldi, C. V. Lopes, "Adaptive Low Power Listening for Wireless Sensor Networks," IEEE Transactions on Mobile Computing, 2007.

[27] T. Schmid, R. Shea, Z. Charbiwala, J. Friedman, M. B. Srivastava, Y. H. Cho, "On the interaction of clocks, power, and synchronization in duty-cycled embedded sensor nodes," ACM Trans, 2010.

[28] G. Lu, N. Sadagopan, B. Krishnamachari, A. Goel, "Delay efficient sleep scheduling in wireless sensor networks," 24th Annual Joint Conference of the IEEE Computer and Communications Societies. Proceedings IEEE, INFOCOM, 2005.

[29] L. Gu, J. A. Stankovic, "Radio-triggered wake-up capability for sensor networks," Real-Time and Embedded Technology and Applications Symposium, 2004.

[30] W. K. Seah, E. Z. Zhi, H. Tan, "Wireless sensor networks powered by ambient energy harvesting (WSN-HEAP) - Survey and challenges," Wireless Communication, Vehicular Technology, Information Theory and Aerospace & Electronic Systems Technology, 2009. Wireless VITAE 2009.

[31] R. J. M. Vullers, R. V. Schaijk, H. J. Visser, J. Penders, C. V. Hoof, "Energy Harvesting for Autonomous Wireless Sensor Networks," Solid-State Circuits Magazine, IEEE , 2010.

[32] http://www.ecfr.gov

[33] http://www.nxp.com/

[34] http://www.impinj.com/

[35] http://www.omni-id.com/products/RFID_tagsultra.php

[36] S. Ondrej, B. Zdenek, F. Petr, H. Ondrej, "ZigBee Technology and Device Design," Proceedings of the ICN/ICONS/MCL 2006 International Conference on Networking, International Conference on Systems and International Conference on Mobile Communications and Learning Technologies, April 2006, pp. 129.

[37] CSL CS468 16-Ports EPC Class 1 Gen 2 RFID Reader http://convergence.com.hk/upload/download/CSL%20CS468

[38] Motorola FX9500 Fixed RFID Reader http://www.motorola.com/web/Business/Products/RFID/RFID%20Readers/FX9500/_Documents/static_files/FX9500_Specifications.pdf

[39] GAO 8-Port Gen 2 RFID Reader http://www.gaorfid.com/

[40] Z. Zhou,H. Gupta, S. R. Das, and X. Zhu, "Slotted Scheduled Tag Access in Multi-Reader RFID Systems," Proc. 15th IEEE Intl Conf.Network Protocols (ICNP), 2007.

[41] M. Abbak, I. Tekin, "RFID Coverage Extension Using Microstrip Patch Antenna Array," IEEE Antennas and Propagation Magazine, vol. 51, no. 1, pp. 185-191.

[42] V. Sheridan, B. Tsegaye, M. Walter-Echols, "ZigBee-Enabled RFID Reader Network," Major Qualifying Project Report, E-project-041706-150556, Worcester Polytechnic Institute, 2006.

[43] K. Leong, M. Ng, P. Cole, "The Reader Collision Problem in RFID Systems," Proceedings of the 2005 IEEE International Symposium on Microwave, Antenna, Propagation and EMC Technologies for Wireless Communications, Aug. 2005, pp. 658-661, Vol. 1.

[44] http://www.gs1.org/epcglobal

[45] http://www.silabs.com/products/mcu/Pages/default.aspx

[46] http://www.austriamicrosystems.com/Products/RF-Products/RFID/AS3992

[47] http://www.jennic.com/products/wireless_microcontrollers/

[48] P. V. Nikitin and K. V. S. Rao, "An Overview of Near Field UHF RFID," IEEE International Conference on RFID, 2007.

[49] M. Buettner, B. Greenstein, A. Sample, J.R. Smith and D. Wetherall, "Revisiting smart dust with RFID sensor networks," In Proceedings of the 7th ACM HotNets, October 2008.

[50] M. Buettner and D. Wetherall, "An Empirical Study of UHF RFID Performance," Annual International Conference on Mobile Computing and Networking (MobiCom 2008), 2008.

[51] P. V. Nikitin and K. V. S. Rao, "Performance Limitations of Passive UHF RFID Systems," Antennas and Propagation Society International Symposium, 2006.

[52] EPC Radio-Frequency Identity Protocols Class-1 Generation-2 UHF RFID Protocol for Communication at 860 MH - 960 MHz

[53] L. Chen, I. Demirkol and W. Heinzelman, "Token-MAC: A Fair MAC Protocol for Passive RFID Systems," IEEE Global Telecommunications Conference (GLOBECOM 2011), 2011.

[54] K. S. Leong, M. L. Ng and P. H. Cole, "The Reader Collision Problem in RFID Systems," Proceedings of IEEE International Symposium on Microwave,

Antenna, Propagation and EMC Technologies For Wireless Communications, 2005.

[55] Q. Zhao, W. Ren, A. Swami, "Spectrum Opportunity Detection: How Good Is Listen-before-Talk?," Signals, Systems and Computers, 2007. ACSSC 2007.

[56] ETSI EN 302 208-2 v 1.1.1 , Electromagnetic compatibility and Radio spectrum Matters (ERM); Radio Frequency Identification Equipment operating in the band 865 MHz to 868 MHz with power levels up to 2 W; Part 2.

[57] D. Simplot-Ryl, I. Stojmenovic, A. Micic, and A. Nayak, "A hybrid randomized protocol for RFID tag identification," Sensor Review 26/2 (2006) 147-154.

[58] R. Kalinowski, M. Latteux and D. Simplot, "An adaptative anti-collision protocol for smart labels," Tech. Rep. LIFL Univ. Lille 1, 2001.

[59] S. M. Birari and S. Iyer "PULSE: A MAC Protocol for RFID Networks," Embedded and Ubiquitous Computing C EUC 2005.

[60] H. Dai, S. Lai and H. Zhu "A Multi-Channel MAC Protocol for RFID Reader Networks," Wireless Communications, Networking and Mobile Computing, 2007.

[61] http://en.wikipedia.org/wiki/Token_ring

[62] M. Ergen, D. Lee, R. Sengupta and P. Varaiya, " WTRPWireless Token Ring Protocol," IEEE Transaction on Vehicular Technology VOL. 53, NO. 6, NOVEMBER 2004

[63] http://wisp.wikispaces.com/

[64] S. Zhang and A. Seyedi, "Analysis and Design of Energy Harvesting Wireless Sensor Networks with Linear Topology," IEEE International Conference on Communications (ICC), 2011.

[65] http://en.wikipedia.org/wiki/Johnson-Nyquist_noise

[66] http://www.impinj.com/products/rfid-reader.aspx

[67] L. Chen, S. Cool, H. Ba, W. Heinzelman, I. Demirkol, U. Muncuk, K. Chowdhury and S. Basagni, "Range Extension of Passive Wake-up Radio Systems through Energy Harvesting," IEEE International Conference on Communication (ICC '13), June 2013.

[68] P. Nintanavongsa, U. Muncuk, D. R. Lewis and K. R. Chowdhury,"Design Optimization and Implementation for RF Energy Harvesting Circuits," JETCAS'12, March 2012

[69] http://www.maximintegrated.com/app-notes/index.mvp/id/1186

[70] H. Ba, I. Demirkol and W. Heinzelman, "Feasibility and Benefits of Passive RFID Wake-up Radio for Wireless Sensor Networks" Proceedings GlobeCom 2010.

[71] N. Pletcher, S. Gambini and J. Rabaey, "A 52 W wake-up receiver with -72 dbm sensitivity using an uncertain-IF architecture, IEEE J. Solid-State Circuits, vol. 44, no. 1, pp. 269C280, 2009.

[72] G. Anastasi, M. Conti and M. Di Francesco, "Data collection in sensor networks with data mules: An integrated simulation analysis," IEEE Symposium on Computers and Communications, 2008. ISCC 2008.

[73] W. Ye, J. Heidemann and D. Estrin, "An energy-efficient MAC protocol for wireless sensor networks," INFOCOM 2002. Twenty-First Annual Joint Conference of the IEEE Computer and Communications Societies. Proceedings. IEEE , vol.3, no., pp.1567,1576 vol.3, 2002

[74] T. V. Dam and K. Langendoen, "An adaptive energy-efficient MAC protocol for wireless sensor networks," 1st international conference on Embedded networked sensor systems (SenSys '03). ACM, New York, NY, USA, 171-180.

[75] J. Polastre, J. Hill and D. Culler, "Versatile low power media access for wireless sensor networks," 2nd international conference on Embedded networked sensor systems (SenSys '04). ACM, New York, NY, USA, 95-107.

[76] A. El-Hoiydi, J.-D. Decotignie, C. Enz and E. Le Roux, "Poster abstract: wiseMAC, an ultra low power MAC protocol for the wiseNET wireless sensor network," 1st international conference on Embedded networked sensor systems (SenSys '03). ACM, New York, NY, USA, 302-303.

[77] M. Buettner, G V. Yee, E. Anderson and R. Han, "X-MAC: a short preamble MAC protocol for duty-cycled wireless sensor networks," 4th international conference on Embedded networked sensor systems (SenSys '06). ACM, New York, NY, USA, 307-320.

[78] C. Petrioli, D. Spenza, T. Pasquale and T. Alessandro, "A Novel wake-up Receiver with Addressing Capability for Wireless Sensor Nodes," IEEE DCoSS 2014, 2014.

[79] B. V. der Doorn, W. Kavelaars and K. Langendoen, "A prototype Low- Cost wakeup radio for the 868 MHz band, Int. Journal of Sensor Networks, vol. 5, no. 1, pp. 22C32, 2009.

[80] P. Le-Huy and S. Roy, "Low-Power Wake-Up radio for wireless sensor networks, Mobile Networks and Applications, pp. 1C11, 2010.

[81] J. Ansari, D. Pankin and P. Mahonen, "Radio-triggered wake-ups with addressing capabilities for extremely low power sensor network applications, International Journal of Wireless Information Networks, vol. 16, no. 3, pp. 118C130, 2009.

[82] S. J. Marinkovic and E. M. Popovici, "Nano-Power Wireless Wake-Up Receiver With Serial Peripheral Interface," Selected Areas in Communications, IEEE Journal on , vol.29, no.8, pp.1641,1647, September 2011

[83] http://en.wikipedia.org/wiki/Energy_harvesting

[84] C. Park and Pai H. Chou, "AmbiMax: Autonomous Energy Harvesting Platform for Multi-Supply Wireless Sensor Nodes".

[85] https://wisp.wikispaces.com/

[86] http://wisp.wikispaces.com/WISP+Challenge

[87] E. M. Tapia, S. S. Intille and K. Larson, "Portable wireless sensors for object usage sensing in the home: challenges and practicalities". In B. Schiele, A. K. Dey, and H. Gellersen. Ambient intelligence: European conference, AmI 2007, Darmstadt, Germany, November 7-10, 2007: proceedings. Springer. p. 23.

[88] http://www.impinj.com

[89] H. Ba, I. Demirkol and W. Heinzelman, "Passive Wake-up Radios: From Devices To Applications," Ad Hoc Networks Volume 11, Issue 8, November 2013, Pages 2605C2621

[90] http://www.ti.com/product/msp430f1611

[91] http://www.ti.com/product/cc2420

[92] H. Yan, J. G. Macias Montero, A. Akhnoukh, L. C. N. de Vreede and J. N. Burghart,"An Integration Scheme for RF Power Harvesting," *The 8th Annual Workshop on Semiconductor Advances for Future Electronics and Sensors,* Veldhoven, Netherlands, 2005.

[93] http://www.eecs.harvard.edu/ konrad/projects/shimmer/references/tmote-sky-datasheet.pdf

[94] https://www.ams.com/eng

[95] http://www.ti.com/product/tps2042b

[96] http://www.powercastco.com/

[97] P. Nain, D. Towsley, L. Benyuan and L. Zhen, "Properties of random direction models," INFOCOM 2005. 24th Annual Joint Conference of the IEEE Computer and Communications Societies. Proceedings IEEE

[98] Chen, L., Cool, S., Ba, H., Heinzelman, W., Demirkol, I., Muncuk, U., Chowdhury, K., and Basagni, S., "Range Extension of Passive Wake-up Radio Systems through Energy Harvesting," ICC 2013, Jun. 2013.

[99] Ba, H., Demirkol, I. and Heinzelman, W., "Feasibility and Benefits of Passive RFID Wake-up Radios for Wireless Sensor Networks," GLOBECOM 2010, Dec. 2010

[100] http://www.ams.com/eng/Products/RF-Products

[101] Merlin, C., Heinzelman, W., "Duty Cycle Control for Low-Power-Listening MAC Protocols," IEEE Trans. on Mobile Computing, Nov. 2010

[102] Zhang, Y., Chen, S., Kiyani, N. F., Dolmans, G., Huisken, J., Busze, B., Harpe, P., van der Meijs, N., De Groot, H., "A 3.72μW ultra-low power digital baseband for wake-up radios," VLSI-DAT 2011, Apr. 2011

[103] Harpe, P., Huang, X., Wang, X., Dolmans, G., De Groot, H., "A 0.37μW 4bit 1MS/s SAR ADC for ultra-low energy radios," VLSI-DAT 2011, Apr. 2011

[104] Huang, X., Harpe, P., Dolmans, G., De Groot, H., "A 915MHz ultra-low power wake-up receiver with scalable performance and power consumption," Proceedings of the ESSCIRC 2011, Sept. 2011

[105] Pletcher, N., Gambini, S., Rabaey, J., "A 65μW, 1.9 GHz RF to Digital Baseband Wakeup Receiver for Wireless Sensor Nodes," CICC 2007, Sept. 2007

[106] Ba, H., Demirkol, I., Heinzelman, W., "Passive wake-up radios: From devices to applications," Ad Hoc Networks, Nov. 2013

[107] Zhang, Y., Dolmans, G., "Wake-up radio assisted energy-aware multi-hop relaying for low power communications," WCNC 2012, April 2012

[108] Ruzzelli, A., Jurdak,R., O'Hare, G., "On the RFID wake-up impulse for multi-hop sensor networks," ACM International Conference on Embedded Networked Sensor Systems, November 2007

[109] http://www.ams.com/eng/Products/RF-Products/RFID/AS3992

[110] www.ti.com/lit/ds/slvs930a/slvs930a.pdf

[111] http://www.lairdtech.com/

[112] http://en.wikipedia.org/wiki/Decibel

[113] Shah, R. C., Roy, S., Jain, S., Brunette, W., "Data MULEs: Modeling a Three-tier Architecture for Sparse Sensor Networks," Intel Research Tech Report , January 2003

[114] http://www.impinj.com/Speedway_Reader_Family.aspx

[115] http://www.powercastco.com/products/powercastertransmitters/

[116] http://www.ece.rochester.edu/projects/wcng/project_genius2.html

[117] http://www.eecs.harvard.edu/~konrad/projects/shimmer/references/tmote-skydatasheet.pdf